Faculty of Science and Technology
Department of Physics and Technology

Investigation of Photovoltaic Energy Yield on Tromsøya by Mapping Solar Potential in ArcGIS

—

Odin Foldvik Eikeland

EOM-3901 Master's Thesis in Energy, Climate and Environment, July 2019

“Success is a science; if you have the conditions, you get the results”

- Oscar Wilde

Abstract

To contribute to the reduction of greenhouse gas emissions, energy production from renewable energy resources should be markedly increased to supply the rising global energy demand (Marchant, 2018). This thesis investigates the solar energy potential in Tromsø which is used as a basis for estimating total energy yield from photovoltaic (PV) systems on rooftops. The energy yield is compared against energy load from Cruise ships visiting Tromsø to investigate the potential for supplying the ships with renewable, local produced PV solar energy to substitute the ships own production of energy.

The aim of this thesis is to investigate the solar potential on Tromsøya by creating a solar map in ArcGIS. The solar map could be used as a basis for investigating energy yield from PV systems installed on buildings. The suitable areas for PV systems on Tromsøya were determined by qualified estimations based on building area statistics and utilization factors. The energy load from Cruise ships was estimated by using given information from Port of Kristiansand, the only harbor in Norway which offer the possibilities for shore power.

This thesis has created the first 0.25-meter resolution solar map ever made of Tromsøya. The resulting solar map shows accurate results with a relative RMSE of 0.007 W/m^2 when compared against averaged pyranometer values at Holt weather station. The resulting potential from buildings on Tromsøya shows that the PV energy yield with 10% integration scenario could cover the load from Cruise ships for all summer months during the tourist season. The solar fraction (SF) shows a positive energy balance between PV energy yield and Cruise ship energy load for all months, except from March where the load was higher than yield. Calculations based on electricity spot price shows that Tromsø municipality could earn economic benefits by selling produced PV solar energy to Cruise ships.

Contents

List of Tables

List of Figures

Acknowledgements

First, I would like to thank my supervisors Matteo Chiesa and Tobias Boström for offering me the opportunity to work on this project. Matteo, who first came up with the idea and explained it in detail with high enthusiasm as always. Tobias has contributed with his expertise and experience in this field to form the idea to a good project. I would also like to tank Bilal Babar for contributing with tips regarding to ArcGIS and for valuable feedback in the end of the master thesis work. In addition, a huge tank to Rolf Andersen at UiT which helped me a lot with accesses needed to create the high-resolution solar map.

Multiple data sources have been applied during this project, and I would like to thank all who contributed with information and non-public data. This includes: Institute for Computer Science at UiT which contributes with weather data from pyranometers, Siril Hafstad at Geodata which helped me in the beginning with ArcGIS and Trond Sikveland which provided needed information about energy load from Cruise ships.

The study period at UiT would never have been the same without my classmates. I want to thank you all for five fantastic years. Unlimited number of memories has been created together.

Thanks to UiT- The Arctic University of Norway for five exciting and challenging years. In addition, thanks for providing me the opportunity to travel and participate in competitions in cycling when I was a student by giving me the status as a top athlete at the University.

Finally, I would like to thank my family. I would never been here if it wasn't for you. You have always supported and advised me in different situations during my life, making it possible to achieve my goals and enjoy a good life.

Best regards,

Odin Foldvik Eikeland

Abbreviations

AM	Air mass
ARC	Arctic Centre for Sustainable Energy
ASR	Area Solar Radiation
CPU	Central processing unit
DEM	Digital elevation model
DSM	Digital surface model
DTM	Digital terrain model
D&T	Diffuse & Transmission
Esri	Environmental System Research Institute
FF	Fill factor
GDB	Geodatabase
GHI	Global Horizontal Irradiance
GIS	Geographic Information System
GPS	Global Positioning System
GW	Gigawatt
IFT	Institute for Physics and Technology
INS	Inertial Navigation System
InSAR	Interferometry Synthetic Aperture
kWh	Kilowatt hour
LF	Load fraction
LiDAR	Light detection and ranging
MAE	Mean absolute error
MVA	Megavolt-Ampere
MW	Megawatt
NIBIO	Norwegian Institute for Bioeconomic
NOK	Norwegian Krone
PF	Power factor
PM	Particulate Matter
PR	Power Ratio
PSR	Point Solar Radiation
PV	Photovoltaic

RADAR	Radio detection and ranging
RMSE	Root mean square error
SF	Solar fraction
SSB	Statistics Norway
UiT	The Arctic University of Tromsø
UTM	Universal Transverse Mercator
VAT	Value Added Taxes

Nomenclature

In this thesis, physical quantities are denoted by italic types. Physical units are denoted by roman. The list is sorted after physical symbols, description and units in alphabetical order. Latin symbols first and then Greek symbols.

Symbol	Description	SI Unit
A	Area	m^2
A_{sol}	Architecturally suitable area	m^2
A_g	Ground floor area	m^2
AM	Air Mass	
E	Energy	J
E_{GO}	Band Gap Energy	J
c	Speed of light	$\mathrm{m/s}^2$
D	Minority carrier Diffusivity	cm^2/s
h	Planck's constant	$\mathrm{m}^2\mathrm{kg/s}$
I	Current	A
I_0	Saturation current	A
I_D	Sunlight intensity	$\mathrm{kW/m}^2$
I_G	Global irradiance	$\mathrm{kW/m}^2$
k	Boltzmann constant	$\mathrm{m}^2\ \mathrm{kg}\ \mathrm{s}^{-2}\ \mathrm{K}^{-1}$
L	Minority carrier diffusion length	µm
m_e	Mass electrons	kg
m_h	Mass holes	kg
n_i	Intrinsic carrier concentration	cm^{-3}
P	Power	$\mathrm{kg\ m}^2/\mathrm{s}^3$
T	Temperature	K
T	Temperature	°C
t	Time	s
u_f	Utilization factor façade	
u_r	Utilization factor roof	
V	Voltage	$\mathrm{kg\ m}^2/(\mathrm{s}^3\mathrm{A})$
q	Electronic charge constant	C
x,y,z	Cartesian coordinates	m
λ	Wavelength	m
η	PV efficiency	
θ	Angle of degree	°

1 Introduction

1.1 Background

The global population continues to rise, and the global energy demand is increasing. As a part of the 2015 Paris agreement, the global warming should be limited to 1.5°C before the end of the century by markedly increase the percentage of energy production from renewable energy resources (Marchant, 2018).

Since the beginning of the new millennium, the global photovoltaic (PV) marked has grown rapidly from less than 1 GW in year 2000 to exceeding 500 GW in year 2018 (Solar Business Hub, 2019). India was one of the countries with highest growth in 2018 with 10.8 GW, Australia close to 3.8 GW, Mexico 2.7 and Korea with 2.0 GW (Solar Business Hub, 2019). The middle east and African countries have also grown, but these results would be more viable in 2019. Europe experienced growth in PV market, with Germany and Netherland as most significant countries. In summary, the global PV marked grew by 99.8 GW in 2018. The total production from PV systems contribute close to 2.6% of the electricity demand in the world (Solar Business Hub, 2019). For 2019, a 25% growth with 129 GW new capacity is predicted to be installed (Sustinable Enterprises Media, Inc, 2019). In the future, PV has the potential to become a major source of electricity with an expected exponential growth. PV systems has the advantage that it could easily vary from small individual production systems to large power plants. To continue rising, the PV marked need to be supported by decreases in battery prices and rapid uptakes of electric vehicles (Solar Business Hub, 2019).

In Norway, the interest in PV has been low with an installed capacity of only 6 890 kW_p in 2004, and the marked growth was low with a yearly increase of 5% from 2004 to 2013. In 2016, the PV marked in Norway exploded with a 75% increase from 2015 and the marked has continued to rise with a 59% increase in capacity from 2016 to 2017 (Multiconsult, 2018). The installed capacity changed from almost 100% off-grid systems to 50% off-grid and 50% connected to grid. In 2018, the solar energy marked continued to rise with 29% from 2017 and the total installed capacity is 68-megawatt peak (MW_P). This extreme increase in PV marked in Norway from 2015 until today is caused by reduced prices for installations, higher

efficiency for modules and a growing interest in renewable energy resources, in addition to several new businesses that are focusing on solar energy.

In conjunction with the increased focus on PV marked worldwide and in Norway, UiT- The Arctic University of Norway has established a PV system for research purposes to increase knowledge about PV system potentials in the Arctic regions. In addition, the Institute for Physics and Technology (IFT) at UiT has installed several instruments in different locations in Troms county to investigate the solar potential. In 2017, UiT established the Arctic centre for Sustainable Energy (ARC) which is an interdisciplinary centre focusing on Arctic challenges and conditions within renewable energy and greenhouse gas management (UiT, 2019).

1.2 Idea and Aim of Thesis

The idea for this thesis was conceived by Professor and leader of ARC, Matteo Chiesa during a discussion with author. We discussed the Cruise ships in Tromsø harbor which emits huge amounts of greenhouse gases and particulate matter due to self-production of energy when in harbor. We were curious about if it was possible to supply these Cruise ships with renewable solar energy from PV systems on Tromsøya. Pollution from Cruise ships is a highly debated field regarding to climate change and supplying with renewable shore power when in harbor is something to consider. To investigate energy yield potential from PV systems, Professor Tobias Boström suggested to create a solar map in ArcGIS which could be used as a basis for mapping the solar potential in Tromsø.

The main aim of this thesis is to create a high-resolution solar map in ArcGIS software that can be used as a basis for mapping solar potential on rooftops on Tromsøya. A solar map for Tromsøya has been created before in a former master thesis but has not been used for PV energy yield purposes. The former solar map has a resolution of 1- meter, while in this thesis a solar map of both 1-and-0.25-meter resolutions is to be created to investigate differences in high-and-low resolution solar maps.

When the solar map is created, it is possible to use this map to evaluate the potential for energy yield from PV systems. Total number of buildings must be identified to thereafter

estimate solar-architecturally suitable roof and façade areas by using utilization factors. The areas could thereafter be used to calculate the total energy yield from PV systems on Tromsøya. The total production could be set in context with energy consumption from Cruise ships visiting Tromsø to investigate if enough energy could be produced by renewable solar energy to supply Cruise ships. Finally, a simple calculation is performed to investigate the opportunities for economic benefit for Tromsø municipality by selling PV solar energy.

1.3 Significance

The PV solar potential conditions in urban environments can vary significantly according to tilt and orientation of roof in addition to surrounding factors as shadowing effects. The local conditions can differ between neighbouring areas because of topography and surrounding buildings, and therefore all areas must be considered when investigating local PV solar potential. In addition, the global solar irradiation varies significantly during the year, especially in Arctic regions. Arctic regions north of the polar circle has 24-hours polar nights during winter where solar irradiation is non- existent. On the other hand, during the summer period in the 8 weeks when sun never sets, PV generation potential could be significant. During this period, the electricity load from Cruise ship is significant with an increased traffic as the tourism in Tromsø is at its peak in summer months.

Creating solar maps can make it possible to visualize the solar potential on both buildings and surrounding terrain. In this thesis, GIS is used as a tool for investigating the solar potential on all rooftops on Tromsøya regarding to orientation, tilt and surrounding effects. This solar map could be a valuable asset when considering where to place a PV system with optimal production.

1.4 Structure of the Thesis

Including the introduction, the thesis consists of 6 chapters: theory, method, results, discussion and conclusion with suggestions for further work.

Chapter 2 provides the theoretical backgrounds needed to understand the methodology in the thesis. The chapter holds an introduction to solar energy and working principles of PV cells. Geographical information system (GIS) is thereafter described.

Chapter 3 presents the methodology used to reach the results. It describes the process of creating the solar map in ArcGIS, case studies, and mapping of total building area, and estimation of energy consumption from Cruise ships.

Chapter 4 provides monthly energy yield from PV systems on Tromsøya and presents the energy yield/need balance between PV systems and Cruise ships. In addition, a case study for one day in June 2018 is performed to show how much area of PV systems are needed to cover a Cruise ship 10 hours energy demand.

Chapter 5 holds a discussion of method based on when creating the map, it debates how the calculation of these solar maps could be done in more efficient ways. The validity of the estimating method for the total building area on Tromsøya is discussed. Finally, uncertainties regarding to estimating energy load from Cruise ships is examined.

Chapter 6 summarizes the results and proposes suggestions for future work.

In addition, monthly solar maps for 1-and-0.25-meter resolution are added in the appendix which could be used for closer investigation of solar potential for specific months. The bibliography with all sources of information is provided in the end.

2 Theoretical background

2.1 Solar energy

Solar energy is the source for almost all energy on the earth. Humans, animals and plants need the sun for heat and food. Humans also use the sun's energy in many other ways than food and warming. For example, fossil fuels are widely used for transportation and electricity generation. Fossil fuel is solar energy which has been stored in millions of years (Honsberg & Bowden, 2018). Similarly, humans use biomass which converts the sun's energy into fuel, and wind energy uses air current that are created by solar heated air and the earth's rotation (Honsberg & Bowden, 2018). Hydroelectricity is also indirectly energy we receive from the sun. The sun heats up water, which evaporates and return to earth as precipitation, and gets stored in dams where we can install hydro power plants to make use of the stored water for hydroelectricity (Honsberg & Bowden, 2018).

The solar energy can be viewed as parcels of energy, where each parcel is in form of photons. The photons have energy given as

$$E = \frac{hc}{\lambda} \tag{2.1}$$

,where λ is the photons wavelength, h is given as the Plank's constant and c is the speed of light and is often considered as constant (Honsberg & Bowden, 2018). Therefore, the energy of the photon is dependent on wavelength λ, where short wavelength photons have high energy, and vice versa. Photons of different wavelength reach different parts of the Earth's atmosphere. As solar radiation passes through the atmosphere, dust, gasses and aerosols absorbs photons. Some specific gasses such as ozone, carbon dioxide and water have high absorption of photons. A big part of the infrared light with high wavelength above 2 μm is absorbed by water vapor and carbon dioxide, while most of the ultraviolet light with shorter wavelength below 0.3 μm is absorbed by ozone (Honsberg & Bowden, 2018).

The absorption of photons by specific gasses is not the only factor which affect the solar radiation trough the atmosphere. The major factor for reduction in power from solar irradiation to surface, is absorption and scattering of light due to molecules in the air and dust. If the sun is not directly overheaded at the surface, the photons must travel longer distance

trough the atmosphere. In this case, higher energy photons with shorter wavelengths are more absorbed and scattered than low energy photons with longer wavelengths. If the sun is directly overheaded at surface, the absorption due to atmospheric elements causes a relatively uniform reduction across the visible spectrum (Honsberg & Bowden, 2018).

2.1.1 What is solar irradiance?

Solar irradiance is the amount of energy from the sun that hit the earth over a square meter per second, and has unit $\left[\frac{J}{sm^2}\right]$ or $\left[\frac{W}{m^2}\right]$ (Garner, 2008).By measuring the irradiance of the sun at a wavelength of light, we find the solar spectral irradiance. The spectral irradiance variations are seen in many photons with different wavelengths. The photons in the visible light and infrared part of the electromagnetic spectrum have long wavelengths, and the photons in the X- ray part has short wavelengths (Garner, 2008). By measuring spectral irradiance, we get more knowledge about which wavelengths are absorbed in the atmosphere, and which wavelengths does reach the surface. Radiation in the visible and infrared spectrum reaching the surface, while ultraviolet and X- ray radiation is absorbed by the atmosphere at higher altitudes (Garner, 2008).

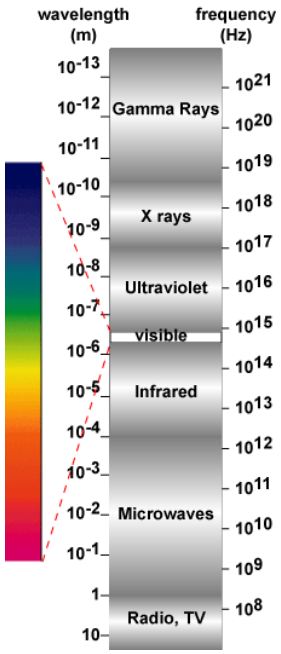

Figure 2-1: The electromagnetic spectrum (Honsberg & Bowden, 2018)

2.2 Atmospheric effects on solar radiation

Since the earth's surface is covered by an atmosphere, the solar radiation which reach surface is affected by atmospheric effects. Some of the major atmospheric effects are reduction of solar radiation intensity due to absorption, scattering and reflection of photons. In addition, the photons will have a change in spectral content due to absorption or scattering. When the photons radiate through the atmosphere, a diffuse or indirect component would occur due to scattering. The final major component which affects solar radiation on Earth's surface is local variations in water vapor contents, pollution and clouds (Honsberg & Bowden, 2018). An overview of atmospheric effects on a typical clear sky situation is given in figure 2-2.

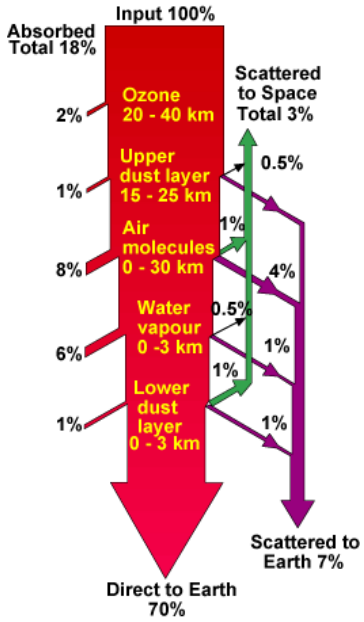

Figure 2-2: Atmospheric effects on Solar radiation (Honsberg & Bowden, 2018)

2.2.1 Air Mass

In addition to atmospheric effects as such absorption, reflection and scattering, the distance the photons travel through the atmosphere affects solar intensity on earth. Air Mass (AM) is the distance the photons travel through the atmosphere normalized to the shortest distance where the sun is directly overhead (Honsberg & Bowden, 2019). Air mass is defined as

$$AM = \frac{1}{\cos(\theta)} \tag{2.2}$$

,where θ is the zenith angle and represent the angle away from vertical. The bigger θ is, the smaller is AM. Therefore, AM represent the reduction of power of light which reach the earth surface with respect to angle. If AM=1, then power of light is only dependent of other atmospheric effects.

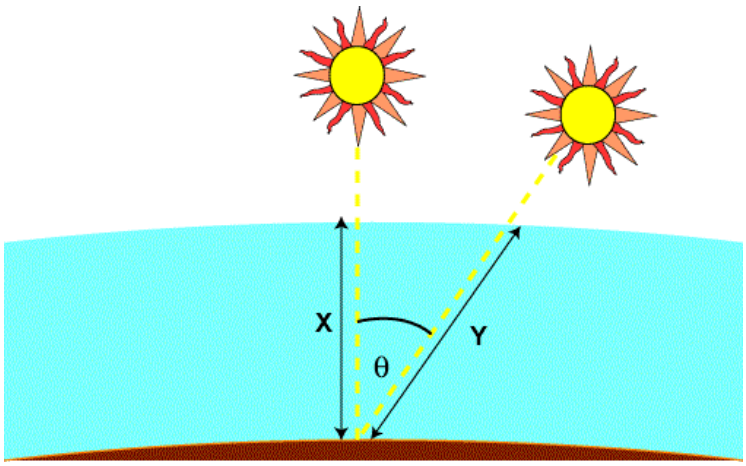

Figure 2-3: Air Mass effect of solar radiation on surface, where θ represent the angle away from vertical (Honsberg & Bowden, 2019).

However, equation (2.2) assumes that the Earth's surface is a flat horizontal layer and is also non-physical at high degrees because of an infinite AM when the sun's angle is 90° at sunrise. Therefore, the curvature of the earth must be considered. Equation 2.3 incorporates Earth's curvature (Honsberg & Bowden, 2019)

$$AM = \frac{1}{\cos(\theta) + 0.50572(96.0799 - \theta)^{-1.6364}} \tag{2.3}$$

Equation (2.3) gives AM at sunrise

$$AM(90°) = \frac{1}{\cos(90) + 0.50572(96.0799 - 90)^{-1.6364}} = 37.9 \tag{2.4}$$

Based on atmospheric effects as scattering, absorption, reflection, change in spectral contents, local variations and AM, it is possible to calculate a value of the direct component of solar intensity on Earth surface. The intensity of sunlight at sea level could be calculated as a function of air mass from an experimentally determined equation with good accuracy

$$I_D = 1.353 \cdot 0.7^{AM^{0.678}} \tag{2.5}$$

Where I_D is the sunlight intensity on a flat disk perpendicular to the sun in $\mathrm{kW/m^2}$. The number 0.7 arises from approximately 70% of the incident radiation is transmitted through the atmosphere. The factor 0.678 is an empirical term which should fit observed data that also takes non-uniformities in atmospheric layers into account. It is important to notice that these constants could be slightly different for calculations above the polar circle, as the sun has lower angle compared to typical conditions at lower latitudes. The constant value of 1.353 is the solar constant given in $\mathrm{kW/m^2}$ (Honsberg & Bowden, 2019).

To achieve an even more accurate value for solar intensity, height above sea level is an important factor as the solar intensity increases with height. With height considered, the direct sunlight intensity I_D could be written as

$$I_D = 1.353 \cdot \left[(1 - ah)0.7^{AM^{0.678}} + ah\right] \tag{2.6}$$

Where a = 0.14 is an empirical constant and h is height above sea level given in kilometers (Honsberg & Bowden, 2019). In addition to direct radiation from the sun, the diffuse radiation is about 10% of the direct component on a clear day (Honsberg & Bowden, 2019). The total global irradiance on a solar module on a clear day could therefore be calculated as

$$I_G = 1.1 \cdot I_D \tag{2.7}$$

This derivation assumes typical atmospherically conditions with given empirical terms and could varies at high latitudes in the Arctic regions where AM is different due to different angle between sun and surface.

2.3 Photovoltaics

Photovoltaics (PV) is the conversion of sunlight directly into electricity by using solar cells (Honsberg & Bowden, 2019). The first PV devices were demonstrated in the 1950s and later used for satellite applications in space. In the beginning, PV's was very expensive to produce and have a low efficiency. In recent years, PV's has lower cost and ever increased efficiency and is the fastest growing energy resource in the world with an investment increase of 16% in 2017 compared to 2016 (Berke, 2018) .

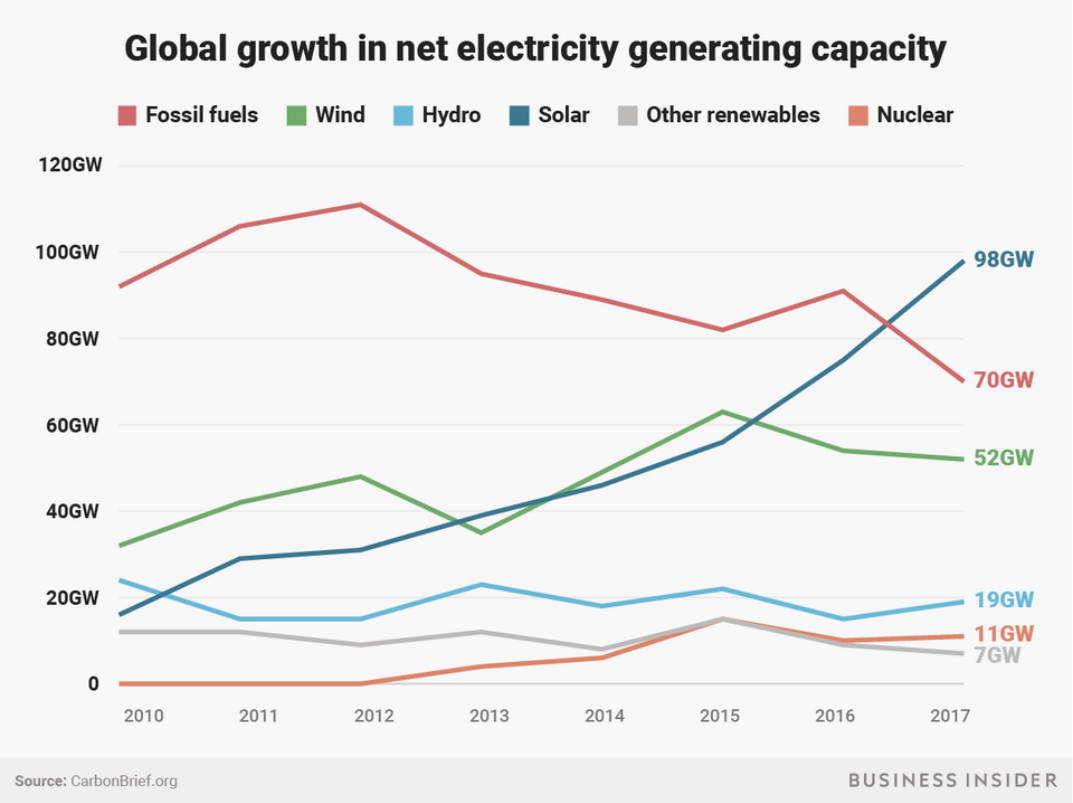

Figure 2-4: Global growth in net electricity generation capacity (Berke, 2018)

2.3.1 Physics of PV

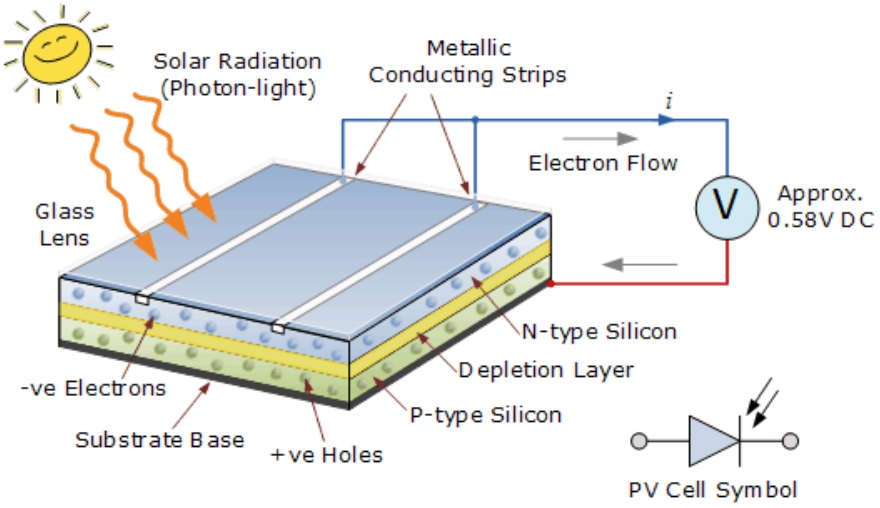

Figure 2-5: Schematic overview of PV cell construction (Alternative Energy Tutorials, 2019)

As the name photovoltaic implies, "photo" means light and "voltaic" represent electricity. When photons with an intensity of global irradiance I_G hits the surface of solar cell, photons are reflected, absorbed or transmitted. The portion of absorbed photons depends on albedo and band gap of a semiconductor material. The albedo gives fraction of radiation that is reflected and is dependent on the properties of the material. Materials with dark surfaces has low albedo and high absorption. Band gap is the minimum amount of energy which is required for an electron to break free of its bound state and get into a free state where it can participate in conduction, which makes it possible to transfer internal energy inside the semiconductor material (Honsberg & Bowden, 2019). Photons with equal or higher energy than band gap will be absorbed, while lower energy photons will weakly interact and gets transmitted through the material (Honsberg & Bowden, 2019).

When a photon gets absorbed, its energy is transferred into a semiconductor material. A semiconductor is a material where the individual atoms are bonded together in a regular, periodic structure where each atom is surrounded by eight electrons (Bowden & Honsberg, 2019). Silicon (Si) is a semiconductor material and the most common material used in solar cell because of low cost and good efficiency. The energy which gets absorbed into the semiconductor material is transferred to an electron surrounding the atom (Seale, 2016). If enough energy is transferred, the electron escapes from its normal position and leaves a hole

behind. The electron is negatively charged, while the hole (empty space where the electron used to be) is positively charged. A photon with enough energy could normally free exactly one electron- hole pair. The electron- hole pair is free to move and could be current carriers under influence of energy from photons (Seale, 2016).

The simplest solar cell has three layers. A top junction made of N- type semiconductors, the depletion region and P- type semiconductor. N- type represent Negatively charged semiconductor composed mostly of negatively charged electrons. This type semiconductor has been doped with certain impurity atoms which is negatively charged and is called donors (Andrews & Jelley, 2013). The depletion region is the absorber layer where interaction between electron and holes occurs. P- type represent the Positively charged layer which compose mostly of positive holes. This type has been doped with impurity atoms which is positively charged and is called acceptors. In the depletion region, a junction between positive layer and the negative layer occurs and is called P-N junction. Inside the P-N junction, an electric field is created. This electric field released by light absorption provides the voltage needed to force the electrons and holes in a certain direction. If we provide an external current path, the electrons will flow through this path from N- side to P- side to interact with holes to provide current (Seale, 2016). Current from flow of electrons and voltage from electric field provides power production from solar cell as power is given as the product of voltage and current

$$P = VI \tag{2.8}$$

Where P represent power from the product of voltage V and current I. To make use of the produced electric current inside solar cell, metallic contact layers are put on top and bottom to allow the electric current to flow in and out of the solar cell. In addition, solar cells are often covered with antireflective coatings to reduce losses from reflection. When installed out in the real world, the cells are often covered with materials which protects from external factors as snow, ice or dust (Seale, 2016).

2.3.2 Effect of temperature

This master thesis is written in Tromsø, which is in an Arctic region with low temperatures. Therefore, it is important to consider temperature effects on production from solar cells. The results in this section will show that solar cells have higher efficiency at low temperatures compared to high temperatures.

Solar cells as a semiconductor device are sensitive to temperature. If the temperature increases, the band gap of the semiconductor reduces. With decreased band gap, the energy of the electrons inside the material increases. Therefore, lower energy is provided to break the bond. In a bond model of a semiconductor band gap, reduction in bond energy reduces the band gap, which provides reduction in band gap with increased temperature (Honsberg & Bowden, 2019).

There are many factors in a solar cell which is affected by a change in temperature. The most significant factor is the open-circuit voltage. The increasing temperature effect for the open-circuit voltage is shown in the figure below

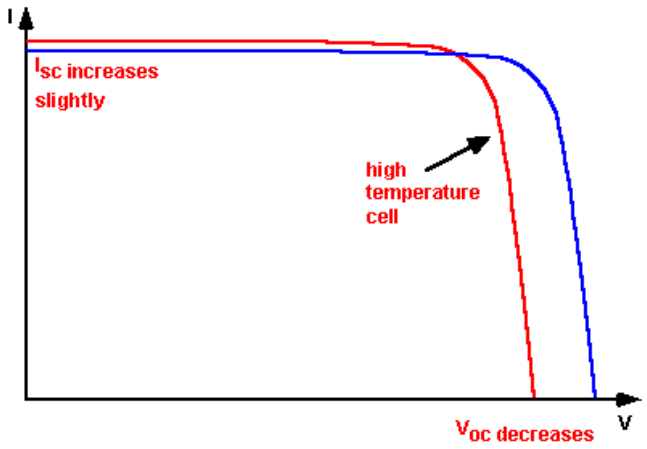

Figure 2-6 Effect of temperature on IV properties on a typical solar cell (Honsberg & Bowden, 2019)

Where I_{SC} and V_{OC} represent short- circuit current and open- circuit voltage respectively. The open circuit voltage decreases with temperature because of temperature dependence of the saturation current I_0

$$I_0 = qA\frac{Dn_i^2}{LN_D} \tag{2.9}$$

This equation measures the current from one side of a P- N junction. The different parameters in equation (2.9) are

q = electronic charge constant
A = Area
D = Diffusivity parameter. Measures the diffusivity of the minority carrier for silicon as a function of doping
L = Minority carrier diffusion length
N_D = Doping
n_i = Intrinsic carrier concentration

Many of these parameters have temperature dependency, but the most significant parameter is the intrinsic carrier concentration (Honsberg & Bowden, 2019). The intrinsic carrier concentration is a measure of number of electrons and holes which participates in transfer of internal energy (conduction). This parameter depends on band gap and the carrier's energy as

$$n_i^2 = 4\left(\frac{2\pi kT}{h^2}\right)^3 (m_e m_h)^{\frac{3}{2}} \exp\left(-\frac{E_{GO}}{kT}\right) = BT^3 \exp\left(-\frac{E_{GO}}{kT}\right) \tag{2.10}$$

Where the parameters represent

T = Temperature
h & k = Planck's constant & Boltzmann constant
m_e & m_h = Masses for electrons and holes
E_{GO} = Band gap energy
B= Constant independent of temperature

Now we can substitute equation (2.10) into (2.9) to get an expression for I_0

$$I_0 = qA\frac{D}{LN_D}BT^3 \exp\left(-\frac{E_{GO}}{kT}\right) \approx B'T^\gamma \exp\left(-\frac{E_{GO}}{kT}\right) \tag{2.11}$$

In equation (2.11) we impose a constant γ to make the temperature dependence for I_0 useful for other materials and set $B = B'$ to distinguish the approximation in (2.11). To further investigate temperature dependence of V_{OC}, we use the expression for the saturation current.

$$V_{OC} = \frac{kT}{q}\ln\left(\frac{I_{SC}}{I_0}\right) = \frac{kT}{q}\ln I_{SC} - \frac{kT}{q}\ln\left[B'T^\gamma\, exp\left(-\frac{qV_{GO}}{kT}\right)\right]$$
$$= \frac{kT}{q}\left(\ln I_{SC} - \ln B' - \gamma \ln T + \frac{qV_{GO}}{kT}\right) \tag{2.12}$$

Where $E_{GO} = qV_{GO}$. Further we assume that the derivative of the open circuit voltage does not depend on the derivative of the short circuit current. This gives expression for circuit voltage

$$\frac{dV_{OC}}{dT} = \frac{V_{OC} - V_{GO}}{T} - \gamma\frac{k}{q} \tag{2.13}$$

Equation (2.13) shows that the temperature sensitivity for a solar cell is dependent on open circuit voltage and band gap, where higher voltage gives less temperature sensitivity. By using typical values for silicon (Honsberg & Bowden, 2019), the decrease in open circuit voltage as a function of temperature is

$$\frac{dV_{OC}}{dT} \approx -2.2\text{mV per °C} \tag{2.14}$$

The increase in short- circuit current for silicon is

$$\frac{1}{I_{SC}}\frac{dI_{SC}}{dT} \approx 0.0006 \text{ per °C} \tag{2.15}$$

Now, to find the temperature dependence for maximum power output for a solar cell, we need to introduce the Fill Factor (FF), a parameter which determines the maximum power output from a solar cell (Honsberg & Bowden, 2019).

FF is defined as the ratio of the maximum power output ($P_{MP} = I_{MP} \cdot V_{MP}$) to the short circuit current and open circuit current for a solar cell

$$FF = \frac{I_{mp}V_{mp}}{I_{SC}V_{OC}} \tag{2.16}$$

With some algebra, FF could be expressed as

$$\frac{1}{FF}\frac{dFF}{dT} = \left(\frac{1}{V_{OC}}\frac{dV_{OC}}{dT} - \frac{1}{T}\right) \approx -0.0015 \text{ per } ℃ \tag{2.17}$$

Finally, the temperature effect for maximum power output P_m can be calculated as the sum of open circuit voltage, short- circuit current and FF

$$P_m = \frac{1}{P_M}\frac{dP_M}{dT} = \frac{1}{V_{OC}}\frac{dV_{OC}}{dT} + \frac{1}{FF}\frac{dFF}{dT} + \frac{1}{I_{SC}}\frac{dI_{SC}}{dT} \approx -(0.005)\text{W per } ℃ \tag{2.18}$$

The results of these calculations show that the maximum power output decreases with approximately 0.005 W or 0.5% per degree Celsius, giving that solar cells have higher efficiency in colder conditions. This gives that a solar cell in cold climate conditions at 0 ℃ will have 10% higher efficiency than a solar cell in warmer climate of 20 ℃.

2.4 Geographical Information System

To map the solar irradiation potential for PV systems on Tromsøya, Geographical Information System (GIS) software is used. GIS is a system for collecting, analyzing and administrating geographical and spatial data. GIS analyses layers of information into visualizations by using maps and 3D scenes, giving deep insight to data rooted in the science of geography. In the past two decades GIS has increased significantly and has become an important part of IT-infrastructure. Today GIS is widely used in many industries, spread from agriculture assessment to space technology and environmental monitoring.

2.4.1 Retrieving Data

Receiving geographical data is either recorded by low altitude aircraft in the atmosphere, or satellites in space. There are two different kind of sensors used for receiving data, passive or active sensors such as LiDAR.

Active sensors have its own source of light and sends a pulse (small packet of electromagnetic energy) towards the surface. The reflected wave gets measured, giving information about the surface under the sensor. Passive sensors measure reflected sunlight and measure the sun's energy when it radiates on Earth's surface (GISgeography, 2018).

(a) (b)

Figure 2-7: Example of (a) Passive sensor which measure reflected solar irradiation. (b) Active sensor which sends his own wave towards earth surface, the wave gets reflected on the surface towards a building and gets reflected to sensor again (GISgeography, 2018)

Depending on surface, the active sensor has the capability of distinguish the surface based on different properties, giving information about how the surface varies with respect to buildings, terrain, water etc.

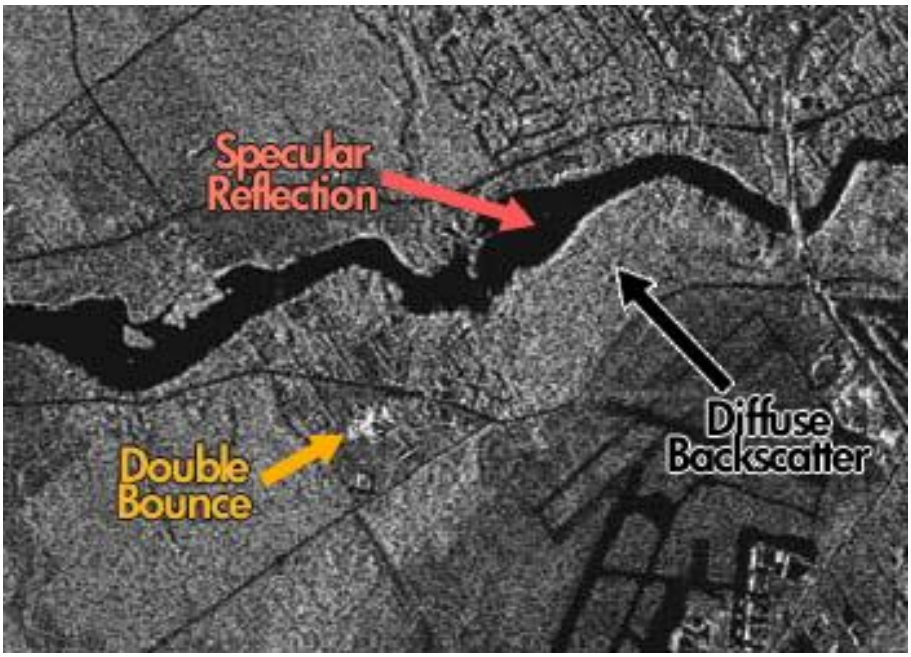

Figure 2-8: Radar image example of a surface with double bounce, specular reflection and diffuse backscatter (GISgeography, 2018)

This radar picture shows the difference in surface properties, the specular reflection gives dark spots which indicates smooth surfaces which in this picture represent a river. The double bounce is visualized with lighter surfaces which could represent urban areas with buildings as in figure 2.7 (b) (wave bounces from surface to building and back to sensor). The Diffuse Backscatter represent rough surfaces as vegetation and agriculture (GISgeography, 2018). In this thesis, LIDAR data which is an active sensor will be used, and the resulting visualizations will clearly show the differences in urban areas, vegetations and smooth surfaces based on radiation properties.

2.4.2 Universal Transverse Mercator (UTM) Projection

When data is retrieved, it needs to be projected to be successfully utilized by GIS software. The projection method is based on the ellipsoid form of the globe. The globe is divided into sixty equal zones where each zone is flattened out. UTM is one of the most common used map projections today and is widely used in GIS. Each UTM zone is 6°, giving 60 UTM zones all over the globe. The Transverse expression is derived as the Mercator uses an upright cylinder for map projection, where the Transverse Mercator takes a cylinder and places it on its side. This method must be done for each UTM zone. See figure 2.9 for UTM zones and cylinder method (GISgeography, 2018)

(a) (b)

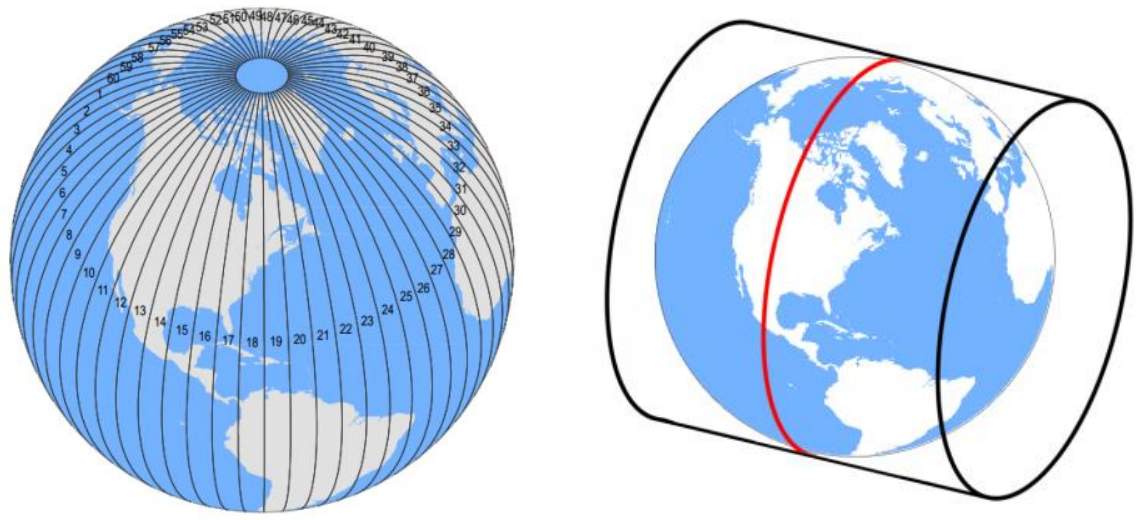

Figure 2-9: (a) UTM zones around the globe (b) Transverse cylinder method (GISgeography, 2018)

This secant cylinder intersects the earth along two small circles parallel to central meridian, giving constant scale along north- south direction, but the scale varies in east- west directions. In addition, two circles are added 180 kilometers east and west of the central meridian with a scale factor of 1, giving 100 meters in the ellipsoid would be the same on the map projection. The central meridian line has a scale factor of 0.9996, giving 100 meters on an ellipsoid would be equal to 99.96 meters on a map (GISgeography, 2018).

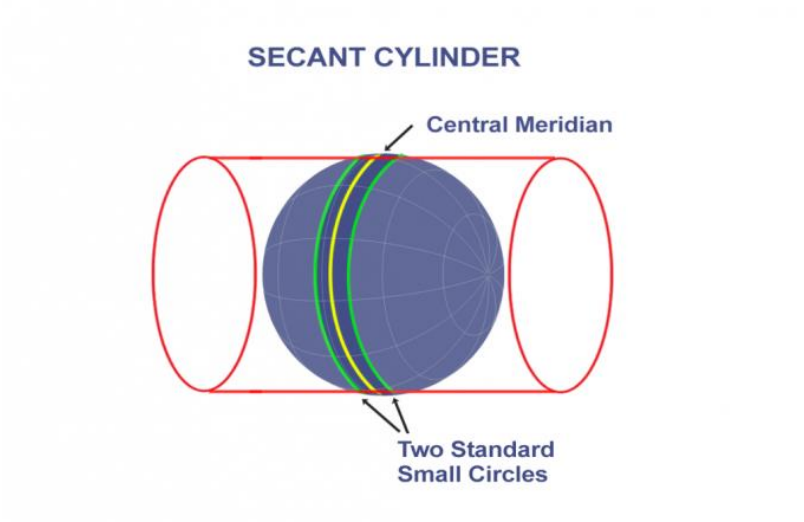

Figure 2-10: Transverse method with added circles in east- west directions (GISgeography, 2018)

In this thesis, the projection methods will not affect the results significantly as the working area will be very small compared to the globe.

2.4.3 Elevation Models in GIS

When data is retrieved and projected into a GIS software, there are two main structures for storing GIS data. i.e. vector and raster. A raster layer consists of pixels organized in matrix form, where each pixel contains information such as temperature, radiation, elevation, buildings etc. The pixel cell must be small enough to capture the surface details, but it should not be too small as it could affect analysis and computer storage efficiency (Esri, 2016).

Vector data consist of points, lines and polygons. The vector points are X-Y coordinates in latitude- longitude directions. Points is often used to display cities and other features which is too small to be represented as polygons. Vector lines represent the connections between vector points and is often used to show features which are linear. Examples of vector lines could be roads and rivers. Finally, to get a complete vector layer polygon connect the vector points and lines. The area inside the closed path gives polygons which is often used to represent city areas, building footprints, agricultural field etc. (GISgeography, 2018)

(a) (b)

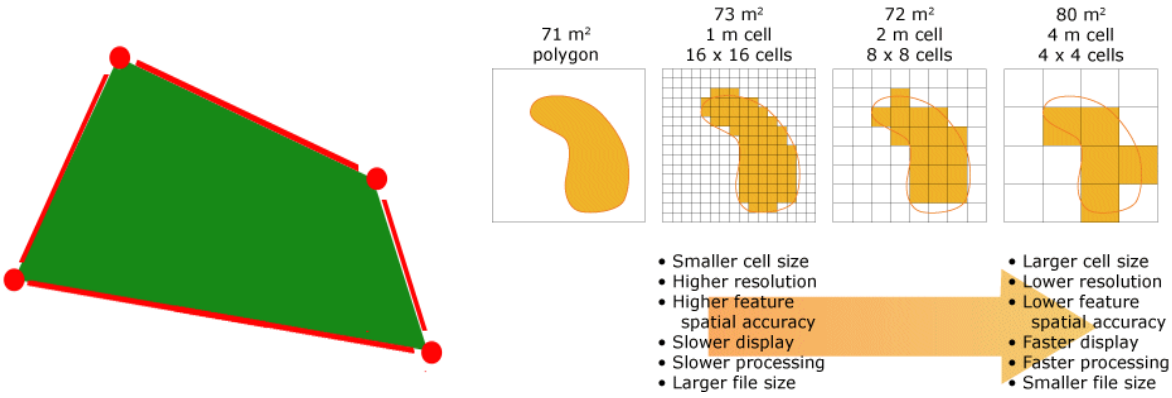

Figure 2-11: (a) Vector layer consisting of red dots and connecting lines in a closed path giving polygon area in green. (b) Raster data in matrix form where each pixel has information about feature. Smaller cells give higher accuracy, but longer computing time (Esri, 2016), (GISgeography, 2018).

When a vector or raster layer contain information about elevation, it is referred as “Digital Elevation Model” (DEM). DEM is a general term which involving “Digital Terrain Model” (DTM) and “Digital Surface Model” (DSM), where DTM represent surface with only terrain and DSM contains both terrain and objects like buildings. For example, a DTM layer would show Tromsøya without any buildings, roads and other types of objects and vegetation, but the DSM layer includes all objects on Tromsøya in addition to bare surface. In this study, DSM will be widely used to calculate and investigate solar irradiation at rooftops on Tromsøya.

(a) (b)

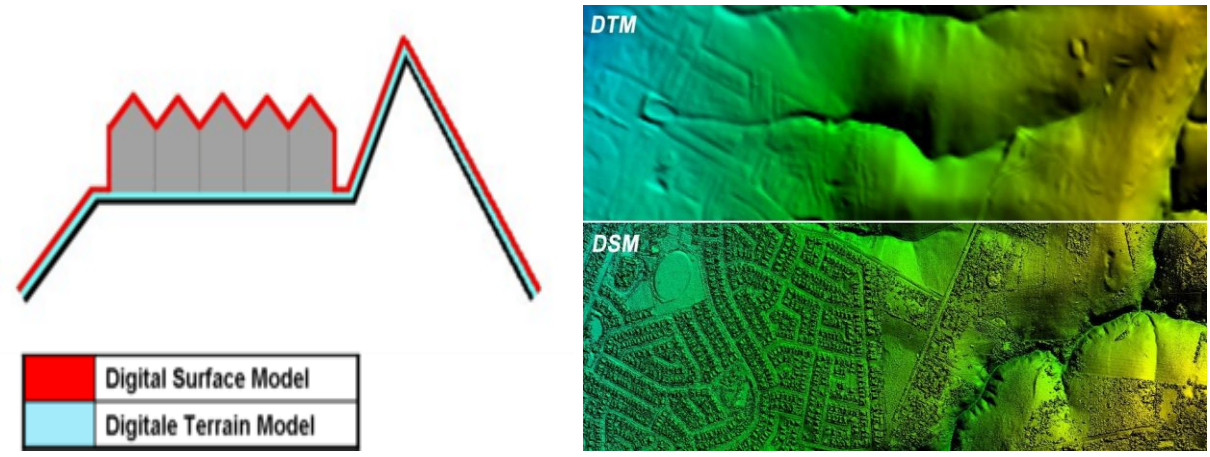

Figure 2-12: Difference between DSM and DTM (a) Schematic horizontal view (b) Vertical view in map (Singh, 2016)

InSAR

To capture elevation surface, some common remote sensing methods are used. Interferometry Synthetic Aperture (InSAR) is an active remote sensing technique which acquires images of the earth and is a powerful technology for modelling surface deformation and elevation mapping. Synthetic Aperture Radar (SAR) acquires images of the Earth in the microwave spectrum with long wavelengths (Milliano, 2016). Waves in this spectrum can penetrate clouds, making SAR sensitive for all weather types and gives good information to the user in many applications. SAR instrument are usually mounted on airplanes, space satellites and terrestrial platforms (Milliano, 2016).

The SAR satellites orbits the Earth at an altitude of 500-800 km and returning to each location on Earth after a specific period. The time between two returning's (repeat cycle) depends on the satellite orbit and vary normally between days to approximately one month. Limitations in orbit control could cause the satellite would not be in an exact same position again after one repeat cycle. The distance between these two spots perpendicular to the satellite viewing direction is known as a "perpendicular baseline". In InSAR acquiring method, this distance causes a 3D effect (Milliano, 2016). These satellites emit radar waves and measures the amplitude and phase of the reflected wave for each pixel in the image. The information from the phase could be very precisely measured and forms the basis for radar interferometry. The simplest form of InSAR combines two SAR images of the same scene into an interferogram where the difference in phase is computed. The resulting interferogram is often displayed in color based on differences in phase, resulting in a colorful image (Milliano, 2016).

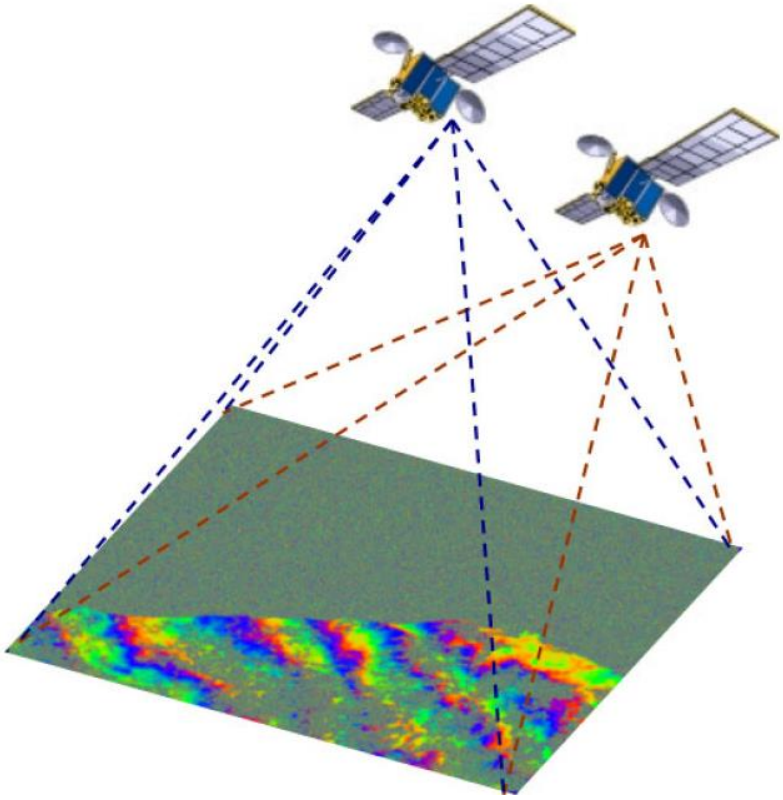

Figure 2-13: InSAR interferogram produces DEM via calculation of phase difference between reflected waves (Tarikhi, 2019)

Photogrammetry

In photogrammetry, photographs or remote data from at least two different points are measured. The basic principles of photogrammetry are like our own vision as we can see depth and perspective as we could vision from separate angles simultaneously. This allows a possibility of calculating distance by trigonometry. The two photos could be two successive, overlapping frames taken during a flight with airplane/satellite, or it could be two photos taken with days and month apart provided steady conditions for land surface. The produced output data is resulting points and contour polylines (The University of Southampton, 2018).

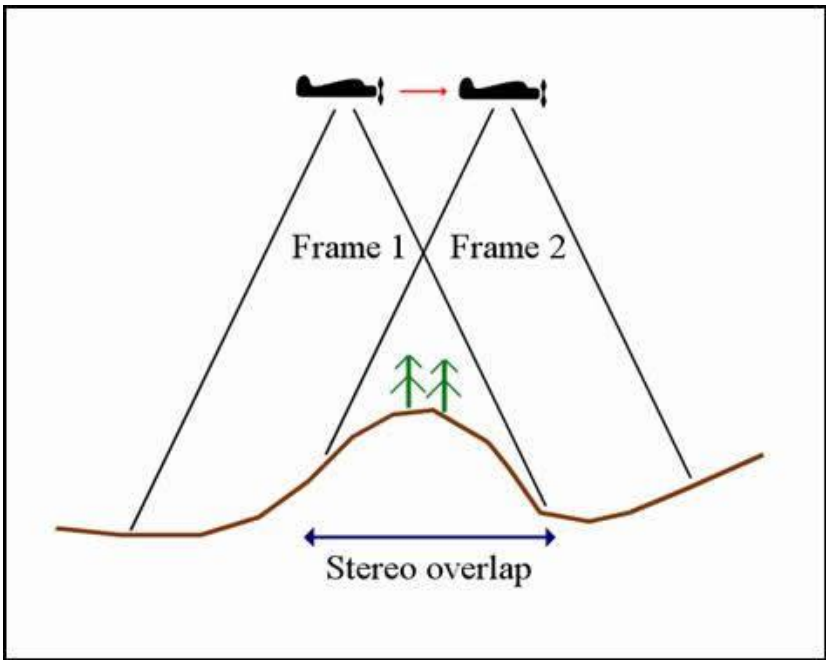

Figure 2-14: Photogrammetry where two photos are taken from different angles (The University of Southampton, 2018)

Inside the area “Stereo overlap”, surface heights are calculated relative to one another, giving an elevation model. The calculated surface height could be referenced to a standard baseline height as mean sea level, giving all measured elevations are relative to the mean sea level height (The University of Southampton, 2018).

LiDAR

The final common remote sensing method which will be considered in this thesis is Light detection and ranging (LiDAR). LiDAR remote sensing will be the main information used for GIS applications in this thesis. LiDAR uses laser light to sample the surface with high density, giving measurements in (x,y,z)- directions with high accuracy. LiDAR is primarily used in airborne mapping applications and is a cost-effective method compared to photogrammetry (Esri, 2016). The LiDAR system hardware components consist of transport equipment as aircraft or helicopter, laser scanner, Global Positioning System (GPS) and Inertial Navigation System (INS) (Esri, 2016). Lidar is an active remote sensor (see figure 2.-7) which sends laser light towards surface and measure the reflected light by receivers in the lidar sensor. These receivers record the time from light was sent towards the surface and returns to the sensor. This recording will measure distance between sensor and surface, in addition will information from GPS and INS give measurements about actual three-dimensional points of the reflected surface. After recording, processing of the collected LiDAR data would give highly accurate (x,y,z)- coordinates by analyzing laser time range, laser scan angle, GPS position, and INS information (Esri, 2016).

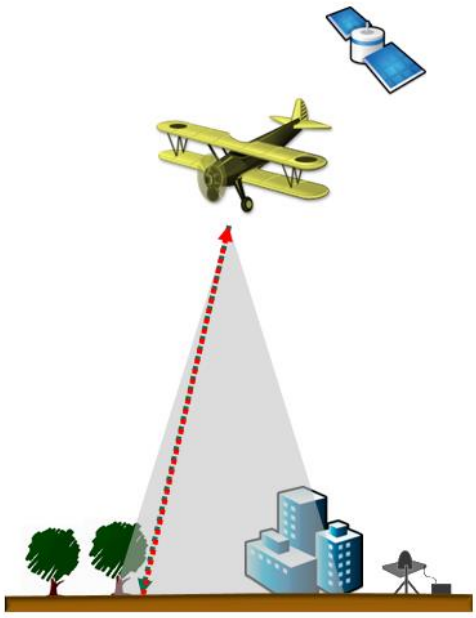

Figure 2-15: LiDAR remote sensing, LiDAR instrument sends a laser pulse towards surface and measures the reflected pulse (Esri, 2016).

The laser pulses are sensitive for object on and above ground surface as vegetation, buildings, roads, giving highly realistic and accurate surface models. The emitted laser pulse can be reflected to sensor in many ways. When the pulse is hitting the surface, it could hit multiple other objects before returning to sensor, giving information about how the surface looks like (Esri, 2016). The first returned laser pulse is the most significant return and is associated with the highest point in the landscape, as a mountain top, rooftops or surface if no higher object is in the area. If the sensor receives multiple returns, it can detect elevation of several objects within the laser footprint of an outgoing laser pulse. The intermediate returns to sensor are associated with vegetation structure, and the last return is for bare- earth terrain models. However, the last return will not always be from a ground return. When a pulse hits a big tree, the pulse will not be able to completely reach the ground. Therefore, this pulse will only contain information about the shape of the tree (Esri, 2016).

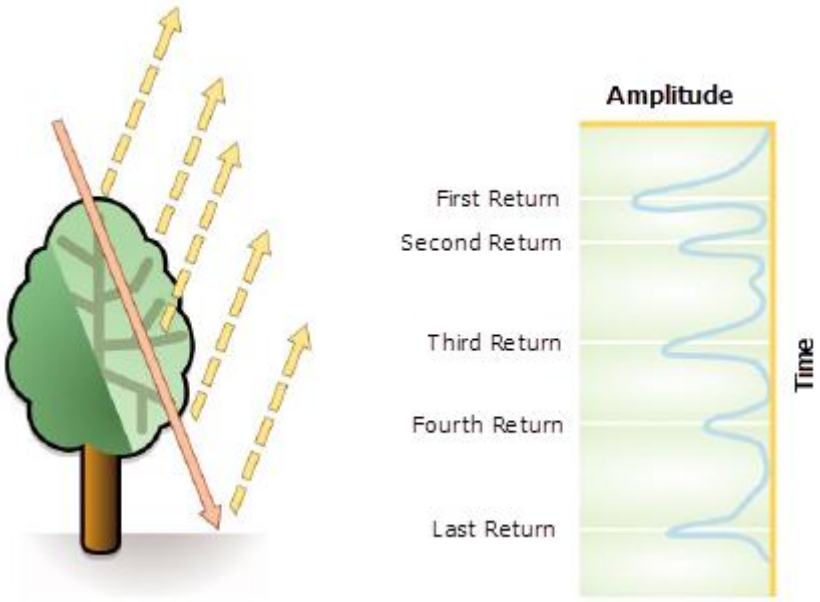

Figure 2-16: LiDAR pulse reaching tree, giving information about shape and high of the tree for the elevation model (Esri, 2016).

In addition to elevation and position values in (x,y,z)- direction, several more information is provided for recorded laser pulse at each lidar point. Intensity, return number, number of returns, point classification values, points at the edge of flight line, red, green and blue (RGB) values, GPS time, scan angle and scan direction (Esri, 2016). Detailed explanation for each of these attributes will not be considered in this thesis as it not relevant for further work. After

processing all attributes, the result is known as point cloud data. The initial point clouds include (x,y,z)- directions giving large collections of 3D points in addition to attributes as GPS time stamps. To distinguish between specific surface features, the laser encounters are classified after the initial point cloud is processed after collection. Specific elevations for ground, vegetation, buildings and everything else which the laser pulse hits during its travel, constitute the point cloud data (Esri, 2016).

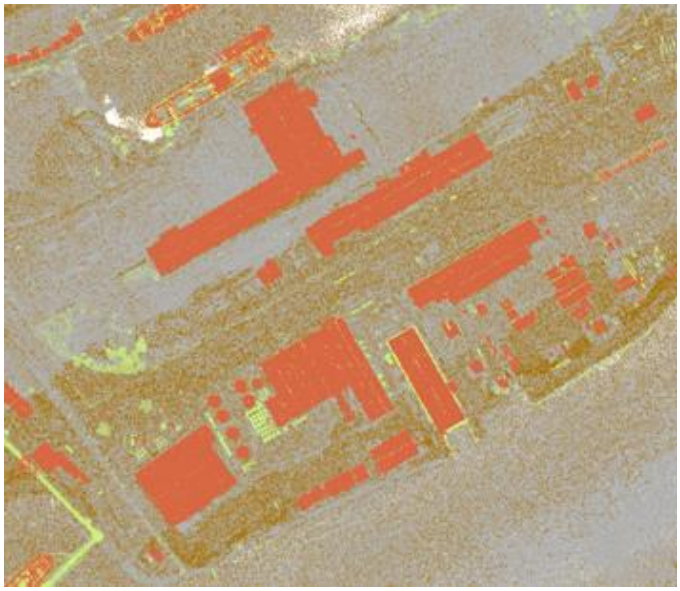

Figure 2-17: DSM produced with LiDAR where buildings are clearly distinguished from other features (Esri, 2016)

To further analyze LiDAR point cloud data in GIS software, it is filtered to produce DEM in vector form or raster formats. With some modifications, both DTM and DSM could be produced from the same LiDAR dataset.

2.5 Pyranometers

To validate the calculated solar irradiation potential on Tromsøya, pyranometers is used as a basis. In the following section, the different types of pyranometers used is briefly explained. In this thesis, three types of pyranometers are used. Two of these types are installed on the roof of Realfagsbygget at the University of Tromsø and one type is installed on Holt.

2.5.1 What is a pyranometer?

A pyranometer is an instrument that measures total solar irradiance that has passed through the atmosphere and reached the surface (Duffie & Beckman, 2013). Total radiation is a sum of diffuse and direct radiation. Direct radiation is unscattered radiation that radiates on a straight line from the sun towards the atmosphere and down to the surface, while diffuse radiation is the radiation which has been scattered by molecules and particles in the atmosphere (ftexploring, 2011). Most of the available solar irradiation data that exists is obtained from pyranometers (Duffie & Beckman, 2013). The detectors in the pyranometers should be able to measure radiation independently of the wavelength in the solar energy spectrum. They should also be able to measure radiation independently of the angle of incidence for the sun, so it can measure direct radiation when the sun is low during the morning and evening (Duffie & Beckman, 2013).There are many different types and models of pyranometers which have different characteristics and benefits according to where the pyranometer should measure radiation. The most common types of pyranometer is the thermopile pyranometer and silicon photocells. In this project, two of the pyranometers is thermopile pyranometers and the third are silicon based.

2.5.2 Thermopile pyranometer

A thermocouples is a sensor that measure temperature and often consists of two different metals (Reotemp, 2011).When the metals are coupled together, a junction between the different metals are created (Reotemp, 2011). When the junction experiences a change in temperature, it will create a voltage. This voltage can then be used to calculate the temperature (Reotemp, 2011). A thermophile is composed of several thermocouples connected in series or in parallel. The working principle for that a thermopile pyranometer could measure radiation, it uses principles of thermoelectric detection (Kipp and Zonen B.V, 2015). The pyranometer consist of a horizontal dark surface with very high absorptance of solar radiation over a wide range of wavelengths (Duffie & Beckman, 2013). When the dark surface is absorbing solar radiation, its temperature increases. This amount of increase in temperature gets measured by thermocouples (Kipp and Zonen B.V, 2015). The amount of temperature change in the thermocouples is a measure of absorbed solar radiation (Duffie & Beckman, 2013).

A typical pyranometer has thermocouples connected in series or series- parallel which makes a thermopile (Kipp and Zonen B.V, 2015). The heated dark surface which receives solar radiation is the active junction of the thermopile, while the passive junction is in thermal contact with the pyranometer housing (Kipp and Zonen B.V, 2015). See schematic figure below for an overview of a typical thermopile pyranometer with hemispherical glass to cover the thermopile with underlying housing.

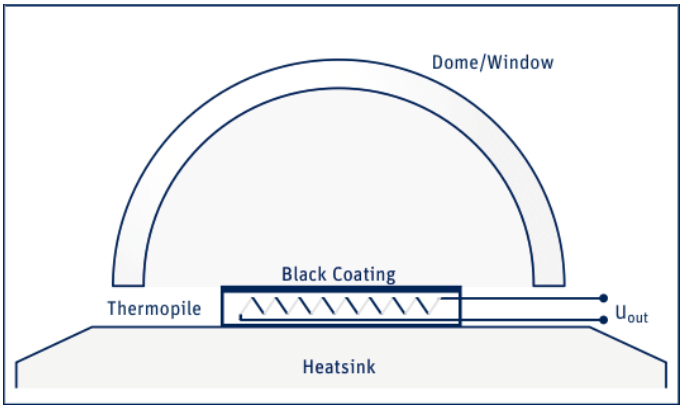

Figure 2-18:Schematic overview of a typical thermopile pyranometer (Kipp and Zonen B.V, 2015)

2.5.3 Silicon Photocells Pyranometer

Silicon photocell pyranometers produces output current similar to how a solar cell panel converts the sun's energy into electricity. (Hinckley, 2017). When the current passes through a shunt resistor, it is converted to a voltage signal with sensitivity of microvolt per watt per square meter (Hinckley, 2017). The silicon pyranometer unlike the thermopile pyranometer, is covered with a plastic diffuser to provide a uniform cosine response at varying sun angles. The silicon pyranometer has a limited spectral response compared to thermopile pyranometers. The thermopile pyranometers could measure the sun's radiation in wavelengths from 0.15 to 4.0 μm, while the silicon pyranometer could only measure the sun's radiation in wavelengths from 0.4 to 1.1 μm. To limit the measurement errors, the silicon pyranometer is calibrated to provide an output like thermopile sensors under clear sky, but this leads to greater measurement errors on a cloudy day. However, silicon pyranometer is often used instead of thermopile pyranometer as the silicon pyranometer is several times cheaper than the thermopile pyranometer (Hinckley, 2017). The typical errors for the silicon pyranometer compared to thermopile pyranometer is about $\pm 3\%$, and is often sufficient for most environmental researches (Hinckley, 2017).

2.5.4 Comparison of thermopile and silicon photocells pyranometers

The following graph shows a comparison between the measured output of a cheap silicon-cell pyranometer, and a more expensive secondary standard thermopile pyranometer. This silicon pyranometer is calibrated to get a correct output under clear sky, which could give measurement errors on a cloudy day. The comparison is done on a clear and a cloudy day to see differences between these two situations (Hinckley, 2017).

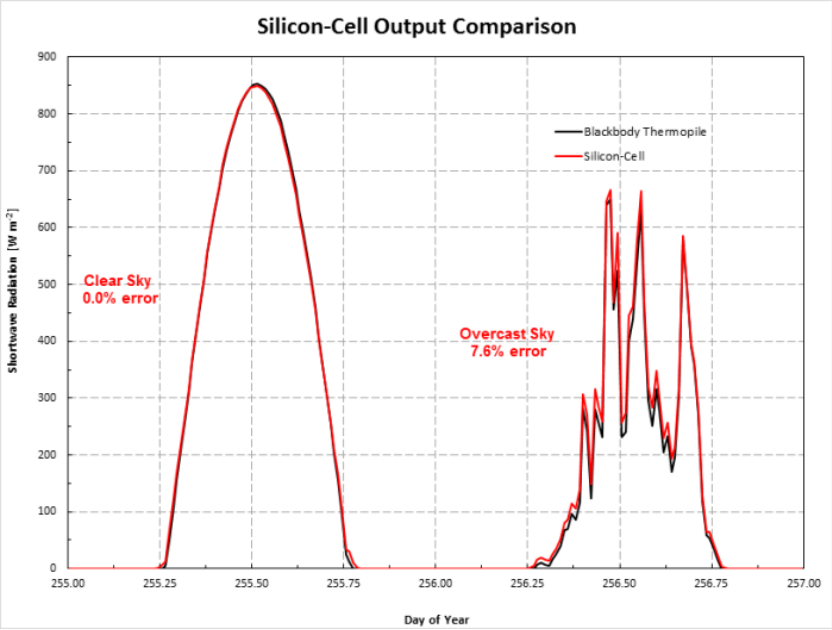

Figure 2-19: Comparison of silicon and thermopile pyranometers under clear and cloudy conditions (Hinckley, 2017)

On a clear day the error is 0.0%, while on a cloudy day the silicon type has an error of 7.6% compared to thermopile pyranometer. For the cloudy day the silicon type tends to measure more solar irradiation than the thermopile. The reason for measurement error when the sky conditions change, is because of the limited spectral response for the silicon pyranometer compared to the thermopile pyranometer, which captures the solar irradiation over a wider wavelength (Hinckley, 2017).

2.5.5 Calibration of pyranometers

For the pyranometer to measure solar irradiation with highest possible accuracy, it has to be calibrated in a correctly. There are several different calibration methods, and the challenge is that some of the methods could give wrong readings after calibration. Therefore, the calibration should have a high-quality standard. The accepted world standards for the calibration of solar radiation measurement instruments is the ISO 9000 standards (Kipp & Zonen, 2018). ISO is the International Organization for Standardization. The ISO 9000 standard is a quality management standard, and the 9000 standards are some of ISO's best-known standards (ISO, u.d.).

One common acceptable calibration method for pyranometers is the ISO 9846 calibration standard. In this method the pyranometer is calibrated against a pyrheliometer (Duffie & Beckman, 2013). A pyrheliometer is an instrument which measures only direct solar radiance at normal incidence (Duffie & Beckman, 2013). A standard method for this calibration is that readings from both the pyranometer and pyrheliometer is taken on a clear day. The readings from the pyranometer should be taken when the pyranometer is both shaded and unshaded, at the same time as readings is taken from the pyrheliometer (Duffie & Beckman, 2013). The calibration constant for the pyranometer is the ratio of difference in output of the shaded and unshaded pyranometer to the output from the pyrheliometer multiplied by the calibration constant of the pyrheliometer and Cos (θ_z), which is the angle of incidence of direct radiation of the horizontal pyranometer (Duffie & Beckman, 2013). We can write this mathematically as

$$\mathrm{C_{pm}} = \frac{\text{Shaded pyranometer} - \text{Unshaded pyranometer}}{\text{Pyrheliometer} * \mathrm{C_{ph}} * \mathrm{Cos}(\theta_z)} \tag{2.19}$$

where $\mathrm{C_{pm}}$ and $\mathrm{C_{ph}}$ are the calibration constants for the pyranometer and pyrheliometer.

The other acceptable ISO standard is ISO 9847. This calibration procedure has two different methods (Kipp & Zonen, 2018). In the first method, the calibration is done outside. Here the test pyranometer is compared to another working standard pyranometer instrument with similar or higher quality. During this calibration it should be clear sky, and the position of sun should be near normal incident on the instrument (Kipp & Zonen, 2018). The second

procedure is done inside in a laboratory. Here the test pyranometer is compared with another working standard pyranometer of same type under a lamp which should be a good approximation for the solar spectrum (Kipp & Zonen, 2018).

2.5.6 Pyranometer models used in thesis

There exist several types of pyranometers which have unique characteristics and benefits for the specific location it is mounted. For example, a pyranometer installed in a desert should have other characteristics than a pyranometer installed in Arctic regions. In the desert, external factors as sand and dust covering the instruments could be a challenge. In Arctic, snow and cold climate is external factors that could affect the pyranometers ability to measure correct values. Troms county is in the Arctic and has cold climate with freezing temperatures and much precipitation of snow during wintertime. This means that a standard pyranometer could easily be covered by ice and snow, which will affect the readings drastically.

2.5.7 University of Tromsø - The Arctic University of Norway (UiT)

There are two types of instruments at the roof of Realfagsbygget at UiT. Digital silicon irradiance sensor from Ingenieurbüro, and thermophile solar radiation sensor 2270 from Anderaa.

The sensor from Anderaa is controlled by the institute for computer science at the university. This sensor is a flexible sensor which have been developed to measure solar and sky radiation under all weather conditions. This pyranometer is a thermopile type with a sensor which employs a high sensitivity thermistor bridge. The sensor measures the temperature rise of the black surface which receives radiation. The highly sensitive thermistor bridge only needs a temperature of $2.2°C$ to obtain a full and correct measurement. Because of this, the instrument does not need double domes (Anderaa Data Instruments AS, 2013).

The sensor from Ingenieurbüro is controlled by the institute for physics and technology at the university. It is a silicon- based sensor which is designed to correspond a PV module, making these sensors ideally suited as a reference for PV systems. The sensor is mounted directly on the PV module and has a corresponding spectral sensitivity with similar incident angle modifier, giving a precise analysis of PV yields by analyzing solar irradiation data.

These instruments have typically uncertainty of 5 $W/m^2 \pm 2.5\%$ for readings (Ingenieurbüro Mencke & Tegtmeyer GmbH , 2019). The instruments on the roof of Realfagsbygget at UiT is not maintained during the year, making the instrument more exposed to covering of from external factors as snow, ice or dust. This could cause lower and inaccurate readings in these situations.

(a) (b)

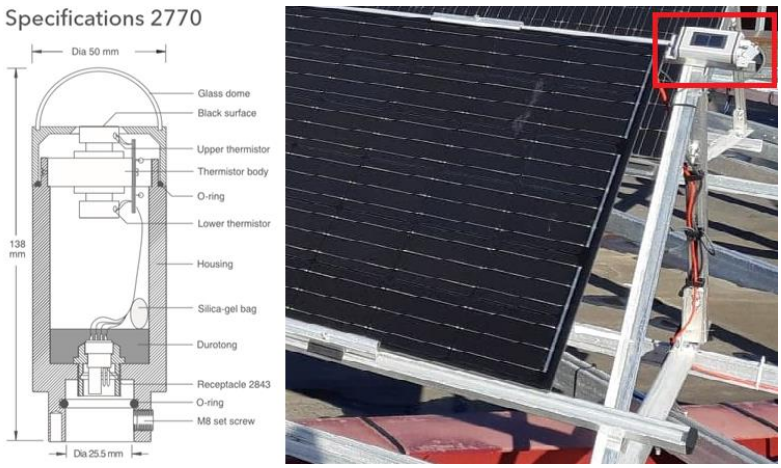

Figure 2-20: (a) Schematic overview for the 2770 instrument from Anderaa (Anderaa Data Instruments AS, 2013). (b) The solar radiation sensor from Ingenieurbüro mounted directly on a 40° PV module (picture by Odin F. Eikeland).

2.5.8 Holt

This pyranometer is installed and operated by NIBIO, a meteorological service driven for collecting meteorological data for alert services and research from the most important agricultural areas in Norway (NIBIO, 2018). They use a CM11 thermopile type pyranometer from Kipp & Zonen. This model has no tilt dependence and can measure solar radiation on inclined surfaces as well as horizontal surfaces. The sensor is maintained daily by employers from NIBIO working on this station, giving good conditions for highly accurate measurements (NIBIO, 2018).

This pyranometer is provided with a thermal detector, where the radiant energy is absorbed by a black disk with high absorption of solar radiation (Kipp & Zonen, 2000). This instrument is calibrated according to the ISO 9847 standard for Kipp & Zonen instruments.

Figure 2-21: Thermophile CM11 Kipp & Zonen pyranometer (Kipp & Zonen, 2000)

3 Method

3.1 Overview

The analysis in this thesis combines mapping of solar potential in the software ArcGIS with estimations of PV energy yield from available roof and façade areas on Tromsø island. The estimated PV energy yield is thereafter combined with the energy demand of harbored Cruise ships in Tromsø to investigate the possibilities of supplying Cruise ships with renewable energy from PV systems. The analysis of PV yield was performed on several scenarios regarding to level of PV integration on roofs and facades. The charging load from Cruise ships is based on statistics from Tromsø Harbor and given information from Port of Kristiansand.

The methodology of mapping solar potential is described in section 3.2. The methodology was applied on Tromsøya in Northern Norway. The solar mapping for the island is performed in the ArcGIS software. The methodology for creating the solar map with 1-meter resolution in ArcGIS is based on similar method as in former master thesis by (Falklev, 2017). When creating the solar map with 0.25-meter resolution, the methodology was far more comprehensive. The methodology of determining solar- architecturally suitable areas on buildings on Tromsø Island is described in section 3.3. The simulation of energy yield from the suitable areas are described in section 3.4. The methodology for estimating energy demand of Cruise ships is described in 3.5. Finally, the Solar fraction (SF) are defined in section 3.6.

3.2 ArcGIS

3.2.1 General Introduction

ArcGIS is developed by the Environmental System Research Institute (Esri), a global market leader in GIS software which delivers a variety of GIS solutions as ArcGIS Enterprise, ArcGIS Online, and ArcGIS pro (Esri, 2019). ArcGIS pro is Esri's latest professional desktop GIS software. ArcGIS pro make it possible to view, analyze, explore, edit and share maps and data. An ArcGIS pro project can contain many maps and layouts, tables, charts and other items. In addition, 3D capabilities are native to ArcGIS pro and any 2D map can be converted to a 3D scene (Esri, 2019).

Some of the tools used to create the solar map in the thesis are complex, while other are simple intermediate tools. The most important for this thesis is the "Area Solar Radiation" tool which is used for making the final solar map. This tool is a part of Esri's Spatial Analyst Tool. The ArcGIS Spatial Analyst tool provides a broad range of spatial modelling and analysis capabilities. With this tool it is possible to create, query, map, and analyze cell- based raster data. In addition, it is possible to derive new information from existing data (Esri, 2019). In this thesis, solar irradiation is derived from existing LiDAR data. The procedure for making the solar map in ArcGIS is given in table 3-1 as:

Table 3-1: Tool procedure for creating solar map in ArcGIS. Step 1-4 is based on similar methodology as in (Falklev, 2017). Step 5-7 is performed to further develop the solar map to highlight rooftops on Tromsøya

Step	Tool
1	"Make raster layer"
2	"Extract by polygon"
3	"Split raster"
4	**"Area solar radiation"**
5	"Make Feature layer"
6	"Feature to Raster"
7	"Diff"

3.2.2 Surface data

Before it is possible to make any map or perform any analysis in ArcGIS, Digital Surface Model (DSM) data must be retrieved. DSM data for this thesis is retrieved from hoydedata.no. This is a website where LiDAR data is published and are freely available for the user. The method of collecting data from this website is as following: Click on "nedlastning" (to the right of start page), then you choose polygon as method for extraction of wanted area. Then you choose "Høydemodell" as product and "Nasjonal høydemodell" as type before you can choose which dataset you want. It is possible to choose between DTM and DSM with 1, 10- and 50-meters resolution (Kartverket, 2019). In this thesis we want a DSM with 1-meter and 0.25-meter resolution. To find the 0.25-meter resolution dataset, choose "Nasjonal høydemodell" as type, and then it is possible to choose "Prosjekt". Thereafter pick "Troms 8pkt 2014 (0.25 m)". This is will give a DSM with a higher accuracy of 0.25-m resolution. This will affect computing time drastically but gives better solar maps which is shown later in a case study for one house on Tromsøya.

3.2.3 DSM Processing

When the DSM data is received and uploaded, it must be processed before doing calculations. When the surface area over Tromsøya is extracted by polygon and sent from Høydedata, two files are sent. The reason is because Tromsøya is in the middle of two map packages with areas covering Tromsø and surroundings. Computing solar maps for Tromsø and surroundings will be a very computationally intense process with a lot of data processing, therefore this thesis is restricted to only include Tromsø island. Before extracting Tromsø island, the two files sent from Høydedata must be merged into one single file. In ArcGIS Pro this is done by using a Data Management Tool which is found on "Analysis/Tools" and thereafter search for the "Mosaic to new Raster" tool in the Geoprocessing pane. The pane view of this tool is shown in figure 3.1

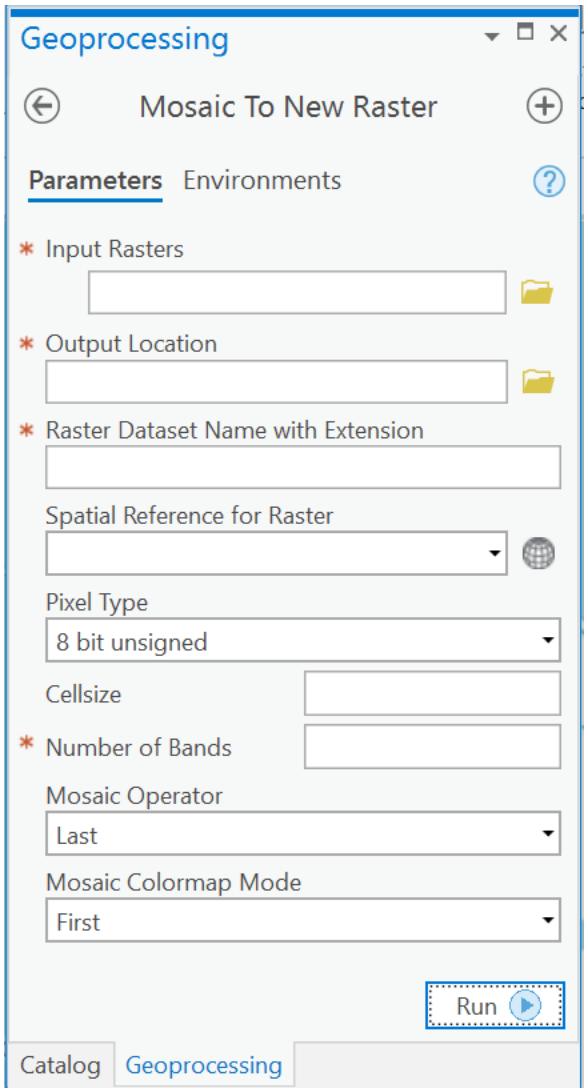

Figure 3-1: The "Mosaic to New Raster tool"

This tool merge raster layers together, and in this case two files are merged which is added into “Input Rasters”. Then you choose where to save the result and give the resulting raster a name with (.tif) extension. The spatial Reference for raster should be UTM-Z33 and pixel type should be 64 to reduce computing time, and for a DSM1 layer the cell size is 1-meter. However, for the high resolution DSM0.25 raster, the cell size for new raster must be 0.25-meter. Number of bands is 1, and the Mosaic operator is not considered in this case as the files does not have overlap. Later in this thesis, the mosaic operator is an important factor when we have overlap between different solar maps. Mosaic Colormap Mode will not affect any results in this thesis.

To extract Tromsø island from the file covering Tromsø with surroundings, the "extraction by polygon" is used. In this tool, coordinates of an area are specified and extracted.

Now it should be possible to calculate the solar map for Tromsø island based on the extracted raster layer covering the whole Island. However, the "Area Solar Radiation" tool is area computing insensitive and calculating solar map for the whole island at one time would be too time procuring (Falklev, 2017). In fact, splitting the island into smaller pieces reduces computing time by more than 5 times (Falklev, 2017). Therefore, the island was divided into 14 pieces by "Split Raster" tool in ArcGIS. This tool works by importing the raster you want to split, specify output location with name before choosing number of tiles as splitting method. This ensures that each region has the same size, giving approximately equal computing time. In addition, an overlap of 250 meter was chosen to make sure that data is not missing at borderline between sections. The raster file ready for computing of solar potential is shown in figure 3.2, where you can see that Tromsø island is the only area of interest, while Tromsdalen and Kvaløya is not a part of the raster file.

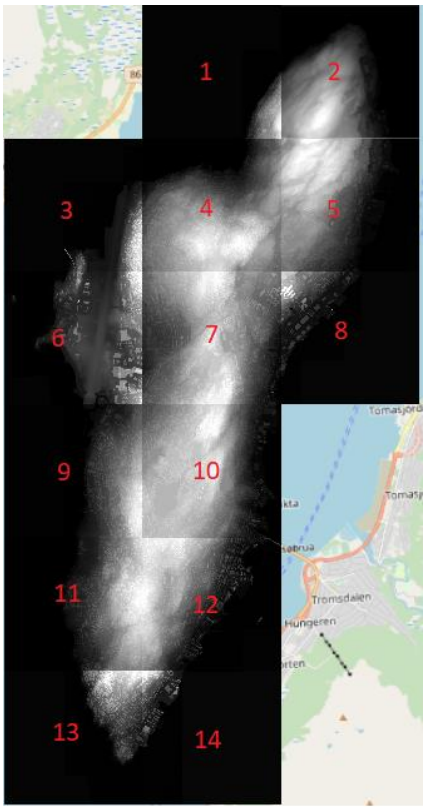

Figure 3-2: Raster file for Tromsø Island split into 14 pieces for LiDAR data with 1-meter resolution

3.2.4 Calculation of solar map

After the raster file is made, it is now possible to calculate solar potential for each region with the “Area Solar Radiation” tool in ArcGIS.

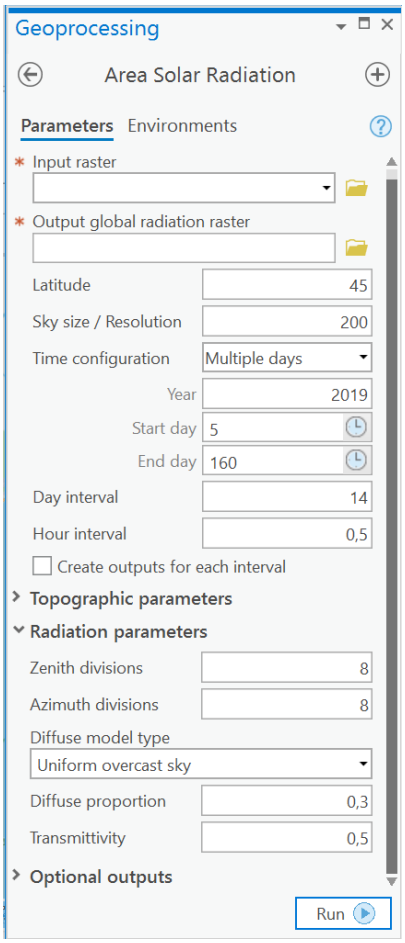

Figure 3-3: The "Area Solar Radiation" Toolbox in ArcGIS Pro

Input raster in this tool is one of the 14 pieces specified in figure 3-3, while output global radiation is the final computed solar radiation raster layer given in $\left[\frac{\mathrm{Wh}}{\mathrm{m}^2}\right]$. The parameters which is important to consider in this tool is the temporal period and radiation parameters like Diffuse proportion and Transmissivity (D&T). Diffuse proportion specify how much of incoming radiation is Diffuse radiation where a value of 1 gives all incoming radiation is diffuse, and 0 gives no diffuse radiation (only direct). Transmissivity represent how much of incoming radiation passes through atmosphere, where 1 gives 100% of incoming radiation passes the atmosphere.

The D&T values varies for each month based on climatology factors and the sun's position. D&T values are usually not available and must be calculated. This is done in former master thesis by (Falklev, 2017), where he has based his calculations on weather data from Holt and the "Points Solar Radiation" tool in ArcGIS. In this thesis, his calculations will not be explained in detail, the important is the resulting D&T values for each month which is given in table 3-2.

Table 3-2: Diffuse and Transmittivity for each month in Tromsø (Falklev, 2017).

Month	Diffuse Proportion (D)	Transmittivity (T)
January	0.9	0.8
February	0.6	0.7
March	0.5	0.6
April	0.4	0.6
May	0.5	0.5
June	0.4	0.5
July	0.6	0.4
August	0.3	0.6
September	0.4	0.6
October	0.5	0.7
November	0.7	0.8
December	X	X

The reason for lack of values in December is due to polar night with low radiation, where the "Point Radiation Tool" in ArcGIS was not able to calculate any D&T values for this month (Falklev, 2017). After plugging in D&T values for specific month, the solar map could be calculated. The resulting output is a raster layer representing the global radiation or total amount of incoming solar irradiation (direct + diffuse) which is calculated for each location of the input surface. The output value is in units of watt hours per square meter [$\mathrm{Wh/m^2}$].

When calculating the solar map, a powerful computer is important. The computer used in this work has the following properties given in table 3-3:

Table 3-3: Information about computer used for calculations

Model	Laptop- GCE5FT43
Processor	Intel(R) CORE™ i5 – 7200 CPU@ 2.50GHz 2.71 GHz
RAM	8.00 GB
Operating system	64- byte

This is not a well-suited computer for heavy computing in ArcGIS, but it works fine for making a solar map for a LiDAR DSM surface with 1-meter resolution. This computer used approximately 45 minutes per month for each of the 14 raster surfaces, giving a total computing time of approximately 115 hours. The processor in the computer has two cores, making it possible to run two calculations at the same time which reduce computing time to approximately 57.5 hours. However, while making the solar map for a DSM surface with 0.25-meter resolution, this computer is not powerful enough to perform calculations in an acceptable time. Therefore, access to a server with high computing capacity is needed when calculating solar map for higher resolution. For this thesis, access to a computer based in Amsterdam via online sky server was given from the University of Tromsø with help from Rolf Andersen, adviser in digital services in science at the University. This computer has 16 virtual cores, making it possible to run maximum 16 calculations in at once. In addition, this computer has the following properties given in table 3-4:

Table 3-4: Information about computer based in Amsterdam

Model	Windows Server 2016 Datacenter
Processor	Intel(R) Xeon® Platinum 8168 CPU @ 2.70 GHz 2.69 GHz
RAM	32.00 GB
Operating system	64- byte

However, issues arise when trying to calculate the solar map for each of the 14 pieces with 0.25- meter resolution. Even with access to the server computer in Amsterdam, the computational requirement goes beyond the hardware specification used, and the ongoing calculations was interrupted. As the “Area solar radiation” tool is area sensitive, the solution was to divide each of the 14 pieces in four, giving 56 pieces in total. Some of the new pieces only include water and were removed, which gives remaining 45 pieces that needed to be calculated separately.

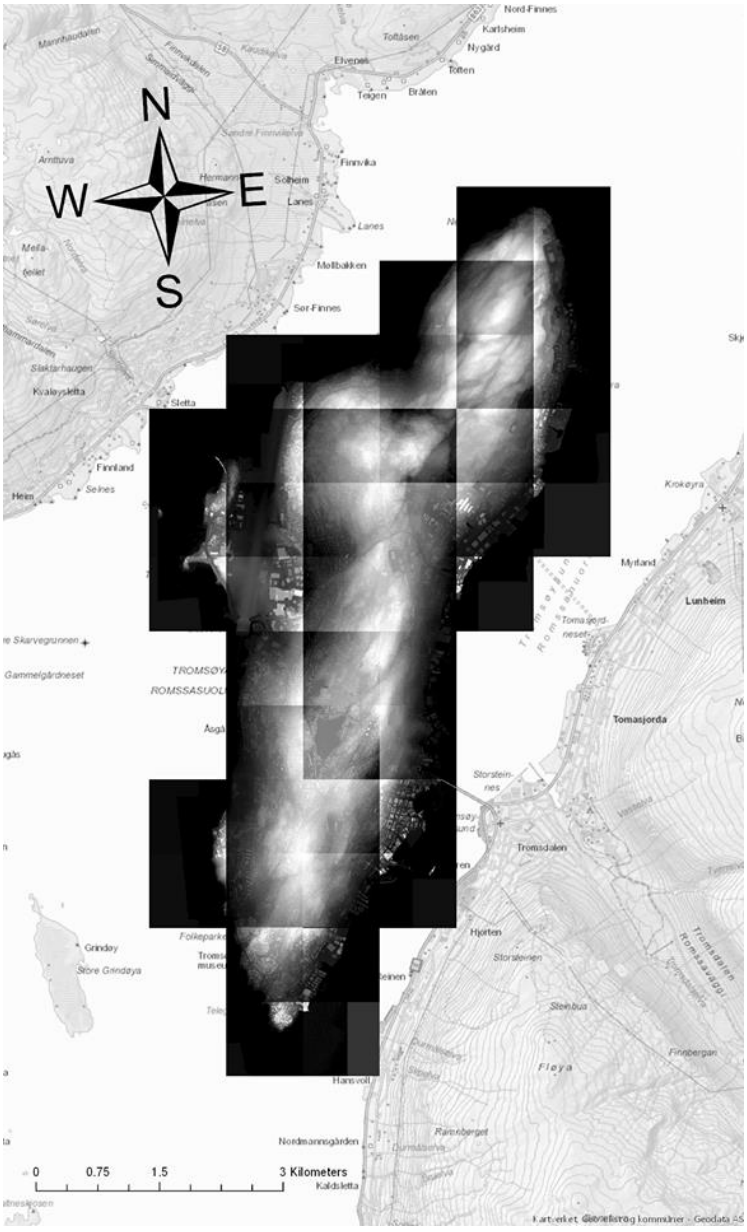

Figure 3-4: Raster layer divided into 45 pieces which all need to be calculated separately for 0.25-meter resolution solar map.

The method for calculating the solar map with 0.25- meter resolution is similar as for 1-meter resolution, but now 15 calculations must be run on the same time (leave one server free). The process would be as following: Start calculation (for example June) on region 1-15. Let the calculation run until finished. Then, start calculation for region 16- 31 before region 32- 45. Then do the same process for next month until finished for all 11 months. This is a very repetitive and time-consuming process but gives a good final solar map. The computer uses approximately 4 hours per section, gives a total computing time of 180 hours for the whole island for one month. As the calculations is run separately for 15 cores, the computing time is reduced to approximately 12 hours for one month. For 11 months, approximately 132 hours was used to create a final high-resolution map for one year on Tromsøya.

After the solar map is completed for each section, the sections needed to be merged together to form a complete map covering the whole island. Again, the "mosaic to new raster" tool in ArcGIS is used. Now we will have overlap between the sections, and therefore the "Mosaic Operator" is important to consider getting a correct result. The possible opportunities are given in the following table as:

Table 3-5: Possible parameters in Mosaic Operator.

First	The value from the cell in the first input raster will be chosen
Last	The value from the cell in the last input raster will be chosen
Blend	The value for the new cell will be calculated by a horizontally weighted calculation of the overlapping cells
Mean	The new value will be the mean of the cell values
Minimum	The minimum value for the overlapping cells will be chosen
Maximum	The maximum value for the overlapping cells will be chosen
Sum	The sum of the cells will be the new cell value

The best result for the final map was received when "minimum" was chosen as Mosaic operator (Falklev, 2017). When all sections are merged together, we get a complete solar map for the whole island per month. Solar maps for each individual month with 1- and 0.25 – meter resolution is given in the appendix. The final step is now to apply "mosaic to new raster" tool again and aggregate all individual months into a map covering the whole year by choosing "Sum" as Mosaic Operator. This would give the final map for Tromsø island given in $\left[\frac{\mathrm{Wh}}{\mathrm{m^2\ yr}}\right]$ which is presented in figure 4-1.

The methodology for creating the solar map of Tromsøya has been based on similar methodology as in former master thesis by (Falklev, 2017). However, the former master thesis did only create a 1-meter resolution solar map covering the whole island. To investigate solar potential on buildings on Tromsøya, it is necessary to identify them by separating buildings from the original solar map. The method of identifying buildings is by creating a feature layer which consist of buildings only. The buildings are received from 3D Clip&Ship service from Geodata, which is their newest 3D service letting you draw a pylogon for area of choice, and thereafter produces a complete 3D scene which could be used analysis in ArcGIS (Geodata, 2019). After receiving 3D buildings from Geodata, the buildings could be imported into ArcGIS by using the "make feature layer". Issues arise when trying to merge the 3D buildings to the solar map since the buildings is classified as 3D feature layer, while the solar map is classified as 2D raster layer. This was fixed by applying the "feature to raster" tool, which converts the 3D buildings into 2D raster layers, giving the buildings footprint as a result. The final step to making a solar map which identifies buildings is to apply the tool "Diff". This tool finds the difference between two raster layers. To create a solar map for rooftops on Tromsøya, the solar map covering both terrain and buildings was extracted by the building footprint layer. The resulting solar map with rooftops highlighted is given in figure 4-5.

3.3 Estimation of solar-architecturally suitable areas for PV systems

Examine suitable areas for installing PV systems by investigating one specific house in the solar map is possible when looking at few houses, but for the whole island this would be inefficient and extremely time procuring. Therefore, another method should be used for Tromsøya. In this thesis, the determination is based on the same method as in paper "Scenario- based modelling of the potential for solar energy charging of electric vehicles in two Scandinavian cities" by (Good, et al., 2018).

3.3.1 Calculation of roof and façade areas

The available areas suited for PV installations is determined by using the method proposed by IEA PVPS Task 7 (IEA Photovoltaic Power System Programme, 2019), where the suitable area A_{sol} is calculated by

$$A_{sol} = A_g \times u_r + A_g \times u_f \tag{3.1}$$

This equation multiplies ground floor area A_g by utilization factors for roof u_r, and façade u_f. In the IEA PVPS Task 7 method (IEA Photovoltaic Power System Programme, 2019), the utilization factors are estimated by considering limitations due to construction, historical considerations and shading for the architectural suitability. For the solar suitability, the relative solar irradiation on surfaces, tilt, location and orientating is considered. Based on number of case studies, the rule- of- thumb values for the solar- architecturally utilization factors are $u_r = 0.4$ and $u_f = 0.15$ (IEA Photovoltaic Power System Programme, 2019).

In present study, the gross building area for Tromsø island is estimated by using statistical data from Statistics Norway (SSB), where buildings are classified in number of buildings per building type (SSB, 2019). The number of buildings is thereafter combined with on the average area of each building type which is given in paper from "Vilni Verner Holst Bloch- Arealstatistikk fra GAB og FKB Bygg" (Bloch, 2002). Gross building area for Tromsø island is not available in the online database, as values are only available at county level. In Good's paper, data for Tromsø municipally was received upon request for SSB (Good, et al., 2018).

Tromsø municipally includes Tromsø island, Kvaløya and Tromsdalen. Therefore, we need to extract buildings which only includes Tromsø island. In 2018, number of inhabitants in Tromsø municipality was totally 75 638, distributed over Kvaløya, Tromsøya and mainland. Some of the biggest towns in Tromsø municipality is; Kvaløysletta on Kvaløya with 8 882 inhabitants, Tromsdalen on mainland with 16 958 inhabitants and Tromsøya with 38 980 inhabitants (SSB, 2019). Based on distributions of inhabitants, a calculated estimate was made assuming that 60% of the buildings for Tromsø municipally is on Tromsø island. Table 3-6 gives the complete overview of number of buildings based on numbers from paper from Good,et al. Gross floor area is calculated based on mean values for different building types. In addition, area for roofs and facades are calculated by multiplying with the utilization factors. The estimated areas are given in table 3-6 as:

Table 3-6: Estimated solar- architecturally suitable areas for PV installations in Tromsø based on paper by (Good, et al., 2018).

Code	Building Type	No. of buildings	Gross building area $[\mathbf{m^2}]$	Area, roofs $[\mathbf{m^2}]$	Area, facades $[\mathbf{m^2}]$
1	Dwelling	18 926	1 940 400	776 160	291 060
2	Industrial building and warehouse	2 451	504 000	201 600	75 600
3	Office and business building	268	120 600	48 240	18 090
4	Transport and communication building	99	23 400	9 360	3 510
5	Hotel and restaurant building	159	31 200	12 480	4 680
6	Building used for education, public entertainment and religious activities	327	166 800	66 720	25 020
7	Hospital and institutional care building	35	21 600	8 640	3 240
8	Prison, building for emergency preparedness etc.	20	4 200	1 680	630
9	**Total**	**22 286**	**2 812 200 ($\mathbf{2.8\ km^2}$)**	**1 124 880 ($\mathbf{1.1\ km^2}$)**	**421 830 ($\mathbf{0.4\ km^2}$)**

Where code 1 represent residential buildings, and code 2-8 represents non- residential buildings. The areas for roof and façade could be set in context with solar potential from the solar map created in ArcGIS to thereafter estimate total PV solar energy yield on Tromsøya.

3.4 Comparison of PV solar energy yield from solar map created in ArcGIS and PVsyst

In paper by Clara et, al. assumptions regarding building orientations and roof tilt was made to estimate PV yield in PVsyst. All residential buildings were assumed to have sloped roofs with 30° roof tilt angle, while all non-residential roofs were assumed to have flat roofs. The utilization factor was assumed to be equal for residential and non-residential roofs. In addition, the building orientations were assumed to be equally distributed in north, south, east and west direction. For sloped roofs, only building's roof orientations between east and west in southern direction were assumed to be suitable for solar energy utilization. In addition, to account for the orientation distribution, the suitable roof area was divided into 12 evenly spaced intervals between east and west. For flat non- residential roofs, it was assumed that a PV system could be placed freely on the roof. For facades, the utilization factor ($u_f = 0.15$) was used for both residential and non- residential buildings, and the façade areas was assumed to be orientated as for roofs (Good, et al., 2018). In this thesis, it is possible to use the solar map to investigate PV yield simulation directly in the map based on roof orientation as in case studies in subchapters 4.2.3 and 4.2.4.

3.4 / Comparison of PV solar energy yield from solar map created in ArcGIS and PVsyst

In PV yield proposals, it is useful to investigate energy yield in $\mathrm{kWh/kW_p}$ in addition to $\mathrm{kWh/m^2}$. This will give energy in terms of kWh per kilowatt-peak instead of kWh per square meter. To investigate energy in $\mathrm{kWh/kW_p}$, the solar intensity in $\mathrm{kWh/m^2}$ is combined with a typical area for solar module, solar cell efficiency, peak power for solar cell and a typical solar power ratio (PR). In this thesis, the same simulated $5.4\ \mathrm{kW_p}$ PV system as in paper from Good et, al. is used, which is given in table 3-7 as:

Table 3-7: Details of simulated $5.4\ \mathrm{kW_p}$ PV system (Good, et al., 2018)

Module	
Type	Jinkosolar, JKM300M-60
Power	300 W_p
Efficiency	18.42%
Module Area	1.637 m^2
Number of Modules	18
Inverter	
Type	AEG, AS-IR01-4600
Inverter power	4.6 kW AC
European efficiency	96.8%
Power ratio (PV array/inverter)	1.17

To get $1\ \mathrm{kW_p}$ for this PV system, approximately 3.33 modules of $300\ \mathrm{W_p}$ is needed

$$3.33\ \text{modules à}\ 300\ \mathrm{W_p} \approx 1\ \mathrm{kW_p} \tag{3.2}$$

Multiply number of modules by module area from table 3-6

$$y = 3.33 \times 1.637\ \mathrm{m^2} = 5.45\left[\frac{\mathrm{m^2}}{\mathrm{kW_p}}\right] \tag{3.3}$$

To analyze the solar potential on different south-facing roof on Tromsøya, the solar map is investigated by clicking on several roofs to find the solar potential. After identifying solar irradiation values on different roofs in the solar map, a mean value of approximately 820 000 $\mathrm{Wh/m^2}$ for south-facing tilted roof seems to be a reasonable value to choose.

Now, multiply this with solar irradiation value given in $\mathrm{Wh/m^2}$ and power ratio to get solar irradiation in $\mathrm{kWh/kW_p}$.

$$a = \frac{820\,000\ \left[\frac{\mathrm{Wh}}{\mathrm{m^2}}\right] \times \mathrm{y} \times \mathrm{PR}}{1000} = 3709\left[\frac{\mathrm{kWh}}{\mathrm{kW_p}}\right] \tag{3.4}$$

Where Power Ratio (PR) is the ratio between PV array and inverter. PR is set to be 0.83. To get this unit in terms of PV system instead of solar irradiation, multiply with efficiency given in table 3-17

$$z = a \times \eta = 683\ \left[\frac{\mathrm{kWh}}{\mathrm{kW_p}}\right] \tag{3.4}$$

The average value for south facing residential roofs in paper from Good et, al. is 730 $\mathrm{kWh/kW_p}$, but it is important to notice that this is a value for 12 months, while the solar map does not take December into account. To compare solar map value and PVsyst value from Good et, al. we divide by number of hours for respectively 11 and 12 months

$$\mathrm{PVsyst} = \frac{730}{8760\ \mathrm{h}}\left[\frac{\mathrm{kWh}}{\mathrm{kW_p}}\right] = 0.0833\left[\frac{\mathrm{kW}}{\mathrm{kW_p}}\right]$$

$$\mathrm{Solar\ map} = \frac{683}{(8760-744)\mathrm{h}}\left[\frac{\mathrm{kWh}}{\mathrm{kW_p}}\right] = 0.0852\ \left[\frac{\mathrm{kW}}{\mathrm{kW_p}}\right]$$

Where 744 is number of hours in December. This shows that the average value in solar map is slightly higher than estimated PVsyst value.

Finally, to get this in terms of $\mathrm{kWh/m^2}$ for a PV system, divide by y

$$b = \frac{z}{y} = \frac{683\left[\frac{\mathrm{kWh}}{\mathrm{kW_p}}\right]}{5.45\left[\frac{\mathrm{m^2}}{\mathrm{kW_p}}\right]} = 125\ \left[\frac{\mathrm{kWh}}{\mathrm{m^2}}\right] \tag{3.5}$$

All results of calculations for residential and non- residential roofs are given in table 3-8.

Table 3-8: Average energy yield for 11 months on residential roofs, non- residential roofs and facades

	Energy yield, residential roofs	Energy yield, non-residential roofs	Energy yield, facades
Avg. $\mathbf{kWh/kW_p}$	683	583	622
Avg. $\mathbf{kWh/m^2}$	125	107	114

The energy yield for facades is assumed to be equal for both residential and non- residential buildings. As the solar map in ArcGIS does not calculate solar irradiation for facades, solar radiation values from the solar energy system mounted on the roof of Realfagsbygget is used as basis. This module has an orientation of 39° south-vest and is bifacial, i.e. it has solar cells on both front and backside to increase energy yield from both direct sunlight and reflected sunlight from surroundings. On Realfagsbygget, two of the modules mounted on façade is bifacial, and one is not bifacial and produces an energy yield of 585 kWh/kW_p for 11 months which is approximately 6% lower than for bifacial modules.

Figure 3-5: Solar modules mounted on facade. Module to the left is non- bifacial, while the other two is bifacial modules. Photo by Odin Foldvik Eikeland

Now, as the average energy yield for residential roofs, non-residential roofs and facades are estimated, this could be multiplied by estimated solar-architecturally suitable areas for roof and façade given in table 3-6 to find the total energy yield from PV systems from buildings on Tromsøya. The resulting total energy yield is presented in figure 4-15 and table 4-5.

3.5 Charging load from Cruise ships in Tromsø Harbor

Electricity generation from PV systems could be used to supply several things which requires energy as for example buildings and electric vehicles. In the paper by Good et, al. the possibilities for charging electric vehicles with solar energy was investigated. This paper concluded that the aggregated electric vehicles charging load can be covered with the total solar energy yield for most scenarios, except for some scenarios with little PV integration and heavy use of electric vehicles during winter (Good, et al., 2018).

In this thesis, electricity load from Cruise ships visiting Tromsø is proposed. If Tromsø can supply cruise ships with renewable energy from PV systems, then Tromsø could be in the front of creating sustainable tourist cities.

In this section, the charging load from Cruise ships is estimated based on statistics received from Tromsø harbor. In section 3.5.2, number of ships which harbored in Tromsø is provided. Section 3.5.3 estimates charging load from the ships harbored in Tromsø.

3.5.1 Tromsø harbor

Tromsø has harbor was grounded in 1827 and has been important for the development of Tromsø city in the last 200 years. (Tromsø havn, 2019). From the 1850s, Tromsø was the center for arctic seal and whaling industries. Early in the 19th century, Tromsø became the starting point for several hunting, research and tourist expeditions to Arctic regions, which contribute to give Tromsø the nickname “The gateway to the Arctic Ocean”. Nowadays, the northern Norwegian state has developed an internationally leading knowledge environment inside climate, environment and utilization of Arctic resources which will play an important role in the development of the northern areas.

Today, Tromsø harbor is one of Norway's largest fishing and cruise ports, and an important logistics hub in the northern regions. Tromsø harbor's goal is to be the preferred port for the entire energy sector in the north (Tromsø havn, 2019).

3.5.2 Cruise ship traffic in Tromsø harbor

Tromsø is a popular tourist city which is famous for northern lights and ski touring on the beautiful mountains during winter, and lot of possibilities for hiking and fishing expeditions in the midnight sun during summer. Tromsø is one of Norway's biggest tourist cities with many cruise ships that come to Tromsø and stays in harbor while the tourist explores Tromsø. Tromsø harbor has published statistics over number of boats which arrives each year from 2012-2018, given in table 3-9:

Table 3-9: Statistics of number of cruise ships in Tromsø harbor (Tromsø havn, 2019).

	2012	**2013**	**2014**	**2015**	**2016**	**2017**	**2018**
Nr. of boats	112	104	112	104	91	103	119
Nr. of passengers	105 490	108 681	111 631	111 190	102 495	125 455	142 348

Tromsø harbor have also published statistics of number of fishing ships, offshore vessels, cargo vessels etc. In total, 8 738 ships visited Tromsø harbor in 2018 (Tromsø havn, 2019). In 2019, the expected number of Cruise ships visiting Tromsø is 132. The statistics is given from Harriet Willassen, marketing Manager at Tromsø harbor. The distribution for number of Cruise ships visiting Tromsø during per month is given in figure 3-6:

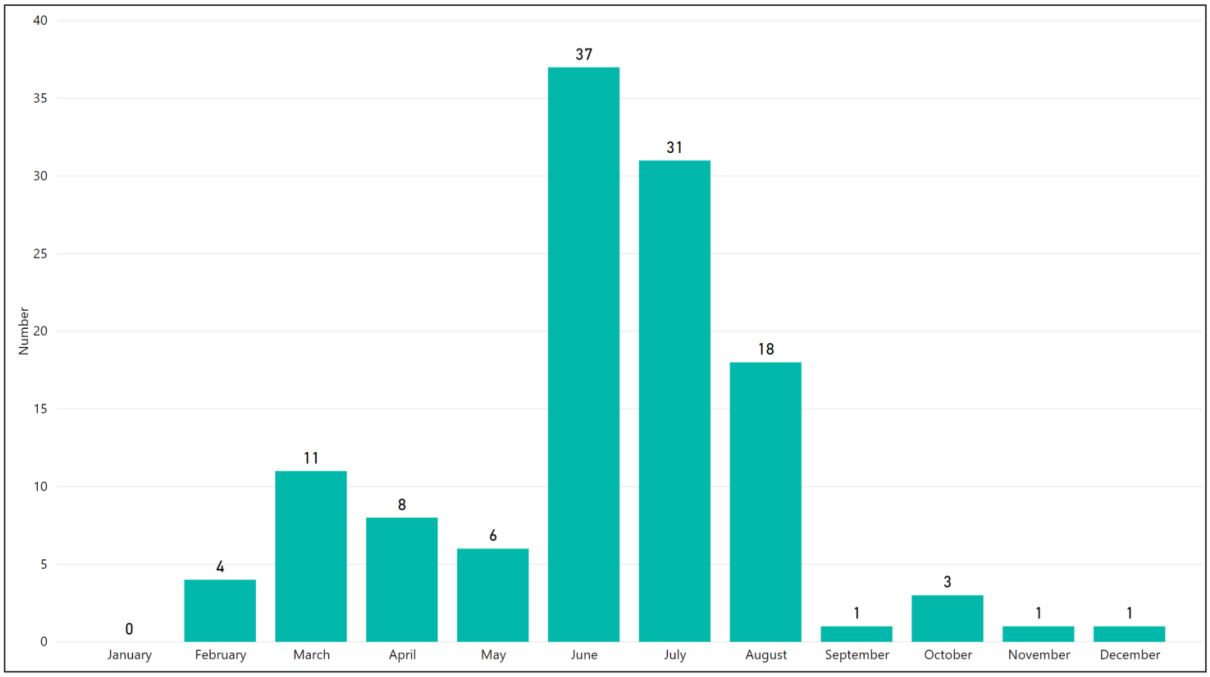

Figure 3-6: Distribution of number of Cruise ships visiting Tromsø per month in 2018

This distribution shows most cruise boats visiting Tromsø during tourist season in June and July. Tromsø is famous for midnight sun and possibilities for trips in a beautiful landscape during summer and is an attractive tourist city worldwide. During wintertime, there is still some cruise traffic as Tromsø is famous for the northern lights and polar nights during winter. Skiing trips on the beautiful mountains around Tromsø is also an attractive tourist goal.

Cruise ships are like small societies which requires lot of energy to function, even when it stands still in port. Water, light, restaurants and heat must be available all the time for passengers and crew. If the harbor does not offer power from land, the ships need to run their own motors to run everything on board which needs power supply. When the boats stand still with motors running, it releases tons of CO_2, SO_2, NO_x and pollution into the atmosphere (Bellona, 2019). This pollution contributes to global warming and low air quality. In addition, the motors are noisy and disturbing for neighborhoods.

In this thesis, an idea of connecting the cruise ships with shore power driven by produced power from PV systems is presented. Then, the ships can turn their motors off when they are in Tromsø harbor and receive sustainable energy from PV systems in Tromsø. This idea could be tested by performing a case study for one day during summer by comparing electricity

generation from PV systems with electricity need from a Cruise ship harbored in Tromsø. First, energy load from cruise ships need to be estimated to figure out how much energy is needed for power supply from PV systems.

3.5.3 Energy load from Cruise ships

Bellona, the independent environment foundation in Norway published in 2016 in cooperation with Siemens, Nelfo and the Electric association a study called "Better climate and smarter economy, Shore power in Norwegian harbors- a feasibility study". This study states when a big cruise ship is in harbor for 8 hours, the ship releases as much NO_x as 10 000 cars which drives from Oslo to Trondheim and correspond the yearly release of NO_x from 700 cars. Performed calculations shows that shore power could reduce NO_x release with 7000 tons, which corresponds to release from 58% of all cars in Norway. Shore power could also reduce release of CO_2 with 360 000 tons, which correspond to 5% of release from all cars in Norway (Bellona, 2016).

Information needed to perform calculations regarding to electricity need from Cruise ships harbored in Tromsø has been provided upon request from Trond Sikveland-Port Area Manager in Port of Kristiansand. Kristiansand harbor is the only harbor in Norway which have the facility to provide Shore power to Cruise ships today (Sikveland, 2019). The information is provided in table 3-10.

Table 3-10: Given information about energy consumption regarding to ship name and passenger capacity (Sikveland, 2019)

Ship name	Passenger capacity	Shore Power possible to connect	Energy needed (MVA/hour)	Energy needed (MW/hour)
Rotterdam	1 404		5.0 -7.0	4.3-6.0
Nieuw Statendam	2 650	Yes	5.5 -6.5	4.7-5.5
Viking Jupiter	930		5	4.30
Costa Favolosa	3 780		5.4-6.5	4.6-5.5
Regal Princess	3 600	Yes	8.5 -13	7.2-11.1
Koningsdam	2 650	Yes	5.5-6.5	4.7-5.5
Amsterdam	1 380	Yes	6.0-7.0	5.1-6.0
Noordam	1 916	Yes	7.0-9.0	6.0-7.7
Oosterdam	1 848	Yes	7.0-9.0	6.0-7.7
Zuiderdam	1 969	Yes	7.0-9.0	6.0-7.7
AIDAperla	4 350		7.5-9.5	6.4-8.1
AIDAprima	3 300		7.5-9.5	6.4-8.1
MSC FANTASIA	4 900	No	9	7.70
MSC MERAVIGLIA	4 500	Yes	9	7.70
MSC PREZIOSA	3 959	No	9	7.70
MSC SEASIDE/SEAVIEW	5 429	Yes	13	11.10
MSC SPLENDIDA	3 900	No	13	11.10

Where the energy needed is represented in Megawatt- Ampere (MVA) per hour. To convert from MVA to Megawatt (MW), the energy need in MVA is multiplied with a power factor (PF) of 0.85 (Sikveland, 2019). The given information shows that the biggest cruise ships with capacity of 4000-5000 passengers uses approximately 11 MW/hour when harbored, and the smallest ship uses 4.3 MW/hour when harbored.

Statistics given from Tromsø harbor shows an average passenger capacity of 1 542 passengers in 2018. The Cruise ships are ported approximately 11 hours between May-October, and 20 hours between November- April. Based on given information and types of boats visiting Tromsø, an estimate of electricity need is possible to perform. Based on the average capacity of 1 542 passengers, assume each boat uses 5 MW/hour when harbored.

Table 3-11: Distribution of electricity need during 2018 based on number of boats and estimated electrical energy consumption

Month	Nr. of boats	Electricity energy need [MWh]
J-18	0	0
F-18	4	400
M-18	11	1 100
A-18	8	800
M-18	6	330
J-18	37	2 035
J-18	31	1 705
A-18	18	990
S-18	1	55
O-18	3	165
N-18	1	100
D-18	1	100

Table 3-14 shows the greatest traffic during tourist season in summer between June and August with a rapid growth from 6 to 37 visiting ships from May-June, and a quick fall from 18 to only 1 ship between August-September.

3.6 Solar fraction

The self-sufficiency and self-consumption of PV solar power in buildings with Electric Vehicles has been previously studied, for example in (Good, et al., 2018) and (Luthander, et al., 2015). In (Luthander, et al., 2015), numerous calculations that are used to describe self-consumption and self-sufficiency are presented. In this thesis, the self-sufficiency of PV solar power from buildings against Cruise ship load is performed.

The PV solar power self-sufficiency are referred to the solar fraction (SF). SF describes how much of the load which can be covered with PV solar energy. The SF are defined as

$$SF = \frac{\int_{t=t_1}^{t_2} M(t)dt}{\int_{t=t_1}^{t_2} L(t)dt} \tag{3.6}$$

,by using the notation in (Luthander, et al., 2015).

In equation (3.6), t represents temporal period, where t_1 is starting time and t_2 is end time. M(t) represent the overlapping part of the load profile L(t) and PV generation profile P(t) and is defined as

$$M(t) = \min\{L(t), P(t)\} \tag{3.7}$$

The value of SF is in the range [0,1], where SF=1 gives the energy demand is fully covered by PV solar energy (Good, et al., 2018). The values depend on integration factor and the time resolution of data, among other factors (Luthander, et al., 2015).

In this thesis, the aggregated SF values were calculated per month. The values are calculated for three different situations; Total monthly PV energy yield against energy load from Cruise ships and monthly PV energy yield against electricity use for one building with and without heating. As in (Good, et al., 2018), the instantaneous SF value are used, and could be defined as:

$$SF = \frac{M(t)}{L(t)} \tag{3.8}$$

4 Results

4.1 Overview

The resulting final solar map covering Tromsøya is provided in section 4.2. A quality control in section 4.2.1 is performed to validate the result. In section 4.2.3 and 4.2.4, case studies for specific buildings is performed to investigate its solar potential. In case study 4.2.4, the potential is compared against theoretical values from PVsyst. In addition, the SF values for case study in 4.2.4 is calculated.

Section 4.3 presents the total PV solar energy yield from production of PV solar energy at rooftops on Tromsøya. The estimation was performed by combining solar potential in the solar map with the methodology in section 3.3 and 3.4. A case study for one day in June 2018 is performed in section 4.3.1 to investigate area needed to cover the electricity load from one Cruise ship visiting Tromsø for 10 hours. Section 4.4 presents the total monthly energy yield from PV systems versus electricity load based on Cruise ships traffics. Finally, an economic benefit calculation is performed in section 4.4.1 to investigate the opportunities for benefitting from selling PV solar energy produced from modules on buildings to Cruise ship visiting Tromsø. The thesis goes not into analyses of how the local system could be organized in order to secure that the benefit from the production is accrued the owner of the solar energy system.

4.2 Final Solar Map of Tromsøya

The resulting solar map obtained from the methodology described in 3.2.4 is given as:

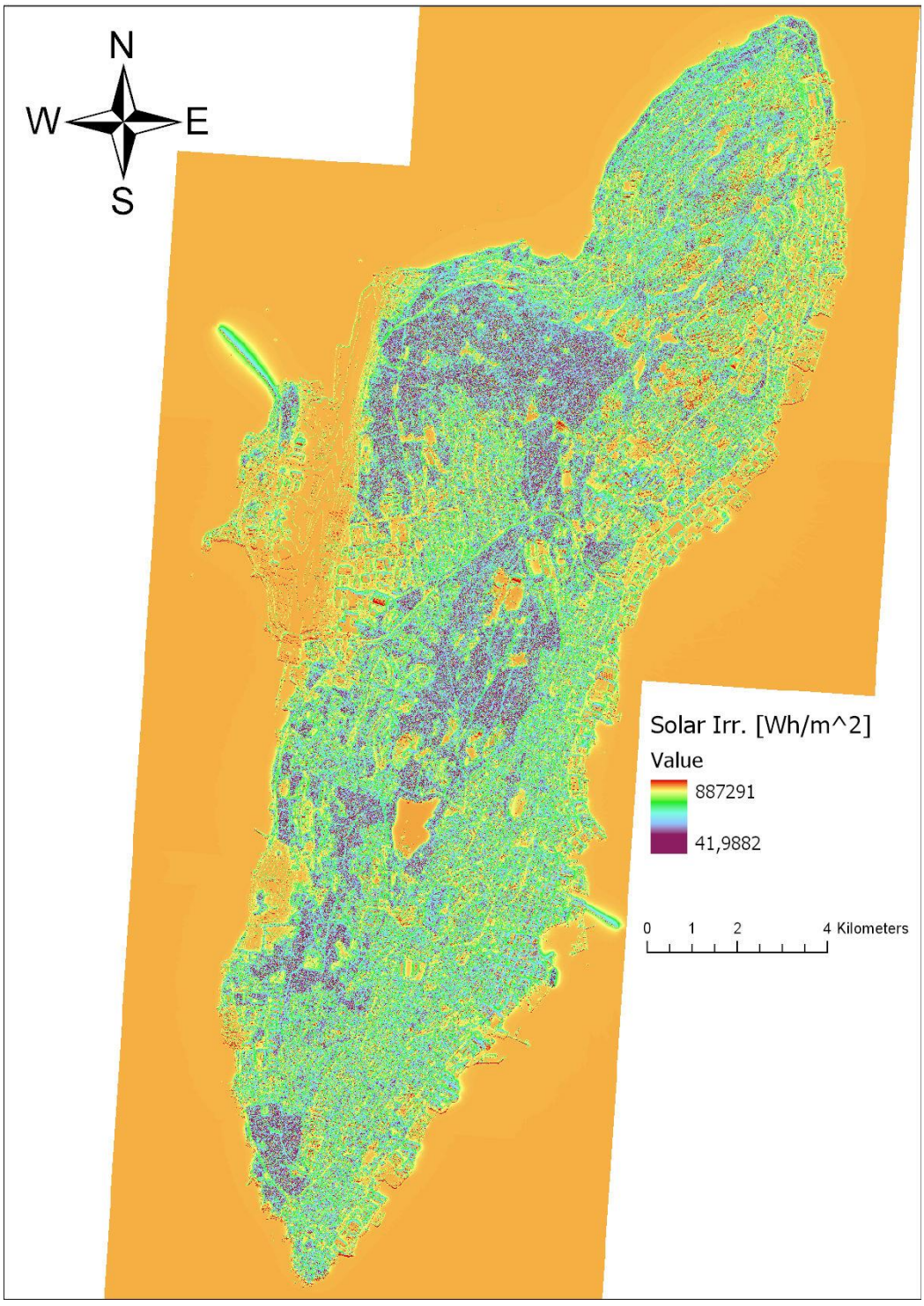

Figure 4-1: The final solar map including Tromsøya.

4.2.1 Validation of solar map

To validate the solar map, a quality control of the solar potential values was performed. The pyranometers installed at Holt and at the roof of Realfagsbygget is used as basis for the quality control procedure. The weather station at Holt was established 1987 and is installed on a lawn. However, this station has had periods where the instrument has not functioned properly, which has given no-or incorrect measurements. Therefore, to make sure of the quality of the data basis, a mean value for the last 10 years is used. There are still some years which is not used because of lack of labels (Falklev, 2017). The years with acceptable data basis are 2009, 2011, 2012, 2014, 2015, 2016, 2017 and 2018 (Falklev, 2017). To compare with the created solar map in ArcGIS, the values for each month in the same area as Holt weather station was used.

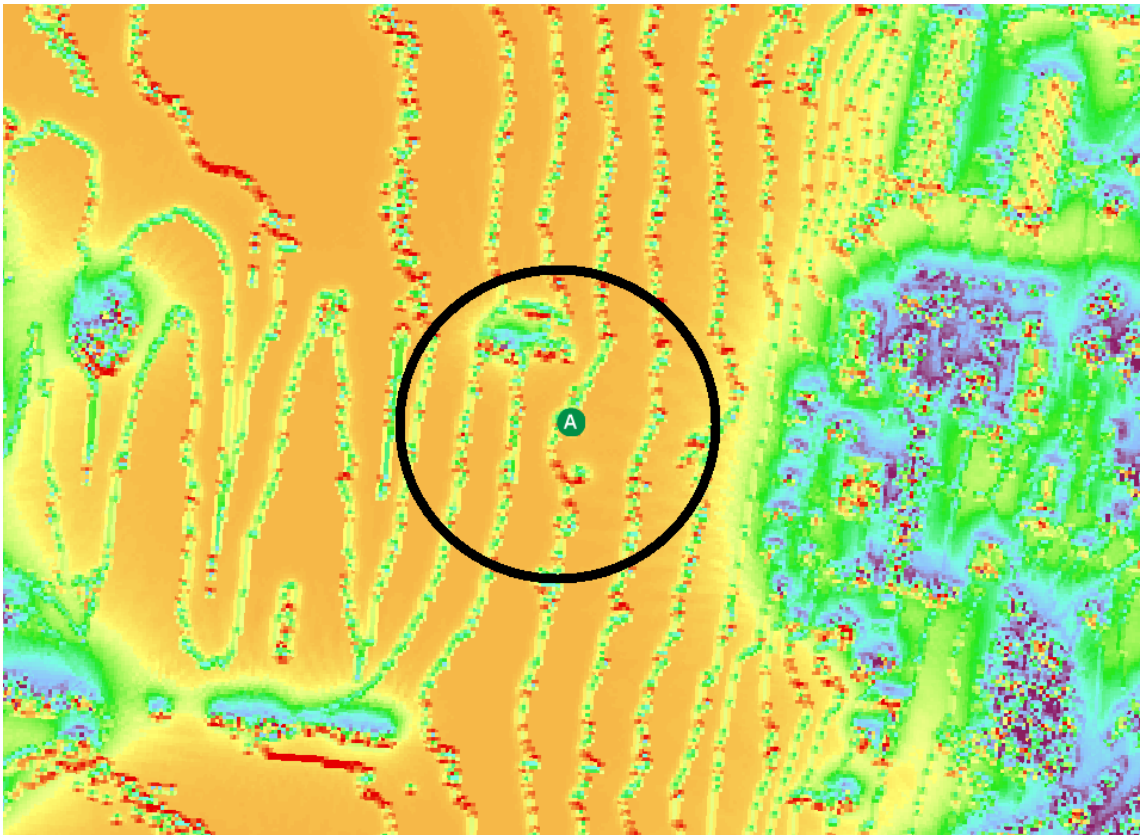

Figure 4-2: Holt Weather station marked with "A" in green, values from solar map is received by clicking on map in the same area as this station.

The resulting comparison is shown in figure 4-3 where monthly solar irradiation values are represented in addition to mean value for one year:

(a) (b)

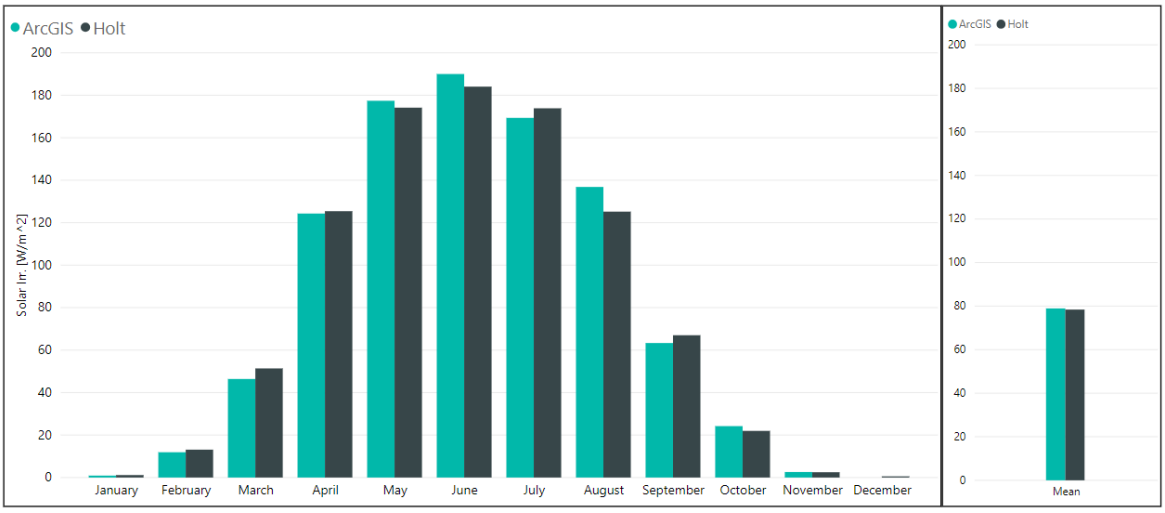

Figure 4-3: (a) Average Solar irradiation values [W/m^2] per month (b) Average solar irradiation values (ArcGIS=79, Holt=78) per year for solar map in ArcGIS and Holt Weather station.

The pyranometers installed on roof of Realfagsbygget has not been operating for as many years as Holt weather station has. Monthly values from the pyranometer operated by institute for computer science (ICS) is averaged for 2016, 2017 and 2018. The pyranometers mounted on the solar modules was not operated before spring 2017, therefore values are averaged for 2017 and 2018 from April to December, while only 2018 values are used for January-March. The pyranometer used for comparison in this thesis is one instrument on a 40°-tilt solar module on the frontside and backside of the module to measure the bifacial effect.

(a) (b)

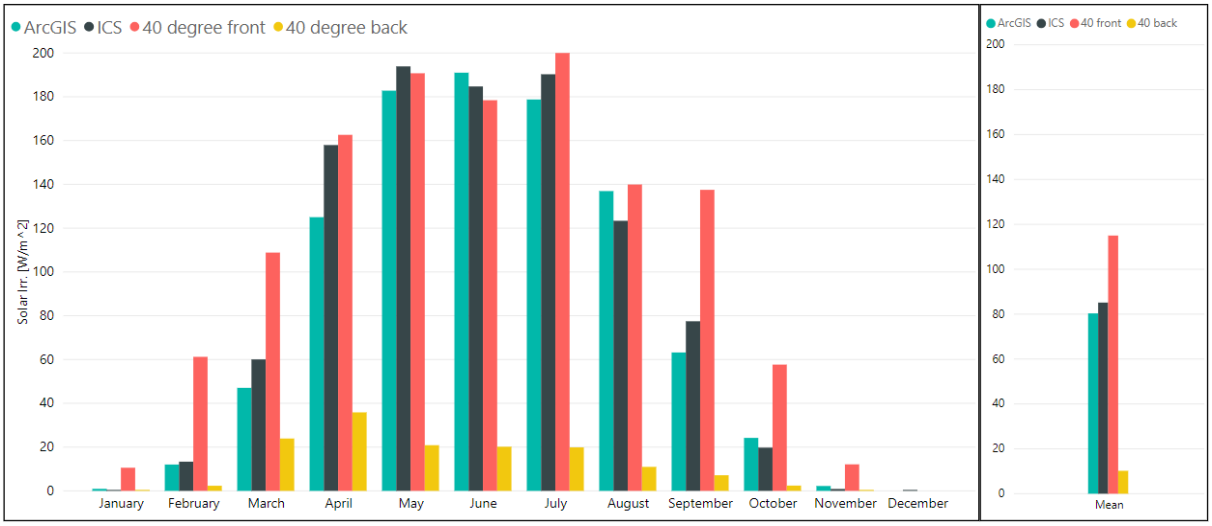

Figure 4-4: (a) Average Solar irradiation values [W/m^2] per month (b) Average solar irradiation values per year for solar map in ArcGIS and pyranometers installed on roof of Realfagsbygget

The pyranometer mounted on solar module measures higher values than both ArcGIS and pyranometer from ICS, especially from September to March. During this period, the sun is low, which gives better angels towards the sun when the measurement instrument is tilted. Moreover, there is a bigger deviation between solar map in ArcGIS and pyranometers at Realfagsbygget than for the instrument placed at Holt. Because of huge differences between ArcGIS map and pyranometers mounted on modules, the root mean square error (RMSE), relative root mean square error, bias and mean absolute error (MAE) is not calculated for these instruments. For the other instruments, the statistical analysis is performed by calculating the errors between ArcGIS and pyranometers. The errors in table 4-1 are given in [W/m^2].

Table 4-1: Statistical analysis for validation of solar map in ArcGIS

Parameter	Holt [W/m^2]	ICS [W/m^2]
RMSE	4.54	12.78
Rel. RMSE	0.07	4.8
Bias	0.57	-0.62
MAE	3.29	9.22

The statistical analysis shows high correlation between measurements for ArcGIS map and pyranometers. The instrument placed in Holt shows lower deviation. A reason for this could be more measurement years for this instrument, giving stronger statistical basis with more measurement data than for the instrument operated by ICS which only has measurement data for three years. In addition, the instrument placed in Holt is maintained and checked daily by employers at NIBIO (NIBIO, 2018), while the instrument operated by ICS is not maintained at all.

However, a relative RMSE of 0.07 for Holt is an accurate result, and a relative RMSE of 4.8 at UiT is also satisfactory for solar energy potential investigations. This indicates that the ArcGIS solar map measures correct solar irradiation values and could be used further for solar energy potential investigations. It is important to notice that the calculations in ArcGIS does not change significantly from year to year, therefore the average pyranometer data should be used for validation. The pyranometer data is sensitive for different climate from one year to another, which will give considerably larger errors if the data is not averaged over several years.

4.2.2 Identification of roofs to investigate solar potential on buildings

The resulting solar map with rooftops highlighted from the original solar map in figure 4-1 is given in the following figure:

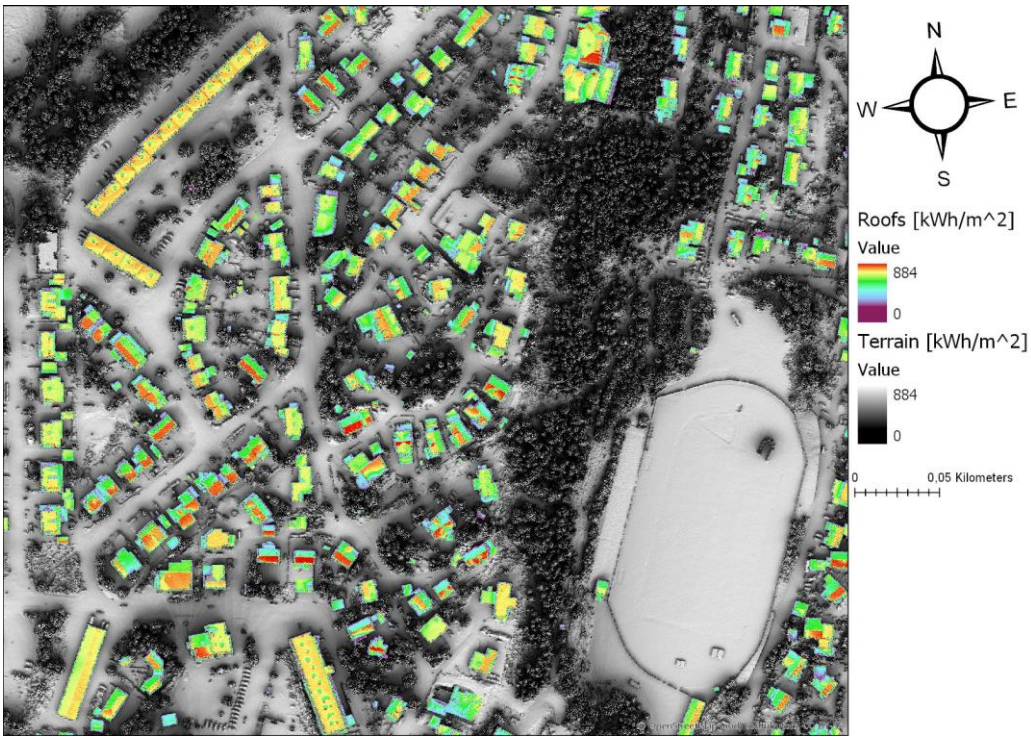

Figure 4-5: 0.25-meter resolution solar map with highlighted roofs on Tromsøya

Figure 4-5 is the 0.25- meter high- resolution solar map for a small neighborhood where the roofs is highlighted by using a color bar. The map demonstrates that the orientation of the roof's matters, where south facing roofs receives more solar irradiation during the year than north facing roofs.

Since the buildings now are classified as a raster layer, it is possible to remove the solar map for terrain, giving a map which shows only the solar irradiation at roofs.

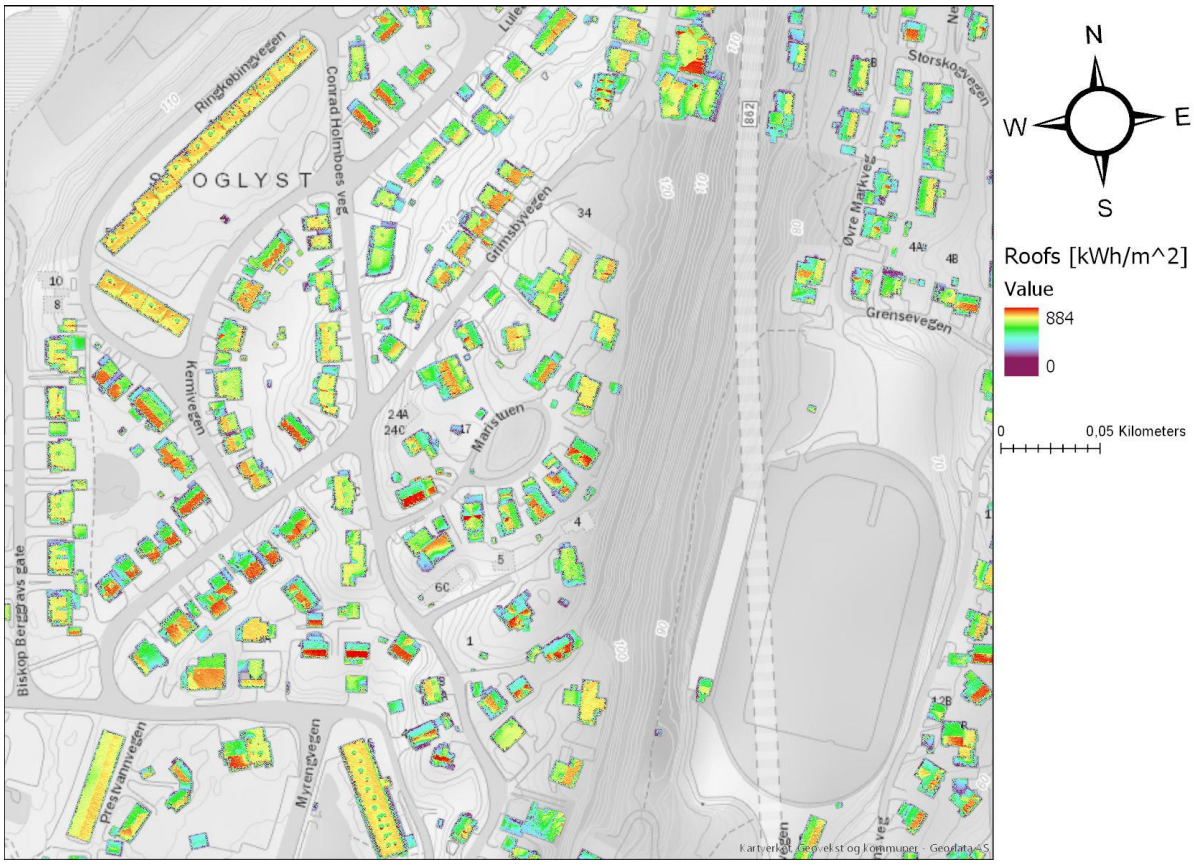

Figure 4-6: 0.25-meter solar map for roofs only with "GeoacheGraatone" as Basemap in ArcGIS Pro

4.2.3 Case study: Investigate solar potential for one house

As the solar map is validated, and roofs are identified, it possible to do a case study for one single house to investigate and analyze solar irradiation. This makes it possible to find potential for solar energy systems, and which roof is most suitable for installing solar modules. In the case study, the 1-meter and 0.25-meter resolution map is used to investigate differences between resolution. The house which is investigated with permission is my supervisor Tobias Boström's house and is located close to "Valhall Stadion" , the athletics stadium on Tromsøya.

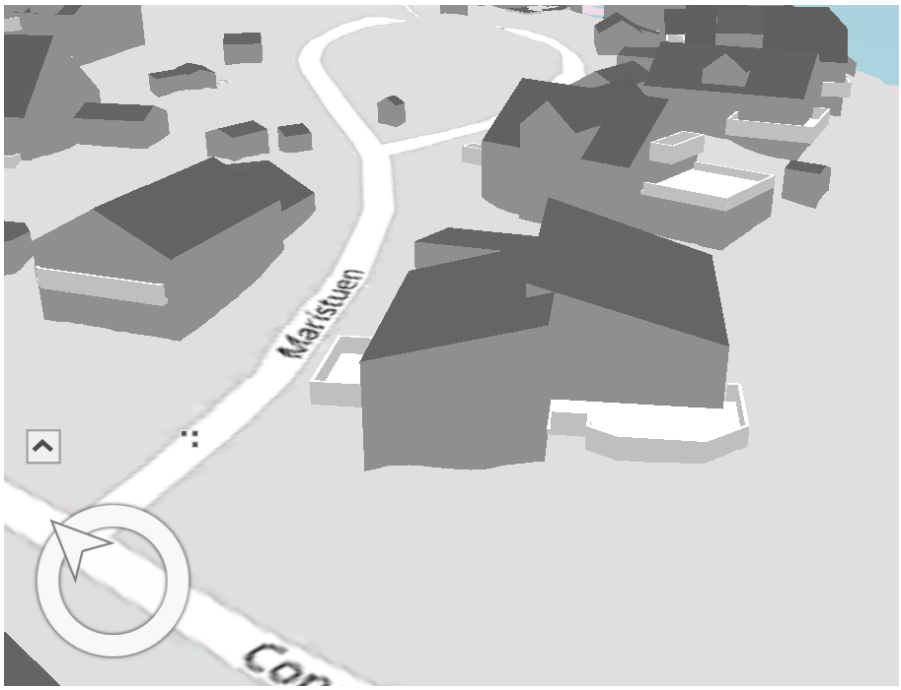

Figure 4-7: Tobias Boström's house with one south and one north-facing roof. Arrow in lower left shows northern direction.

The house has two big roofs which should be suitable for mounting solar modules on, and the south- facing roof would be the roof which receives most sun during the year. In addition, the house has a small forest in front of the south-facing direction which causes shadowing when the Sun has a low angle. Figure 3-11 shows a solar map for the house with some neighborhood houses for 1- and 0.25-meter LiDAR resolution data. In this figure, the solar map for surrounding terrain is included to show shadowing from forest for south- facing roof.

(a) (b)

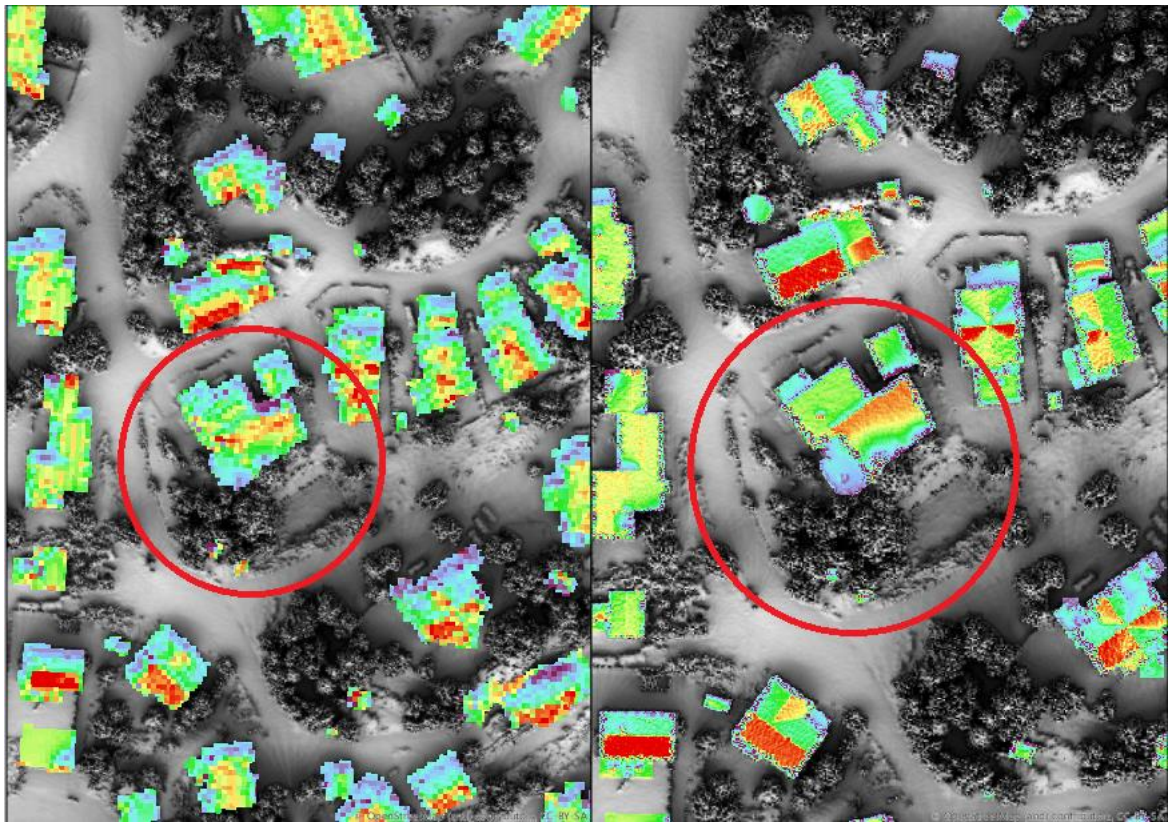

Figure 4-8: (a) Solar map with 1- meter resolution for house and 0.25- meter resolution for surrounding terrain (b) Solar map with 0.25- meter resolution for house and surrounding terrain.

This map shows differences between resolutions on Boström's house. The low- resolution solar map looks grainy and unclear while the high- resolution map is more detailed. The high-resolution map shows shadowing effect from the forest as a line between green and orange color on south facing roof, while on the 1-meter resolution map it is more difficult to identify the shadowing effect. In addition, the differences between north and south-facing roof is more significant for high resolution than for low resolution map. This could be due to lack of data points for the lower resolution LiDAR data, which misses datapoints where the roof has tilt. Differences between high- and low-resolution LiDAR data are most prominent for higher roof tilt (Lingfors, 2017). For flat surfaces, the difference is negligible.

As the low- resolution data is not able to perceive correct roof tilt and shadowing effects, the 1- meter resolution map measures higher average solar irradiation during the year than for

0.25- meter resolution map. In ArcGIS Pro, it is possible to plot the distribution which shows number of pixels within a certain interval of solar irradiation potential in the raster layer. The following figure shows how the solar irradiation for Tobias's house varies on 1-and-0.25-meter resolution raster layer.

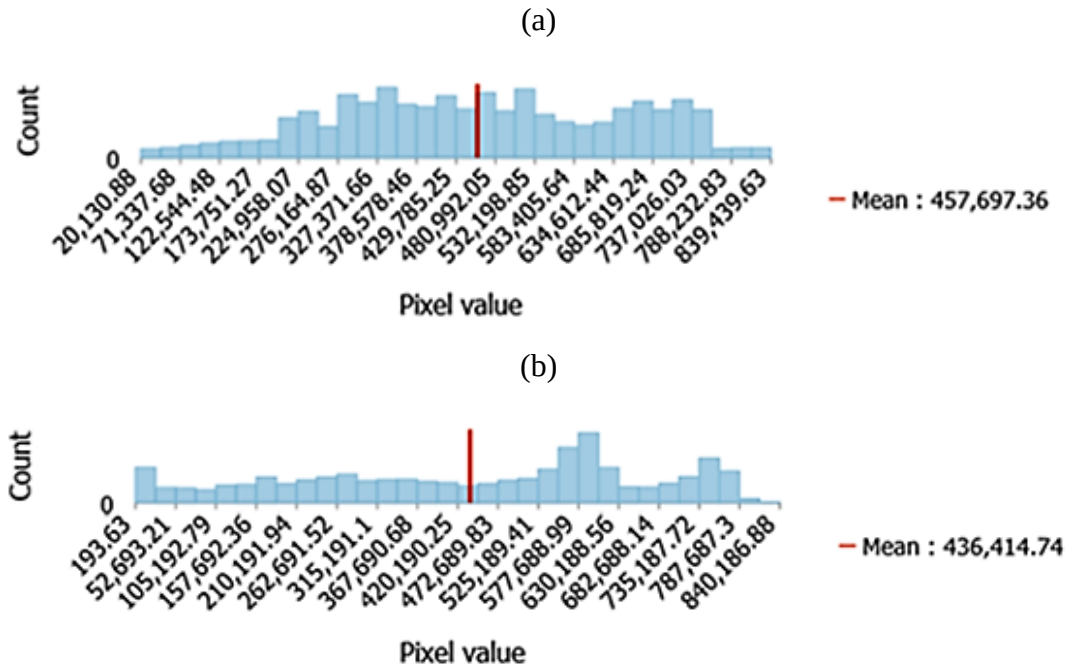

Figure 4-9: Distribution of number of pixels with certain Solar Irradiation values for (a) 1-meter resolution and (b) 0.25-meter resolution solar map. The pixel values are represented in $\mathrm{Wh/m^2}$.

The distribution shows that the 1-meter resolution map has lower ability to distinguish solar potential on the house, gives approximately equal number of pixels between 300 $\mathrm{kWh/m^2}$ and 750 $\mathrm{kWh/m^2}$. The high-resolution solar map distinguishes more clearly between well suited and bad suited areas for solar potential. For 0.25 and 1-meter resolution map, the average solar irradiation value is respectively 436 $\mathrm{kWh/m^2}$ and 458 $\mathrm{kWh/m^2}$ for 11 months. The low-resolution data is overestimating due to the lower availability to distinguish between north and south-facing roof, gives bigger areas with higher solar potential than expected. In addition, the shadowing effect from the forest in front of the south facing roof is not captured. It is important to be aware of this is an average value for the whole house which includes areas which is badly suited for installing solar energy systems.

Therefore, when considering installing a solar energy system it is possible to set a lower limit for solar irradiation in the solar map to investigate areas which is well suited for a solar energy system. In "Oslo solar map", a solar irradiation value above 800 kWh/m^2 per year is characterized as good, and a value above 900 kWh/m^2 is characterized as really good (Oslo Kommune, 2019). These values correspond to 732 kWh/m^2 and 824 kWh/m^2 for 11 months. Tromsø has far more days with rainy and cloudy weather than Oslo, gives fewer days with sunny conditions during the year. Therefore, a value of 700 kWh/m^2 could be set as a suitable lower limit in the solar map to investigate where to install solar energy systems on Tobias's house. This is done by selecting the 0.25-meter resolution map as basis, and thereafter classify the pixel values by different colors. Then it is possible to remove all colors with lower values than 700 kWh/m^2 and stay left with the suitable area.

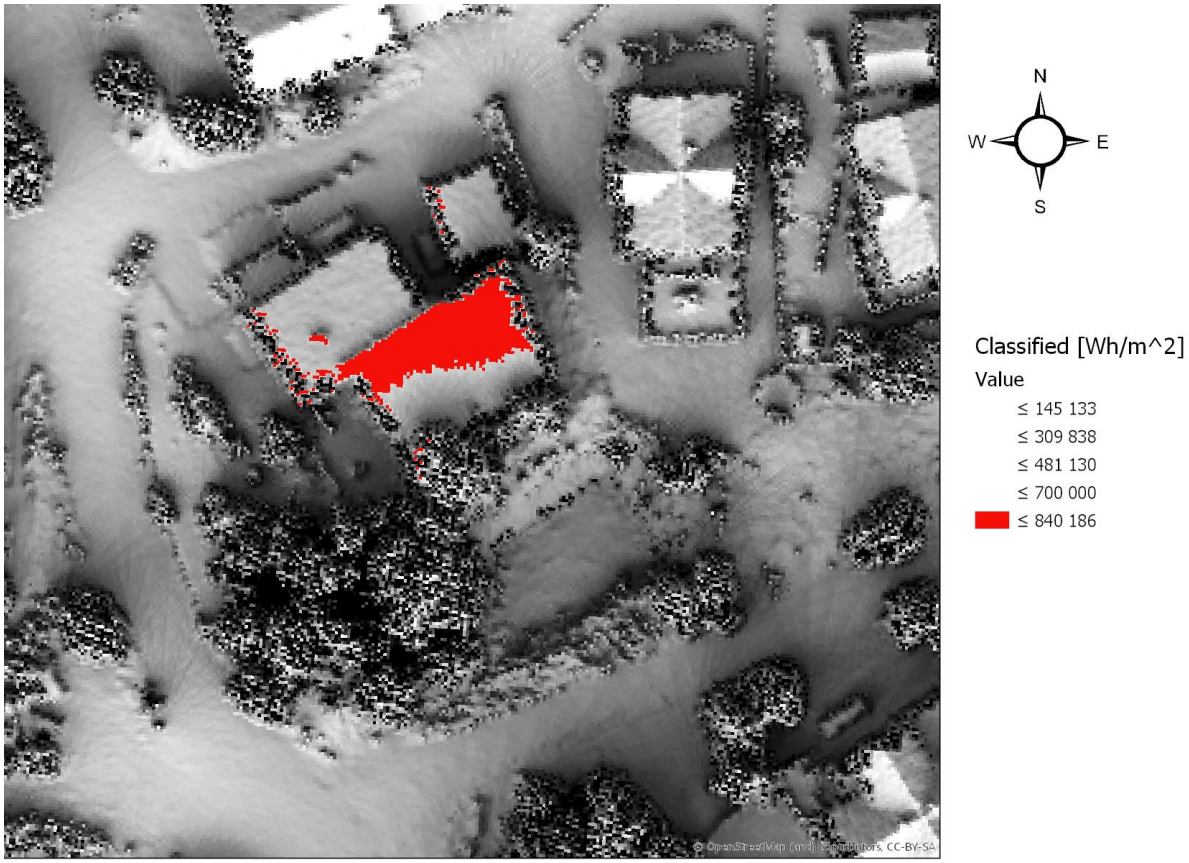

Figure 4-10: Suitable area for installing solar modules with a lower limit of 700 kWh/m^2

This map shows where solar irradiation on Tobias's roof is above the lower limit of 700 kWh/m^2 for 11 months, and the suitable area is on the uppermost part of south- facing roof above the area which being shadowed by the small forest. The map shows that this house has good conditions for solar energy system installed on the house if it is mounted on the correct area, as values between 700-840 kWh/m^2 is characterized as satisfactory values.

4.2.4 Case study: Potential yield of PV system using software PVsyst

Another way of calculating the solar irradiation potential on rooftops is by using the software PVsyst. For the thesis, a trial PVsyst version is used. PVsyst is a PV software package for the study, sizing and data analysis of complete PV systems (PVsyst, 2019). The theoretical solar potential was calculated using data from Meteonorm V7, which provides average monthly meteorological data for all locations on earth (Meteonorm, 2019). For this propose, the monthly data from Meteonorm is collected from a weather station on Langnes (close to airport) on Tromsøya. For the case study, the theoretical solar potential is calculated for a south facing roof with a 30° tilt. This house is addressed on Biskop Berggravs gate 33, close to Prestvannet on Tromsøya. The distribution of solar potential on tilted south facing roof and flat surface is given following figure.

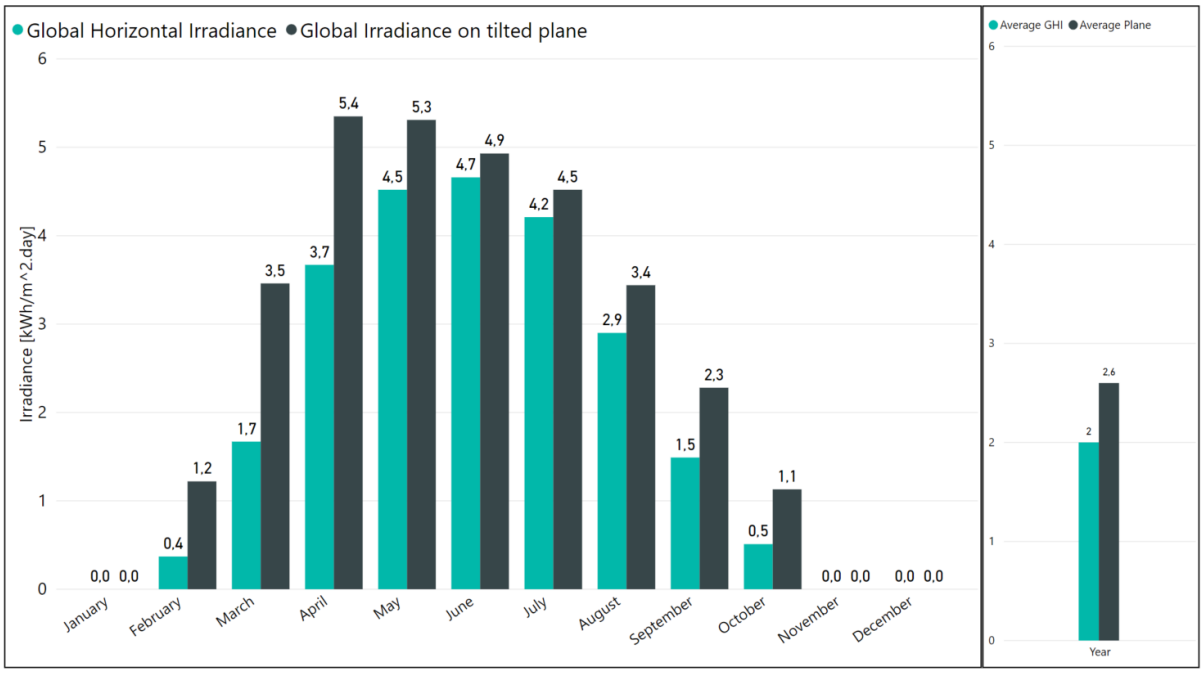

Figure 4-11: The monthly solar irradiation potential on flat surface and 30° tilted south-faced roof calculated in PVsyst software.

To validate the theoretical values, it is possible to compare these values against the solar map created in ArcGIS. Based on average irradiation of 2.0 [kWh/m^2. day] and 2.6 [kWh/m^2.day] for respectively flat surface and tilted surface, it is possible to find the average yearly irradiation and thereafter compare with the solar map. The average yearly theoretical solar irradiation calculated in PVsyst is 668 kWh/m^2 for flat surface and 868 kWh/m^2 for tilted surface. Notice that this is kWh for 11 months as the solar map in ArcGIS is calculated for 11 months due to lack of D&T values in December. The average yearly solar irradiation calculated in ArcGIS is approximately 660 kWh/m^2 and 850 kWh/m^2 respectively for a flat and tilted surface. This gives a deviation of 1.2% for flat surface and 2.1% for tilted roof.

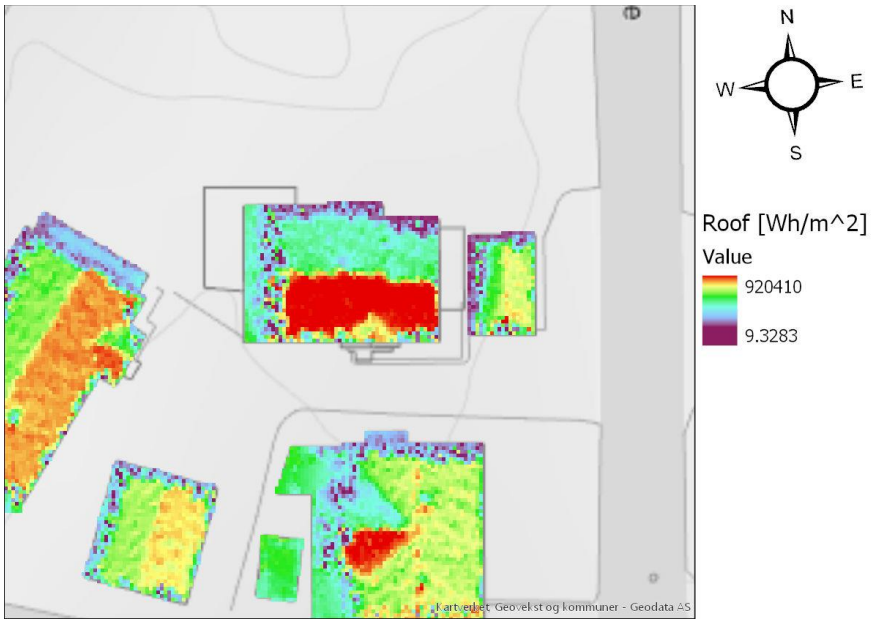

Figure 4-12: 0.25-meter resolution solar map of the solar potential on south-facing roof in case study

When specifying location, meterological data, roof tilt and orientation in PVsyst, several more information is provided in addition to solar potential. PVsyst is designed to give information about how much energy it is possible to generate with PV systems (thereby the name PVsyst). To simulate the energy yield, the PV system needs to be specified. Based on information about plane and façade for this house, the south facing roof was calculated to be 44.5 m^2. Given this area, a 7.1 kW_p PV system with standard modules and monocrystalline silicon cells with an efficiency of 17.57% was simulated in PVsyst. Based on solar irradiation potential, PV system specifications and roof area, the monthly and yearly system output is given as:

Table 4-2: Estimated monthly solar irradiation and PV system output for a 44.5 m^2 roof covered with solar modules with an efficiency of 17.57%.

	Gl. horiz. kWh/m^2.day	**Coll. Plane** kWh/m^2.day	**System output** kWh/day	**System output** kWh
January	0.00	0.00	0.00	0
February	0.37	1.22	7.33	205
March	1.67	3.46	20.75	643
April	3.67	5.35	32.06	962
May	4.52	5.31	31.78	985
June	4.66	4.93	29.53	886
July	4.21	4.52	27.06	839
August	2.90	3.44	20.61	639
September	1.49	2.28	13.65	410
October	0.51	1.13	6.78	210
November	0.00	0.00	0.00	0
December	0.00	0.00	0.00	0
Year	2.01	2.64	15.83	5 779

Based on monthly PV system output from this roof, it is possible to investigate if enough energy is produced to supply a typical home of this size with electricity. There are lack of online statistics showing average monthly energy use for households in Norway. Even the houses have approximately the same size, there is big varieties in monthly energy use. The energy consumption per household varies significantly according to building type, age, heating system, outdoor climate etc. Therefore, it is hard to give a precise estimate of how much electricity one household uses. However, a typical electricity use per year for one household is approximately 20 000 kWh for a detached residential house (Fjordkraft, 2019). Information from house owner of the building in this Case study shows that the electricity consumption was 15 000 kWh in 2018. This is a 150m^2 modern house which uses two air to air heat pumps for heating. Given the yearly electricity consumption, an average monthly energy use is possible to estimate. In (Realfsen, 2007) the monthly electricity consumption is estimated regarding to time of the year, vacations, average household, and a typical use of energy in daily life. The monthly energy use is given table 4-3:

Table 4-3: Monthly electricity consumption assuming a yearly energy consumption of 15 000 kWh (Realfsen, 2007)

Month	Weighting [%]	Consumption [kWh]
January	12.25	1 838
February	10.83	1 625
March	10.61	1 592
April	10.28	1 542
May	6.56	984
June	5.81	872
July	4.80	720
August	3.96	594
September	6.49	974
October	7.31	1 097
November	9.31	1 397
December	11.78	1 767
Year	100	15 000

The overview shows biggest consumption during wintertime because of cold climate which requires more energy to heating than during summer. The weighting column shows how many percent of 15 000 kWh is consumed per month. January, which is usually the coldest month, has highest weighting of 12.25%. July and August, which is associated with the warmest months of the year has lowest weighting. In addition, people are often on vacation and leaving the houses empty, which give lower energy consumption during summer. To compare the energy yield versus estimated typical electricity need, it is possible to make a figure showing the distribution of energy over one year.

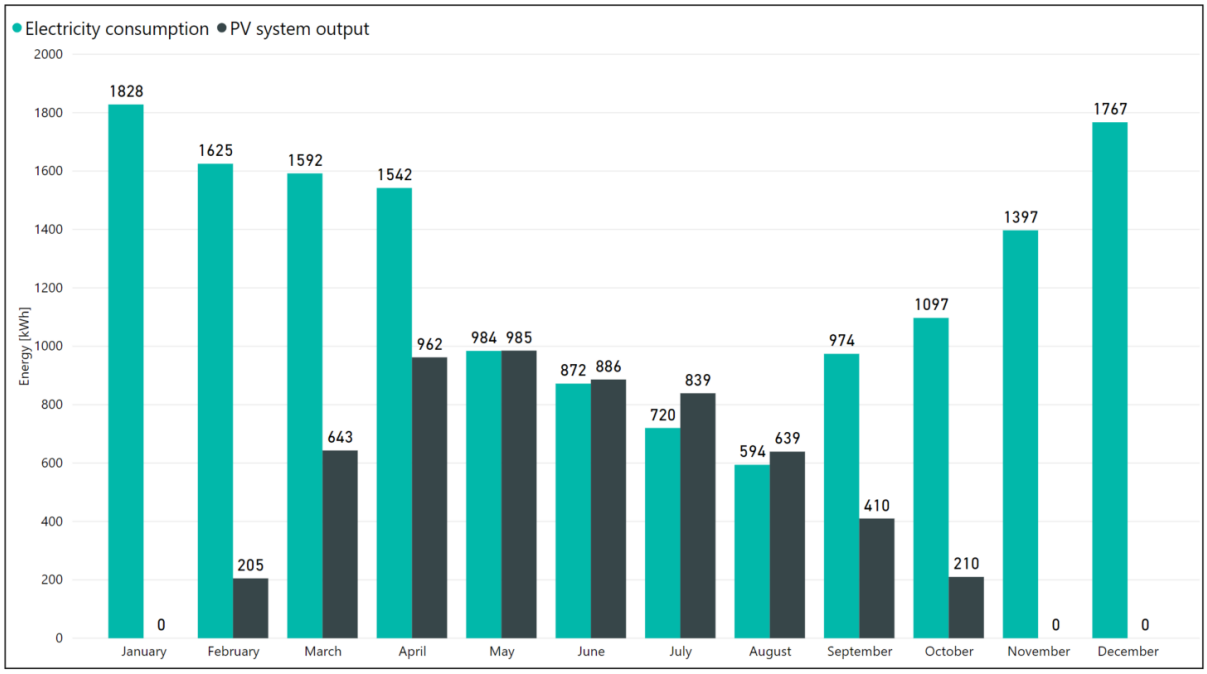

Figure 4-13: Distribution of energy consumption for an average household versus energy yield from the PV system for this case study

The figure shows that during summer period between May and August, the PV system output is enough to fully cover the electricity consumption of the household. This figure shows also that consumption and yield have opposite distribution, with highest energy consumption during winter when the production is lowest and vice versa. However, the energy consumption will vary significantly for different households. Newer houses with smarter energy solutions and lower energy leakage will need less electricity for warming than old houses.

The electricity consumption from houses is mostly due to heating. Especially in Norway, where the climate is cold during winter. When excluding the electricity consumption due to heating, the average electricity consumption is approximately 5 000 kWh per year (Energy Facts Norway, 2019). Instead of using own energy for heating up the building, heating could for example efficiently be provided by district heating. When heating is excluded, the electricity use in homes is approximately equal each month. This will give following distribution of power system output versus electricity consumption with heating excluded.

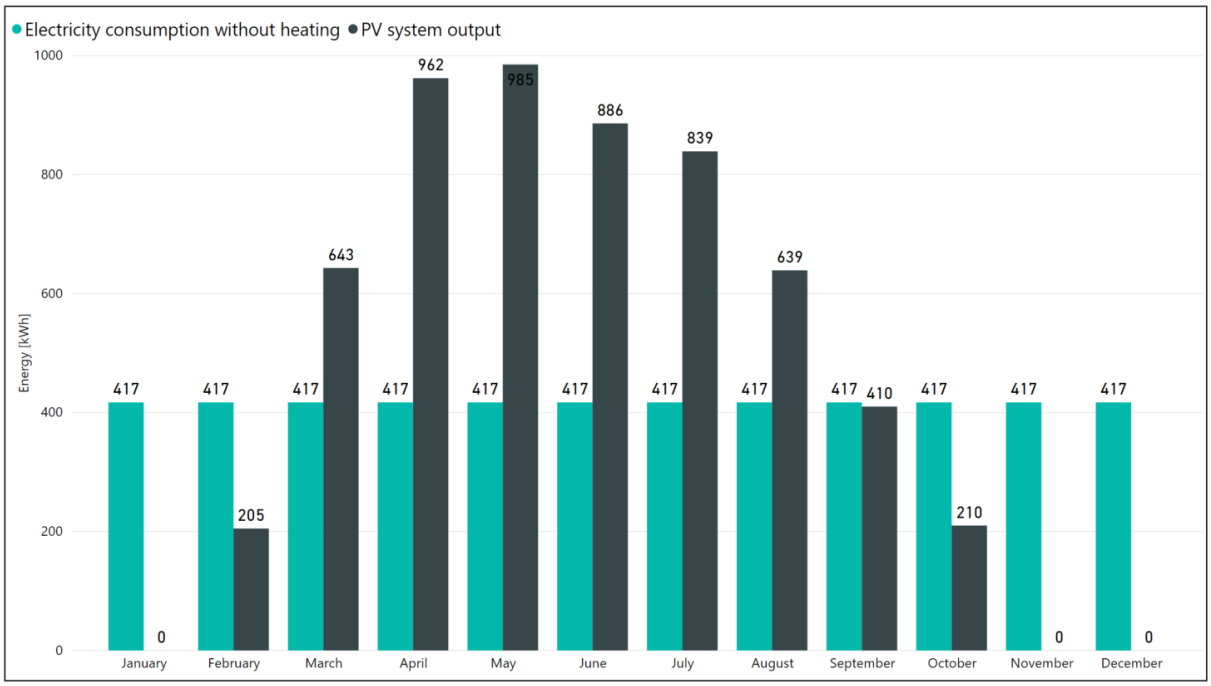

Figure 4-14: PV system output versus electricity consumption without heating. The yearly use of 5000 kWh is assumed to be flat, i.e. the consumption is equal per month.

From figure 4-14, the PV system output is far enough to cover the electricity consumption between March and August if heating of building is excluded. During winter between October to February, the energy yield is not sufficient, as expected due to low solar potential. Between November to January, the PV solar potential is non-existent due to Polar nights.

Solar fraction

The monthly aggregated SF values for PV energy yield versus the energy consumption is provided in tables 4-4. These values are defined in section 3.6, where SF describes how much of energy load is covered by generated PV energy. When SF=1, the electricity consumption for the building is fully covered by the generated PV energy. In the following table, green color represents months with positive energy balance where PV energy yield is higher than consumption, and red color represent months with negative energy balance.

The situations in figure 4-13 and 4-14 were heating of the building is included and excluded are provided to investigate monthly differences in energy balance.

Table 4-4: Aggregated monthly SF and LF values. The red color represents months with a negative energy balance. The green color represents a positive net balance where PV energy yield is higher than consumption.

Month	SF (Heating inc.)	SF (Heating exc.)
January	0.00	0.00
February	0.13	0.49
March	0.40	1.00
April	0.62	1.00
May	1.00	1.00
June	1.00	1.00
July	1.00	1.00
August	1.00	1.00
September	0.42	0.98
October	0.19	0.50
November	0.00	0.00
December	0.00	0.00

Table 4-4 shows a positive net energy balance between May-August with heating included, and a positive net energy balance between March- August where heating of the building is excluded. The higher SF value, the more PV solar energy could be used to cover energy load. The high SF value of 0.98 in September shows that the energy yield is almost enough to fully cover the electricity consumption with heating excluded. This shows that heating of buildings during winter and autumn contribute significantly to electricity consumption, which is expected as Tromsø has colder climate during this period.

4.2.5 Publicly available solar map

To make it possible for inhabitants on Tromsøya to investigate the solar potential from their buildings, the 0.25- meter resolution solar map is shared online. This was easily done via the "share" tab in ArcGIS Pro. This web map is available for everyone who want to use it, with no need for access via ArcGIS. To find the solar map, google "ArcGIS Online" and search for "High resolution solar map for Tromsøya". This will give several different solar maps for Tromsøya as a result. The results are either classified as "Layer", "Web Map", or "Map Package". Choose "Web Map" to investigate the solar map online without downloading. The "Layer" classification could be used to add this as a layer on an existing basemap on ArcGIS online. For further analysis and investigations, it is possible to download this map to ArcGIS pro by choosing "Map Package". This package is 10 gigabytes large and requires long downloading time.

In addition to a freely available solar map on a computer, this solar map is also available on mobile version. The methodology for investigating this map on mobile phone is by downloading the app "ArcGIS explorer", then click "Continue without user" after the app is installed. Again, search for "High resolution solar map for Tromsøya" to find the solar map.

The web map has some limitations compared to ArcGIS pro. The color bar which represents solar potential does no longer shows the solar irradiation value. Therefore, it is not possible to identify exactly how much solar irradiation you have per pixel on your roof just by clicking in the map as in ArcGIS pro. To investigate solar potential in web mode, the color on your roof must be your guidance. Yellow to red color represent high to very high solar potential, while green to blue color represent low to very low solar potential.

Therefore, this map suits as a good teaser, but if a more detailed analysis is required, ArcGIS Pro must be installed. The "Map Package" version of the solar map could be downloaded freely from ArcGIS online after installed ArcGIS Pro.

4.3 Total PV power output on Tromsøya

By using an average energy yield for different building types based on the solar map created in ArcGIS, it is possible to multiply the energy yield by the estimated average area for roofs and facades. Then, the total energy production on Tromsøya could be estimated if all buildings are covered with solar energy systems. However, it is reasonable to assume that all roofs and facades are not completely covered with solar panels. Therefore, PV production from houses is estimated for five scenarios with increased PV integration level. The integration level (percentage of suitable roof and façade area) is simulated for scenarios with 10%, 25%, 50%, 75% and 100% integration, as suggested by (Good, et al., 2018). The distribution of estimated monthly energy yield from PV solar systems mounted on all buildings on Tromsøya with 100% integration level is given in figure 4-15:

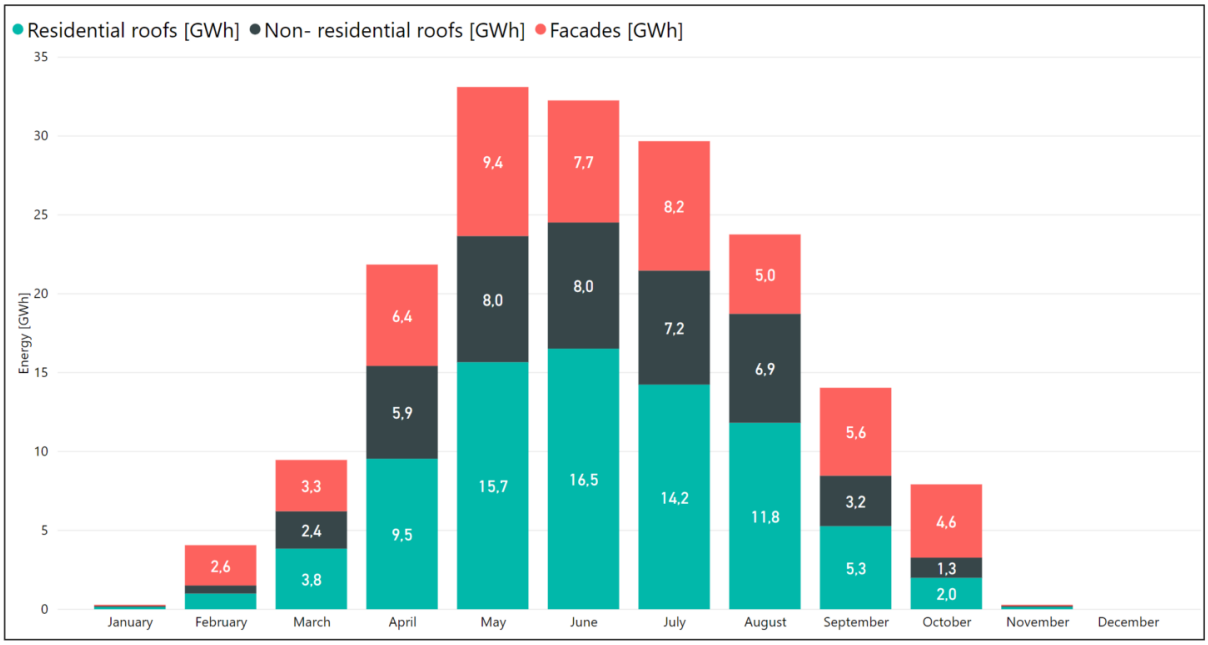

Figure 4-15: Estimated monthly energy yield from PV systems with 100% integration level on buildings on Tromsøya

The distribution shows that the energy production from façade is more stable during the year with higher relative production during wintertime than summer compared to residential and non-residential roofs.

In May, the production from facades is high relatively to the other modules. This occurs because of low Sun angle, giving optimal conditions for production from façade modules.

The estimated total energy yield from solar systems on Tromsø island with different integration levels are given in table 4-4.

Table 4-5: The yearly annual energy yield from PV installations on suitable areas on Tromsøya

PV int. level	Res. roofs	Non- res. roofs	Facades	Total
	GWh	GWh	GWh	GWh
10 %	10	4	5	19
25 %	24	9	12	36
50 %	49	19	24	92
75 %	73	28	36	137
100 %	97	37	48	182

If all buildings were 100% covered with PV systems, a total power production of 182 GWh for 11 months could be expected. The solar potential on Tromsøya calculated in ArcGIS was found to be best from residential buildings with sloped roofs. The residential roofs accounted for approximately 60% of total energy yield from roofs.

When the sun has high angle during summertime the flat roofs gives good power production, but over 11 months the tilted residential roofs give better power production in total. The relative solar potential from facades gives higher power production during winter due to lower sun angle and less exposure to snow coverage. The modules mounted on facades also makes efficient use of the reflected solar irradiation from snow on surface during winter. The facades account for 26% of total production from PV systems.

4.3.1 Case study: Electrical generation from PV versus electrical need from Cruise ship for one day in June

Based on given statistics from Tromsø harbor, the average cruise ship passenger capacity was 1 542 in 2018. The case study estimates the electricity need for a Cruise ship harbored in Tromsø for approximately 10 hours. The ship should have close to equal of the average passenger capacity. Then, the electricity generation from PV systems could be estimated to investigate the possibilities for supplying the Cruise ship with sustainable energy. The following case is presented: 17.06.2018, the cruise ship "VIKING SEA" visited Tromsø. This cruise ship has a maximum capacity of 930 passengers and stays in Tromsø from 08:00 to 18:00, i.e. 10 hours. Based on given information about electricity need given in table 3-10, an electricity consumption of 43 MW when ported for 10 hours could be chosen as a reasonable consumption for this ship.

The production data is received by analyzing a typical summer day in Tromsø in June. The weather statistics from June 2018 is received from "Yr", a weather forecast service (yr, 2019). The statistics for June show many days with weather as rain and cloudy conditions, but also days with sunny weather. On 17. June 2018, the temperature ranges from 7.1°C during the night to 14.1°C at maximum on daytime. The weather varies from cloudy with some rain during night to sunny conditions at afternoon.

As the solar map created in ArcGIS gives monthly average solar irradiation values and not daily values, production values from solar energy system on roof of Realfagsbygget is used. For this case study, production data from 40- and 20-degree modules is associated with residential and non-residential buildings respectively (assume that 20- degree modules are mounted on flat non- residential roofs). Production data from façade is the same for both residential and non- residential buildings. Production data for each module is given in the following figure:

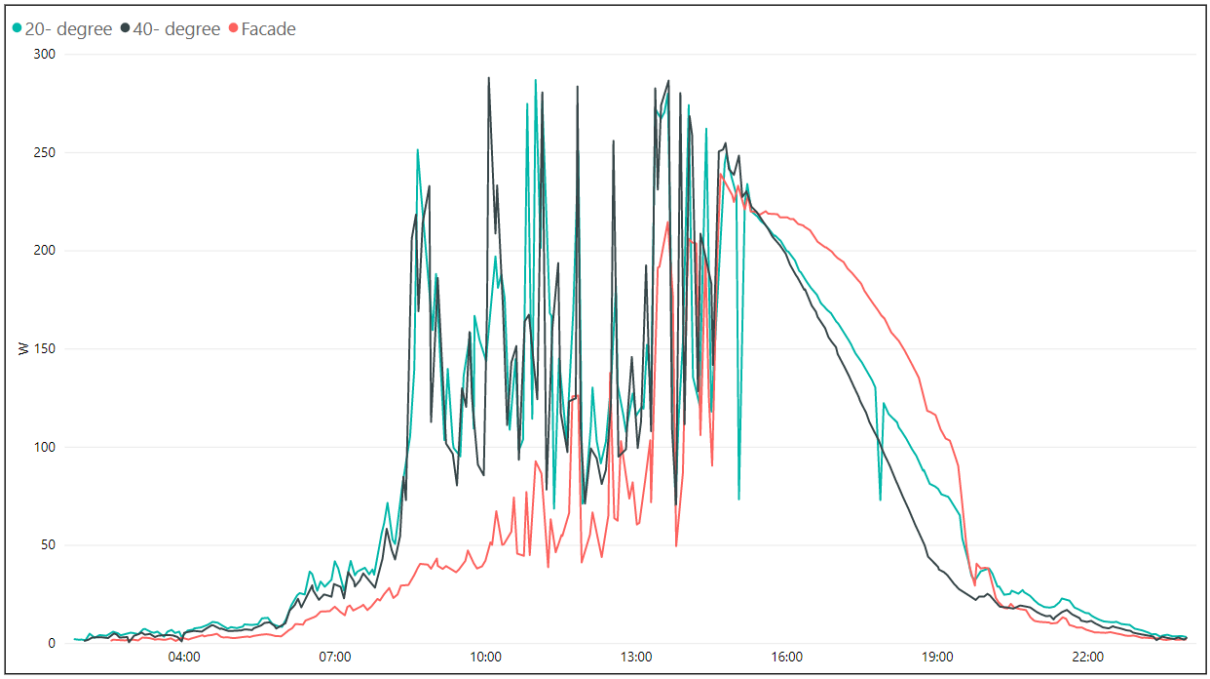

Figure 4-16: Power production from bifacial PV modules 17. June 2018

This figure shows low irradiation during night until 08:00, then the production grows rapidly to its maximum value around 10:0 to 14:00 before decreasing again. As the façade modules is facing south-west, the modules do not receive much irradiation before 14:00. Notice the stability of production from the façade module during afternoon as the sun is low and facing more directly towards the façade module. The average total production for each module from 08:00 to 18:00 is given as:

Table 4-6: Production from PV modules on roof of Realfagsbygget

Module	**20°**	**40°**	**90°**
Production [Wh]	1628	1573	1375
Production [Wh/m^2]	995	961	840

Where the production per module has been divided by the module area of 1.637 m^2 to get production per square meter. The production from these modules is far from enough to supply the Cruise ship with enough energy, therefore PV systems must be integrated on several buildings on Tromsøya to reach 43 MW. Assume a scenario where 25% of each building on Tromsøya are covered with PV modules, both on roof and façade. Multiplying production per

square meter with estimated solar-architecturally suitable areas of roofs and façade given in table 3-7 would give total production

Table 4-7: Total production from PV systems 17.06.2018 for all buildings on Tromsøya from 08:00- 18:00 with 25% integration level

	Non-res. (20°)	Res. (40°)	Facade	Total
Total production [kWh]	86 744	186 472	88 584	361 800

This is more than the electricity consumption of 43 MW needed from the Cruise ship. Therefore, it is possible to investigate how many buildings covered with PV systems are needed to supply the cruise boat with enough electricity. Instead of assuming all buildings are covered with solar energy systems both on façade and roofs, a scenario where only non-residential buildings are covered with PV system on roofs are performed. To supply the cruise ship with totally 43 MW, the following area with PV systems on non-residential roofs are needed

$$\text{Roof} \cdot \ 995 \left[\frac{\text{Wh}}{\text{m}^2}\right] = 43\,000\,000\ [\text{Wh}] \rightarrow \text{Roof} = 43\,216\ \text{m}^2 \qquad (3.6)$$

The average roof area for a non- residential building as a factory building or production hall is approximately 1 100 m^2 (Bloch, 2002). Therefore, approximately 43 non-residential roofs at Tromsøya need to be covered with PV modules with 20° tilt to supply the Cruise ship "VIKING SEA" with enough electricity from 08:00-18:00 in Tromsø harbor with this weather conditions.

4.4 Total monthly PV generation versus electricity need

To investigate the possibility for supplying all cruise ships visiting Tromsø with the total power generated from all PV systems on Tromsøya, a scenario with 10% PV integration level is performed. The production includes total production from residential, non-residential roofs and façade. The monthly PV yield versus monthly electricity need is given in the following figure:

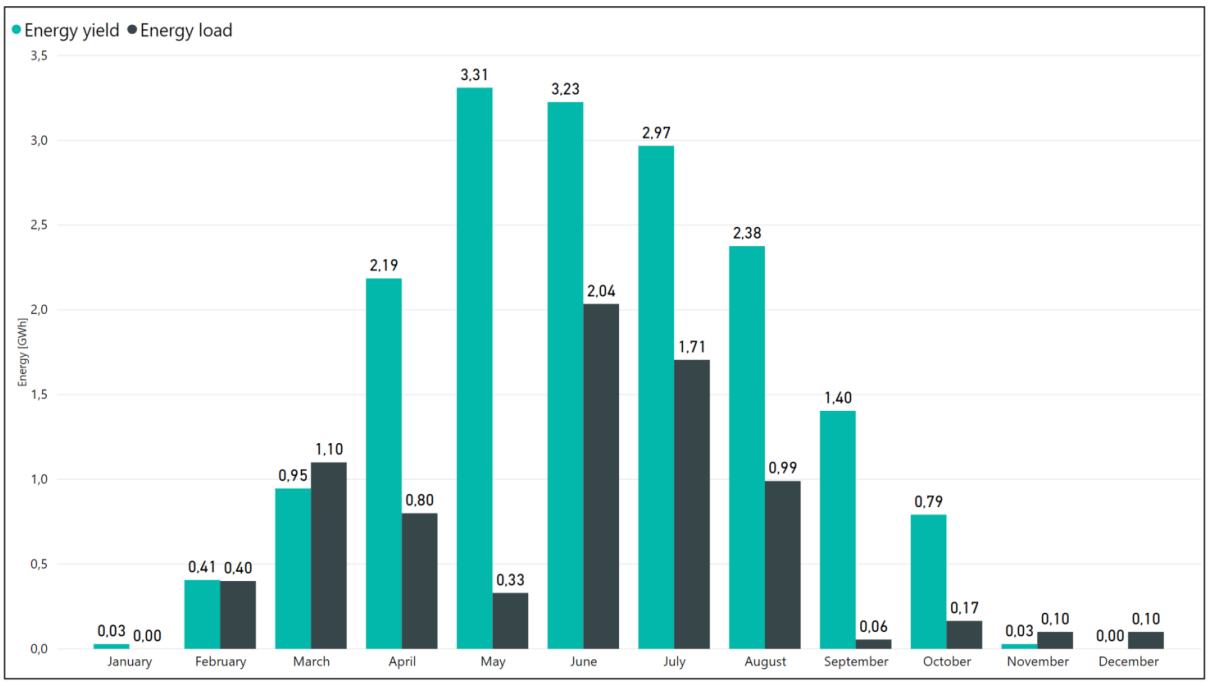

Figure 4-17: Monthly Energy yield in GWh from PV systems with 10% integration levels versus energy need from Cruise ships

Figure 4-17 shows that generated energy from PV systems with 10% integration scenario are enough to cover the cruise ships visiting Tromsø during tourist season in the summer. In winter months as March, November and December the energy load is higher than energy yield. It is important to notice that in this scenario, all the power generated from PV systems is only used to supply the Cruise ships. Nothing is used to supply homes or electrical vehicles. It is also important to notice the generation per month assumes that the PV systems is operating continually with no down time or errors. Therefore, the PV systems will generate electricity when there are no Cruise ships visiting Tromsø. For example, in May 2018 where

the difference is most significant only six ships is visiting Tromsø, and this is the month with greatest energy generation from PV systems. The SF values with 10% integration level is given in the following table as:

Table 4-8: Monthly aggregated SF for 2018 in Tromsø. Green color represents a positive balance between energy yield from PV systems and Cruise ship energy load.

Month	SF
January	1.00
February	1.00
March	0.86
April	1.00
May	1.00
June	1.00
July	1.00
August	1.00
September	1.00
October	1.00
November	0.30
December	0.00

Table 4-8 shows a positive aggregated energy balance for all months except from March, November and December. The high SF value of 0.86 in March shows that generated PV power is almost enough to fully cover the energy consumption from Cruise ships. As there is produced more energy than needed for Cruise ships during summer, Tromsø municipality will have surplus energy which could be used to supply other industries as well. In the thesis, only cruise ships have been focused on, but Tromsø harbor has also several other types ships visiting Tromsø during the year, and energy from PV systems could also be used to serve these ships with electricity.

4.4.1 Economic benefit for selling PV generated power to Cruise ships

As there is enough generated power from PV systems to supply Cruise ships visiting Tromsø during tourist season, it is possible for Tromsø municipality to sell the produced energy to the cruise ships, and thereafter earn an economic benefit by having installed PV system. The electricity price in Norway has been stable since 2014 but it almost doubled from 2017 to 2018, with an average spot price of 24 [øre/kWh] to 41 [øre/kWh]. The price is expected to continue to rise in the future, and in January 2019 the price was 50 øre/kWh compared to 30 øre/kWh in 2018 (LOS, 2019). The monthly electricity price is given in table 4-9:

Table 4-9: Development of monthly electricity price in Tromsø. The price is given in øre/kWh (LOS, 2019).

Month/Year	2019	2018	2017	2016	2015	2014
January	50.10	30.00	23.43	26.78	27.23	27.57
February	44.13	36.14	24.69	18.06	24.48	25.42
March	39.98	43.00	22.10	19.75	21.87	22.59
April	39.70	38.09	22.34	19.45	21.64	22.72
May		34.10	24.14	20.82	19.10	28.13
June		42.82	22.01	23.14	11.68	24.64
July		48.18	18.47	24.21	7.84	24.60
August		48.25	19.34	24.09	10.78	27.38
September		46.34	25.87	22.97	18.34	29.77
October		41.74	26.55	25.30	18.87	27.09
November		45.04	30.60	29.02	20.96	26.96
December		49.64	29.06	25.23	16.36	28.35

This price is excluded Value added tax (VAT) and grid rent. Private households in Northern-Norway is exempt from VAT, therefore the electricity price in Tromsø should be excluded VAT (Troms Kraft, 2019). For public buildings other regulations apply. The grid rent is an extra tax and varies between types of households. For a typical private household in Tromsø, the grid rent is 172 EUR/year (Troms Kraft, 2019). However, this will vary depending on electricity supplier. The electricity prices expected to continue to rise, which is isolated a reason for selling the generated electricity from PV systems to e.g. Cruise ships. Based on

monthly energy load from Cruise ships given in table 3-11, an estimation of the economic benefit could be performed. The following total price in Euro (EUR) is given in table 4-10 as:

Table 4-10: Total price in EUR based on monthly electricity price and Cruise ship traffic.

Month	Total Price [EUR]
J-18	0
F-18	14 766
M-18	48 315
A-18	31 126
M-18	11 494
J-18	89 008
J-18	83 909
A-18	48 792
S-18	2 603
O-18	7 035
N-18	4 601
D-18	5 070

The total price is calculated by using a Norwegian krone (NOK) to EUR exchange rate where 1 EUR is 9.79 NOK. If the energy needed for supplying Cruise ship traffic produced from PV systems on rooftops on Tromsøya is sold to marked prices, this selling will give incomes of approximately 89 008 EUR at it most in June. Over several years with increasing electricity prices and Cruise boat traffic, there could be some economic benefit from selling PV generated energy. An example could be e.g. a local actor organizing the production and marketing, where Tromsø municipality organization could benefit from this. Section 5.3 includes a short discussion of actors that could be included in an actual local system. In addition, based on total electricity generation from PV systems, there are more surplus energy which could be sold to other industries.

5 Discussion

This thesis has created a solar map for Tromsøya based on a similar methodology as in a former master thesis by (Falklev, 2017). The former thesis did only create a 1-meter resolution solar map, which was not used for PV energy yield investigations. This thesis further developed the methodology by creating a 0.25-meter resolution solar map where rooftops on all buildings has been highlighted to investigate PV system potentials. The differences between the resolutions has also been investigated, where weaknesses of the 1-meter resolution solar map has been discussed. This is the first high-resolution solar map for Tromsøya ever made, and it could be used as a basis for PV solar energy investigations in future projects. The process of creating this solar map required access to a computer with high computing capacity which was provided from Rolf Andersen at UiT. The solar map was published online as validation of the solar map shows correct radiation values and the solar potential on each rooftop is easy to visualize. This web map is available for any purposes and is also published as a mobile app version for smartphones.

The calculation of solar-architecturally suitable area for roof and façade on Tromsøya was based on methodology in (Good, et al., 2018), where number of buildings in Tromsø municipality was provided from Statistics Norway (SSB). Number of buildings was estimated by assuming that 60% of all buildings in Tromsø municipality is on Tromsøya. The total energy yield from PV systems on Tromsøya was thereafter compared against electricity load from Cruise ships visiting Tromsø harbor. The Cruise ship traffic statistics was provided from Tromsø Harbor, and electricity load regarding to maximum passenger capacity was provided from Trond Sikveland-Port Area Manager in Port of Kristiansand.

This chapter provides a discussion of the methodology and results in this thesis. Chapter 5.1 discusses the methodology for creating the solar map in ArcGIS, uncertainties and possible errors connected to the final map. In section 5.2, the uncertainties regarding to mapping the electricity generation based on total number of buildings on Tromsøya is discussed. In this section, the possible errors of the statistical estimations are analyzed. Finally, section 5.3 discusses possible sources of errors when estimating electricity consumption from Cruise ships.

5.1 Solar map in ArcGIS

The solar potential on Tromsøya was created in ArcGIS. It visualizes different solar potential from both rooftops and surrounding terrain. This solar map is validated against pyranometer data and estimated solar potential in PVsyst. The result shows high agreement with acceptable deviation which means that the solar map could be used as a basis for investigating solar potential. The different resolutions of 0.25- and 1-meter are tested against each other to identify if there are significant differences in result. The comparison between high and low resolution shows that the low-resolution solar map has less ability to identify shadowing effects and correct angles on roof because of lack of datapoints. Therefore, the 0.25-meter resolution solar map should be used as basis for investigation of solar potential on different houses.

5.1.1 Limitations and uncertainties

Creation of the solar map in ArcGIS was by far the most time-consuming process during this thesis. Several tools in ArcGIS Pro was used to achieve the result. The LiDAR dataset with both 1-and-0.25-meter resolution was successfully imported to the software, but problems occurred when creating the map. Several splitting methods of the original raster layer covering the whole island was used to try to reduce the calculation time. The most efficient method was to divide the raster layer covering the whole island into as many subareas as possible, and then run several calculations simultaneously. With access to server computer based in Amsterdam, 15 calculations could be performed at the same time. However, this requires the need to be accurate in calculating all areas in the right order. For the 0.25-meter resolution map with 45 different areas, each area must be calculated for each month of the year minus December, with different temporal periods with corresponding D&T values. This process includes 45 areas times 11 months which was calculated separately, giving total 495 operations, which needed to be calculated correctly. Thereafter, all these areas must be merged together again to make a map covering the whole island. However, validations of the final map show that this process has been done correctly as the solar map shows correct values. An even faster method is to split the LiDAR raster layer to even smaller areas, but more layers makes the risk for mistakes during the process higher.

Area Solar Radiation tool

The “Area Solar Radiation” tool in ArcGIS is based on Python codes which is a general-purposed programming language. These codes are possible for developers to modify in a way which could make the calculations faster. For this thesis, this opportunity was not considered as the process for modifying the Python codes would be very time consuming itself. In worst case, modifications of the code will cause errors when calculating the solar radiation. However, if high resolution solar maps should be created more often in the future, modifying the python codes could be necessary to make the process more efficient.

In addition to calculate on smaller LiDAR areas and modify python codes, the “Area Solar Radiation” tool has several input parameters which could be changed to increase the calculation efficiency. Except from input raster layer, latitude, time configuration and D&T values, all other input parameters were chosen to be default. The “Area Solar Radiation” parameters are divided into two different sectors. Topographic parameters and radiation parameters. Topographic parameters are divided into “Z factor”, “Slope and aspect input type” and “Calculation directions”. The z-factor adjusts the units of measure to avoid wrong results when z units are in feet’s and x,y units are in meters. The slope and aspect input type are set as “From the input surface raster”. In addition, number of calculations directions must be specified. The default value is 32, which is adequate for complex topography. The topographic parameters are all set to default as changing these parameters would most likely lead to wrong results. The Radiation parameters are categorized into Zenit and Azimuth divisions which specifies number of divisions used to create sky sectors in the sky map. These parameters are set to 8 as default value. The radiation parameters are categorized into “Diffuse model type” and D&T values. D&T values are specified for each month, and the diffuse model type is chosen as default which is uniform overcast sky. This input parameter assumes that the incoming diffuse radiation is the same from all sky directions (Esri, 2019). Faster calculations could be achieved by changing some of the input parameters as for example Zenith and Azimuth divisions, but this would most likely occur wrong and less accurate results and therefore default values were chosen to use for all input parameters.

LiDAR dataset

One error is easily identified after the solar map was created for 0.25-meter resolution. The LiDAR dataset received from geodata is not up to date, and the latest available dataset is from 2014, which means that all buildings built after 2014 are not a part of this solar map. Some examples are the new Tromsø harbor building which was finished 2017 and the new swimming pool on Tromsø skiing stadium. Once a new and updated LiDAR dataset has been created, it is possible to create a new solar map which also will include new buildings.

Figure 5-1: Tromsø skiing stadium, the new swimming pool is not a part of the solar map as the LiDAR dataset was created in 2014.

5.2 Electricity generation from PV systems on Tromsøya

The electricity generation potential from PV systems on Tromsøya was achieved by using the solar map combined with estimated roof and façade area of buildings on Tromsøya. The production was compared against estimated values in PVsyst performed by (Good, et al., 2018). The comparison shows good agreement between the solar map created in ArcGIS and estimated values in PVsyst.

The result shows high production and could be used for supplying industries releasing greenhouse gases with renewable energy. Different scenarios with 10%, 25%, 50% and 100% integration factors were used as basis for mapping total production from Tromsøya. Total energy yield with 10% integration factor was compared against estimated electricity need from cruise ships when ported in Tromsø harbor. The energy yield with 10% integration factor was enough to supply cruise ships each summer month in 2018.

5.2.1 Limitations and uncertainties

The estimated values for electricity generation from PV systems on Tromsøya is created by using statistical data on building ground floor area combined with rule-of-thumb utilization factors for shading, obstacles, orientation, and unstable areas on roofs and facades. It does not exist statistics for gross building area on Tromsøya. The gross building area in Tromsø municipality was estimated based on same methodology as in paper by (Good, et al., 2018), where the number of buildings in Tromsø municipality was received from SSB and thereafter multiplied with average areas for different building types. For Tromsøya, an educated guess was performed to find the ground floor area of buildings. Based on number of inhabitants, 60% of all buildings in Tromsø municipality were assumed to be located on Tromsøya. Assuming 60% of all buildings in Tromsø municipality is located on Tromsøya is a rough estimate. For a more accurate estimate, the number of buildings on Tromsøya should be received upon request from SSB. This was not done in this thesis as the total production yield should be compared against paper by (Good, et al., 2018). The ground floor area on individual buildings can vary significantly, even if the buildings are of same type. This could be a source for potentially large errors in estimations of façade and roof area. For example, industrial

buildings and warehouse which is categorized as code 2 in table 3-9 has an estimated average gross building area of 206 m^2, but the recycling warehouse at Remiks environment park has a roof area of approximately 3000 m^2. There are not many of these examples on Tromsøya, but a few can potentially cause big errors.

When the estimations of roof and façade area are performed, a good estimation of tilt angle and orientation for roofs on residential buildings are hard to perform, even when the solar map is created. In this thesis, an average potential of 820 kWh/m^2 for residential roofs was chosen based on investigations of several houses regarding to roof tilt and orientation. However, far from all houses on Tromsøya was investigated, therefore a qualified guess was made. If only a few houses are investigated, the solar map is well suited for accurate estimations of solar potential. The does only consider solar energy systems on buildings. Solar energy systems mounted on non-building areas are not considered and could be an area of interest for other studies.

As the solar map does not have the ability to investigate solar irradiation in 3D, the solar potential on facades was not possible to calculate. Therefore, the solar energy system on Realfagsbygget at UiT was used to receive production data. This is also a rough estimation, as this façade is standing still facing 39° south-west. This is not the situation for all houses on Tromsøya. In addition, the production values are received from bifacial modules which gives higher production than standard modules. However, due to great amount of low sun and reflection from surrounding snow, bifacial modules should be considered when setting up PV systems in Tromsø.

In case study 4.2.4, the total power production from a PV system covering 44.5 m^2 on a south-facing roof was compared against electricity consumption. The SF values shows a positive net energy balance between May-August and March-August with heating respectively included and excluded. However, the SF values are aggregated monthly values and will varies significantly if hourly values are used instead. For example, for a temporal period of 24 hours, the SF values will most likely show a positive net energy balance during the day, and negative energy balance during nighttime. However, this could be solved by using battery packages to store surplus energy during daytime, which could be used to heat the building or charge the electrical vehicle at night.

5.3 Electricity need from Cruise ships visiting Tromsø

Greenhouse gas emissions, as well as emissions having local impacts on air quality, from Cruise ships is a highly relevant and debated field in today's climate change-and local environmental focuses. Instead of the ships emitting e.g. greenhouse gases by keeping the engines running while in harbor, an idea of supplying cruise ships with shore power from solar energy systems was presented. Solar energy systems could be local coming to organization of the production as well as opportunities for securing benefits from the production for local organizations or the owner of the production units. Therefore, a simple economic calculation was performed to investigate the economic benefits by selling PV solar energy based on electricity price and Cruise ship traffic.

The statistics of number of boats that visiting Tromsø during the year is freely available online at Tromsø harbor's website. In total, 8 738 boats visited Tromsø in 2018. The boats are categorized in loading ships, speedboats, cruise ships, fishing vessels, research vessels, offshore boats, leisure boats and other types. Statistics of monthly cruise ship traffic was received upon request at a meeting with marketing Manager Harriet Willassen at Tromsø harbor. This statistic does also include how long each boat was visiting Tromsø. Information about electricity load based on type and passenger capacity for Cruise ships was provided from Trond Sikveland at Port of Kristiansand.

5.3.1 Limitations and uncertainties

The given information about energy load from Cruise ships shows that even when the boats has approximately same size, the electricity consumption varies drastically. Therefore, it is hard to perform an estimation with high accuracy. The big deviation in energy consumption occurs due to differences in age, construction type, motors, energy efficiency etc. Newer ships are planned and being built to reduce energy consumption, emissions etc.

The resulting balance between yield and load shows that the energy yield from PV systems is enough to supply cruise ship traffic for all scenarios during tourist season at summer. There are several factors which needs to be considered when investigating the balance between electricity load and supplying. For example, if a large cruise ship with 4 000 passengers are

visiting Tromsø one day in June and arrives at 22:00 pm before leaving at 08:00 am next morning, the production from PV systems will not be enough to supply this ship directly. Therefore, big battery packages must be introduced to store the produced surplus energy during daytime when energy yield is high. A well-suited energy storage system regarding to PV energy storage, is production of hydrogen which being used as a battery for long term energy storage. This solution will however require huge investment cost, areas, optimal location etc. ASKO, a food supplier in Norway has a terminal outside Trondheim where a complete solution has been installed. PV systems on the terminal produces hydrogen which being stored on tanks and being used to goods transport out to shops etc. ASKO received approximately 19 million NOK in grants for this project from Enova (Sikveland, 2019). Enova helps other companies financially with renewable and climate-friendly projects (Enova, 2019). If energy is stored on tanks ready to supply boats with PV solar energy, shore power facilities must be available. Currently Tromsø harbor does not offer these facilities. Today, only Kristiansand offers shore power to ships in Norway. Bergen harbor is in process with it, and several other harbors are expected to invest in these facilities in the future. On the other hand, the cruise ships do also need to have the possibility for connecting to shore power. From information given from Port of Kristiansand in table 3-10, only 9 of 17 ships has this facility.

The economical calculation is very simplified. Many factors as transportation of electricity from houses to ships, eventually extra taxes and several political questions are not considered when calculating how much Tromsø municipality could earn when selling the produced electricity. The electricity could either be sold directly from inhabitants, or via power companies such as Troms Kraft. If the electricity is sold directly from inhabitants, all inhabitants must be connected to grid which lead to shore power supply facility in Tromsø harbor. Another possibility is that inhabitants could sell surplus energy to power companies in Tromsø municipality as Troms Kraft. Troms Kraft could thereafter sell the surplus electricity to Cruise ships. In addition, cost including energy solutions as smart grid systems and battery storage are not considered in this thesis. A scenario could be that Tromsø municipality covers the installation cost when inhabitants are investing in PV systems. Thereafter, when the surplus energy is being sold to Cruise ships, Tromsø municipality will earn some part of the economic benefit.

6 Conclusion

6.1 Summary

The solar energy potential on Tromsøya has been evaluated by creating a solar map with solar analyst tools in ArcGIS. The resulting solar map shows solar potential on both terrain and rooftops which has been highlighted in the original map. The solar map was calculated for two different LiDAR raster datasets, a low-resolution dataset of 1-meter and a high-resolution dataset of 0.25-meter. To compute the high-resolution dataset, access to a server in Netherland was given. Because of long processing time, several different methods were performed to find the most efficient process. The solution was to calculate on small areas and then merge all areas together to form a map covering the whole island. Once the final map was completed, the high- and low-resolution solar maps was compared to investigate possible differences.

The resulting solar map shows high accuracy with a relative RMSE of 0.07 W/m^2 when compared to averaged pyranometer values from Holt weather station. The investigation shows that the low-resolution map has lower ability to discover shadowing effects from surroundings, and differences in solar potential for north-and south-facing roof was lower than expected. These errors occur because of lack of datapoints, which give lower ability to discover surrounding effects and the tilt of the roof is assumed to be “flatter” than actual for low-resolution dataset. Because of this, the high-resolution solar map was chosen as the basis for investigating solar energy potential. In the resulting high-resolution solar map, the solar potential on rooftops are easily identified by looking at the color bar. Because of high usability and accuracy radiation values, the solar map was published online, where anyone who might be interested can identify the solar potential from specific buildings. This high-resolution solar map is the first ever made of Tromsøya and could be a valuable asset for future PV solar energy projects.

The potential for PV solar energy systems was evaluated by multiplying solar energy potential per square meter with average gross building areas. The gross building areas were combined with utilization factors for roof and facades to estimate solar-architecturally suitable areas for PV installations. The total energy yield was estimated for different

integration levels of PV in urban environments. The energy yield shows good production from PV systems, especially during summer months, as expected. The energy yield for different scenarios was compared against energy load due to Cruise ship traffic in Tromsø harbor in order to investigate the possibilities for supplying the ships with renewable PV solar energy when harbored in Tromsø.

The electricity need from Cruise ships can be covered by the total energy yield from PV systems with 10% integration factor during tourist season at summer. The monthly aggregated SF values shows a positive energy balance between energy load and energy yield for all months, except from the winter months March, November and December. The month with highest total energy yield from PV systems on residential, non-residential roofs and facades, is May. If neglecting PV systems on facades, June has the highest production. The high production from facades during May compared to June and July is due to lower sun and surrounding snow which reflects towards facades and gives better production. Figure 4-15 shows that production from facades are high during February-May and September-October relatively to residential and non-residential roofs.

The statistics for Cruise ship traffic was obtained upon request from Tromsø harbor. As the statistics from Tromsø harbor did not cover electricity consumption, information was provided from Kristiansand harbor (Sikveland, 2019). The estimation method for monthly consumption was done by combining energy load regarding to passenger capacity with average visiting time for winter and summer periods. A case study for one day during June 2018, shows that approximately 43 factory buildings must be covered with solar modules of 20° to supply a cruise ship directly with electricity from PV systems.

Based on electricity yield versus consumption, an economic benefit calculation was performed. Based on electrical spot price given in øre/kWh and electricity need in kWh from the ships, it was possible to estimate how much Tromsø municipality could earn by selling renewable electricity to the tourist industry. The calculations show that Tromsø municipality could earn some economic benefit by selling electricity. Investment of PV systems in Tromsø could therefore be a good idea as the electricity price is expected to rise and the cost of PV systems are expected to decrease in the future.

6.2 Further work

During this thesis, a solar map covering Tromsøya has been created which later has been used as a basis for investigating energy yield based on statistics for ground floor building areas. There are several possibilities for further work based on the methodology and results in this thesis. Some suggestions are:

- **Update solar map**
  The LiDAR dataset which has been the basis for creating the high-resolution solar map is from 2014. The map will become more and more outdated the more buildings being built. As soon a new updated high-resolution LiDAR dataset is available, a new solar map should be created to include new buildings.

- **Modify Solar Radiation tool in ArcGIS**
  Creating the solar map is time procuring and inefficient, especially for higher resolutions. A future assignment could be to immerse into the python code the "Area Solar Radiation" tool is based on. If it's possible to reduce the processing time, a high-resolution solar map could be created for Tromsø municipality.

- **Create a better online freely available solar map**
  The publicly available solar map created in this thesis suits good as a teaser. The map is available for anyone who would like to investigate the solar potential, but the web map has some limitations which should be improved. A suggestion is to create a solar map as Oslo solar map, which gives the user a lot of information about solar potential from its own house. The process of creating a better online solar map has already started in collaboration with Rolf Andersen at UiT. Creating a suitable online map will most likely need economic resources. The website could be made in collaboration with institute for computer science at UiT. The resulting website would however be useful in many situations for solar potential investigations at UiT.

- **Revising mapping of building areas**

  Instead of using rough estimates about building areas from SSB, a more detailed investigation should be performed to get a more accurate result. In addition, the tilt angle and orientation of buildings should be more closely investigated to identify how much potential there actually is for installing a PV system. Since the solar map includes all buildings (built before 2014) on Tromsøya, it is possible to look directly into the map and investigate potential. This would take time but will give accurate results.

- **A complete cost benefit analysis of PV system investment**

  When estimating economic benefit by selling electricity, a cost estimate should also be performed. A detailed economic analysis for the PV system marked is not performed in this thesis as it is not considered highly relevant for a master thesis in physics and technology. This could be an interesting field to investigate more in detail in collaboration with e.g. students in economy. The analysis would could focus on investment issues of relevance for PV systems in a city as Tromsø in the future. The resulting cost benefit analysis could be presented to Tromsø municipality to discuss organizing of a local solar energy system covering production, distribution, marketing and redistribution of the values achieved to the local community.

7 Appendices

7.1 A Monthly solar maps with 1-meter resolution

The solar map for each month is zoomed into one area covering the University of Tromsø with surroundings. With a map covering the whole island, is it difficult to investigate solar irradiation on roofs. If a solar map for another or bigger area is wanted, please get in touch with author of this thesis.

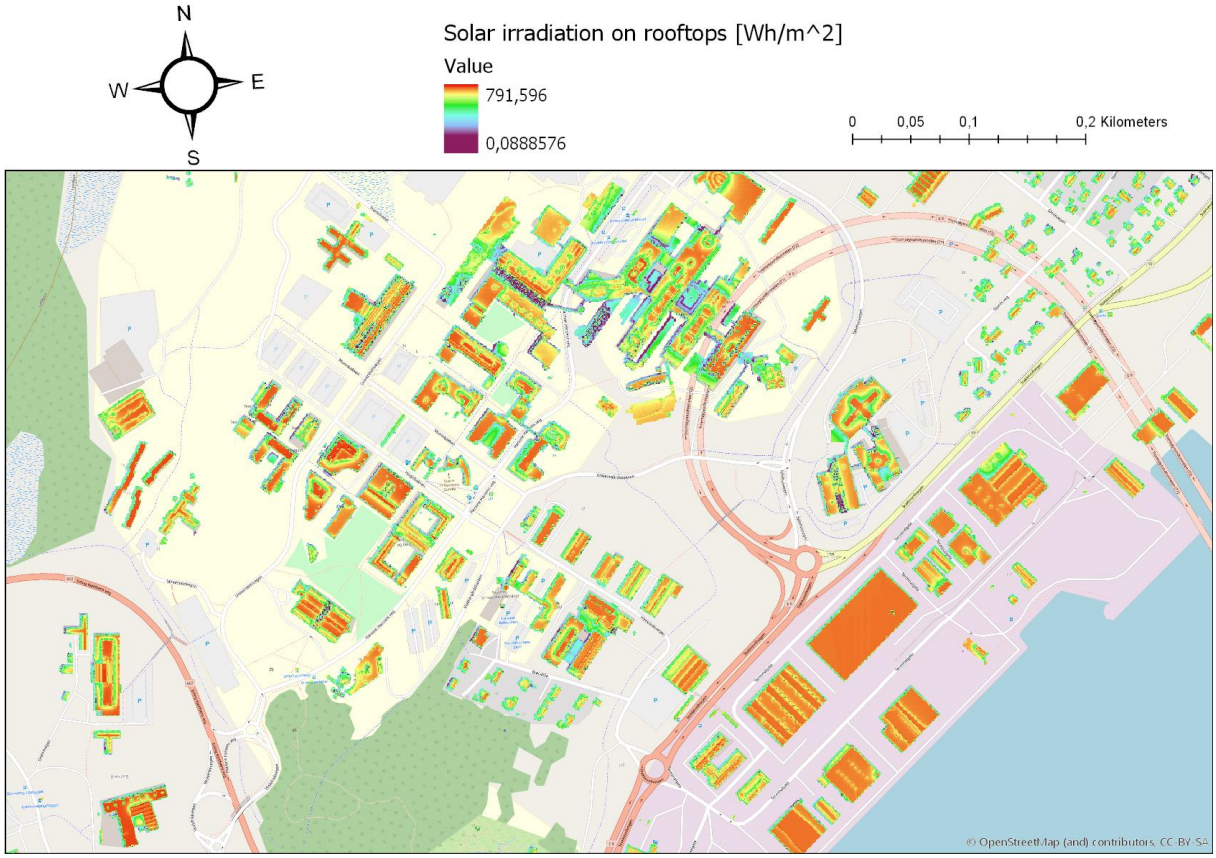

Figure 7-1: Solar map for rooftops in January

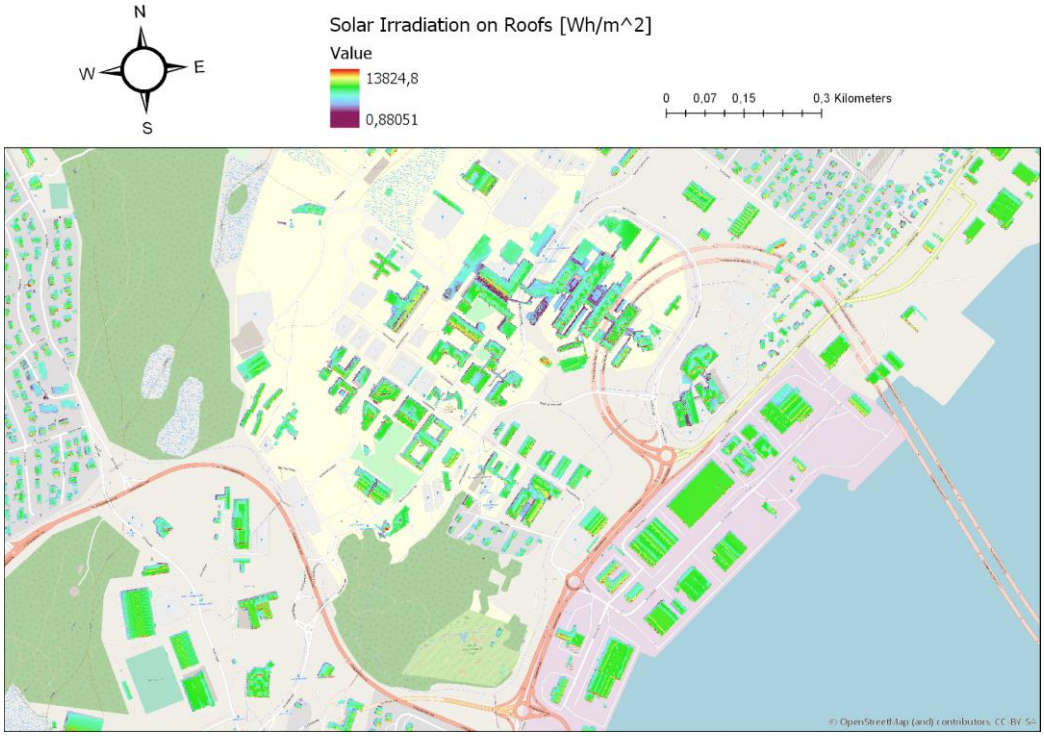

Figure 7-2: Solar map for rooftops in February

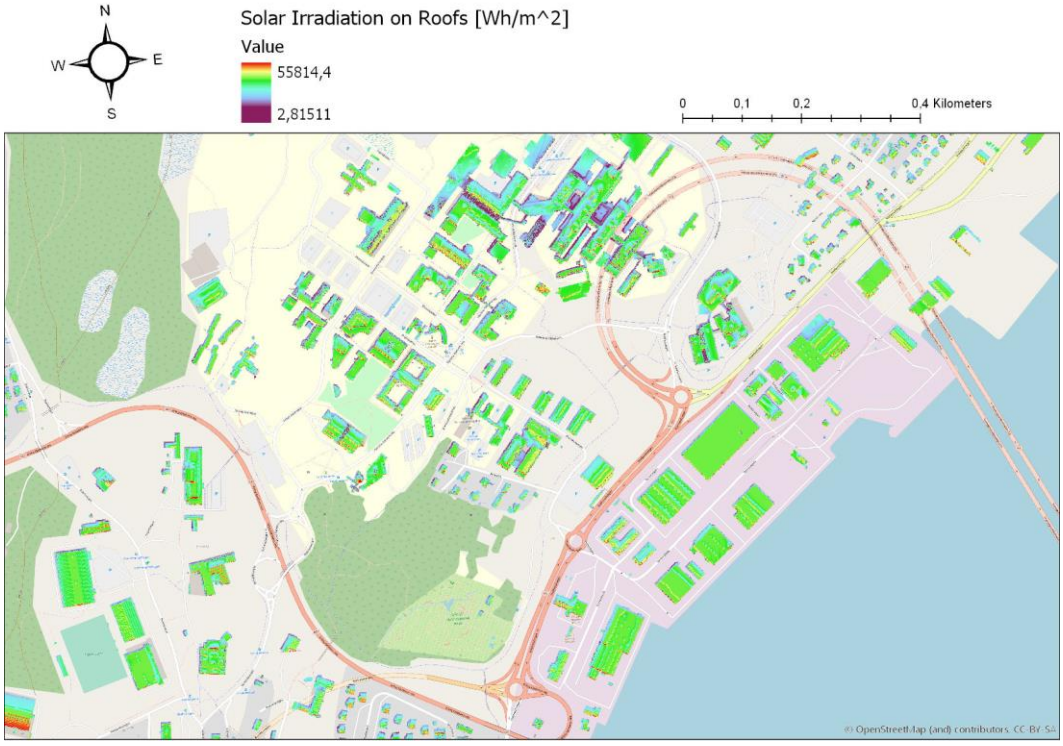

Figure 7-3:Solar map for rooftops in March

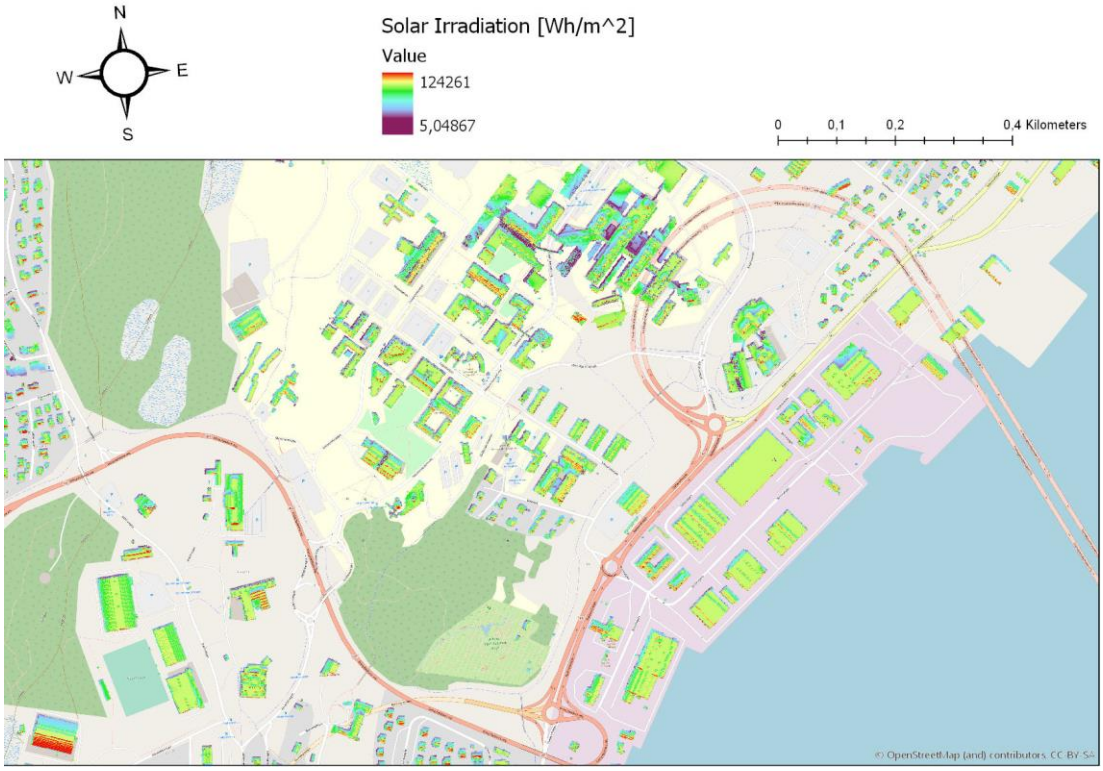

Figure 7-4: *Solar map on rooftops in April*

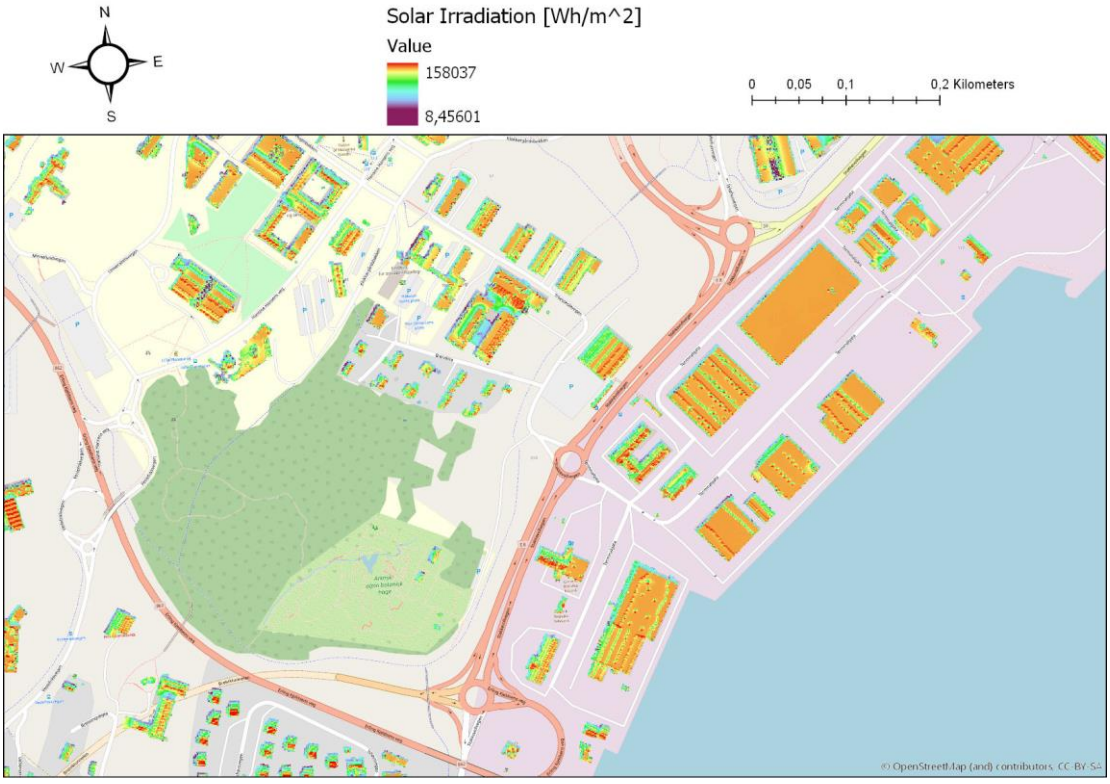

Figure 7-5: Solar map on rooftops in May

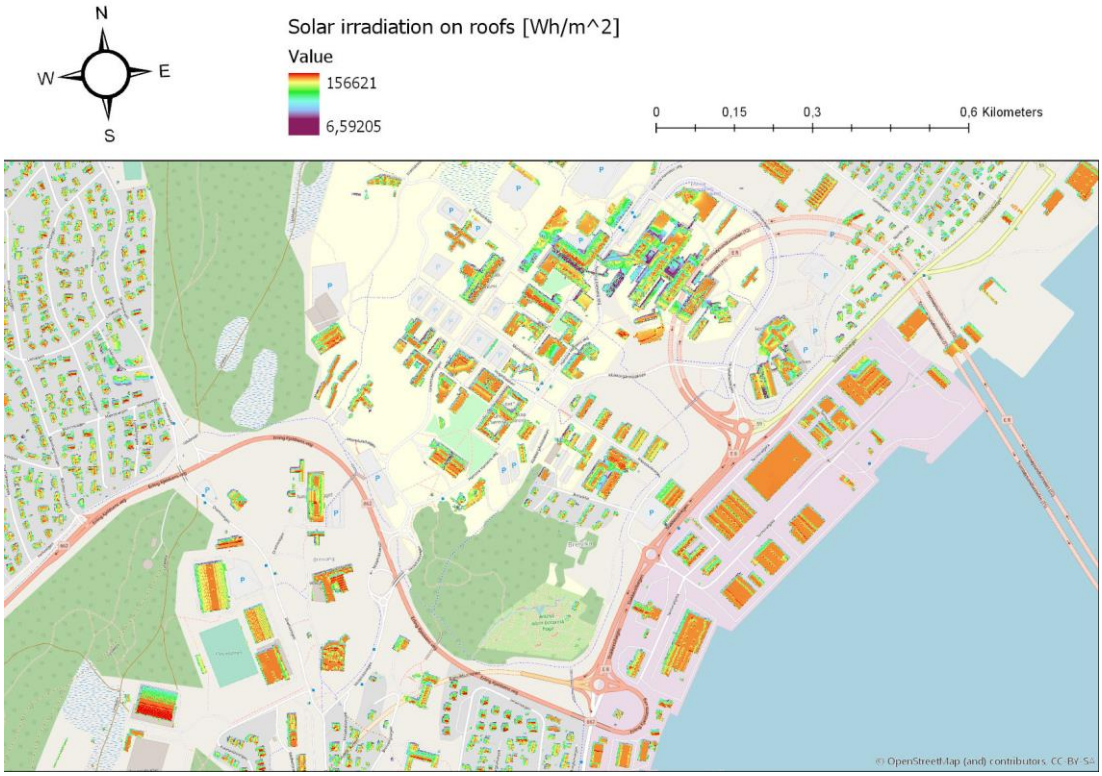

Figure 7-6: Solar map on rooftops in June

Figure 7-7: Solar map on rooftops in July with "GeoacheGraatone" as basemap

Figure 7-8: Solar map for rooftops in August

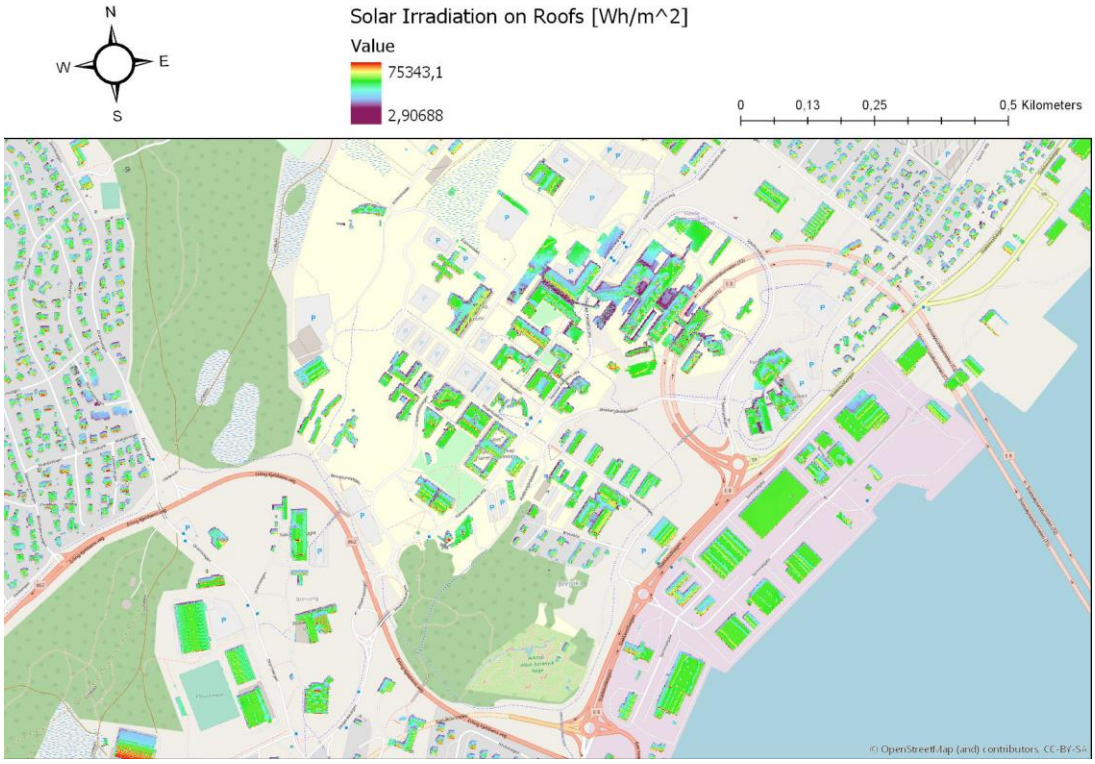

Figure 7-9:Solar map for rooftops in September

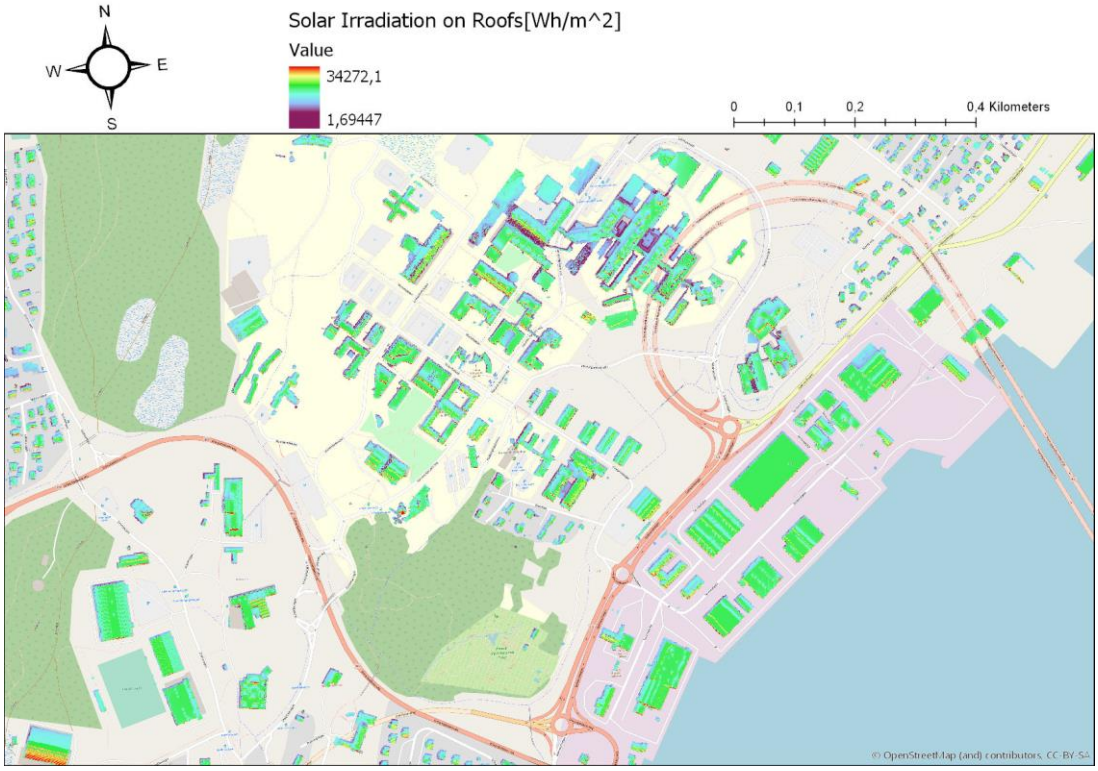

Figure 7-10: Solar map for rooftops in October

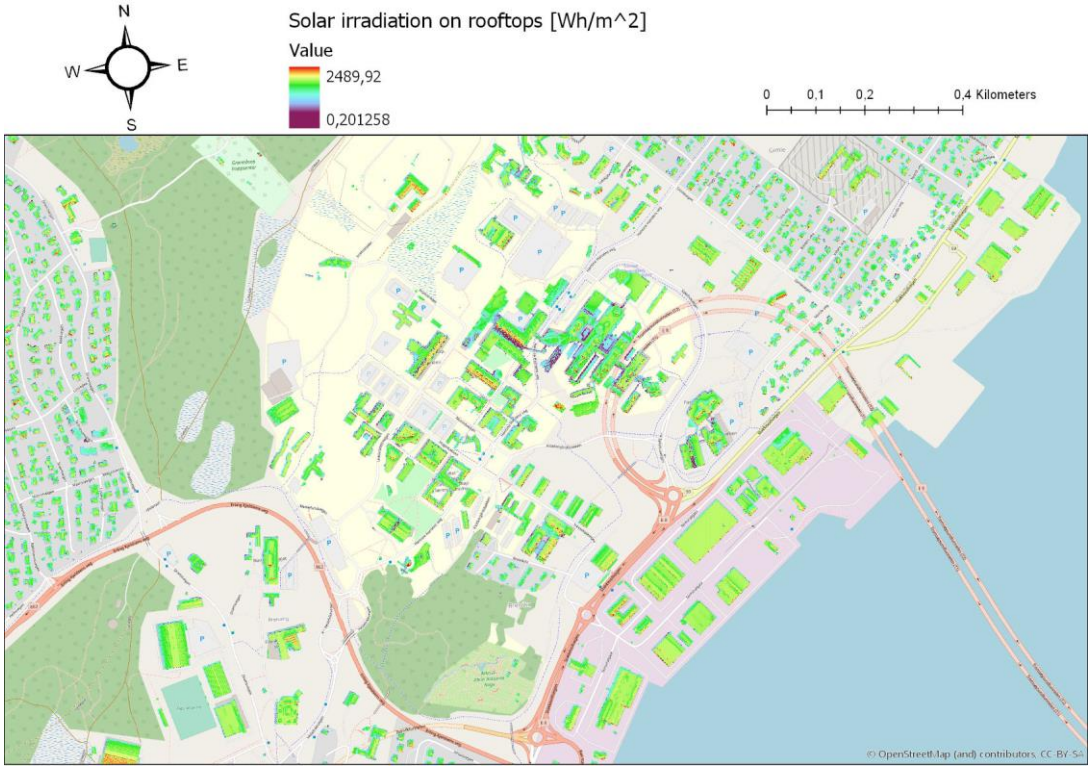

Figure 7-11: Solar map for rooftops in November

7.2 B Monthly solar maps with 0.25-meter resolution

For 0.25- meter resolution solar map, the map is zoomed into the area covering Tromsø running station with surroundings.

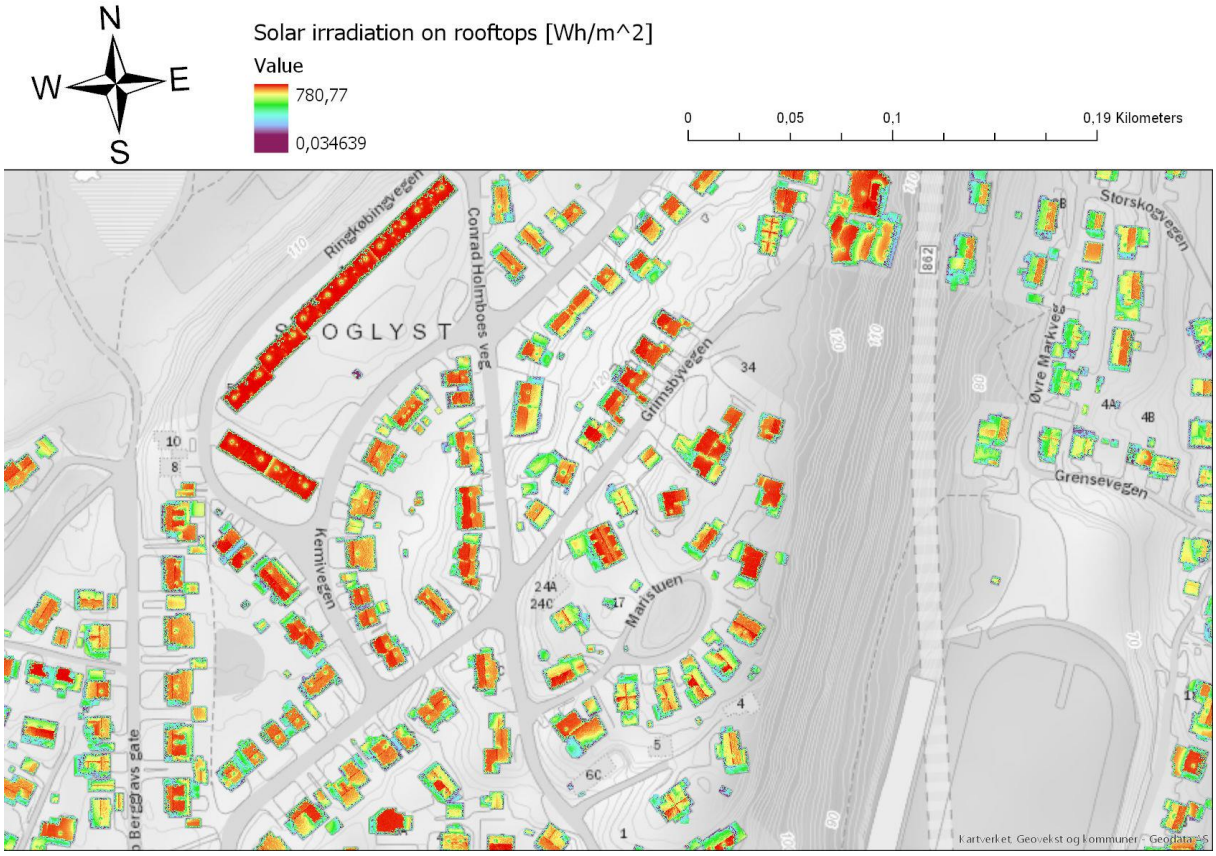

Figure 7-12: High resolution solar map on rooftops in January 2018

Figure 7-13:High resolution solar map on rooftops in February 2018

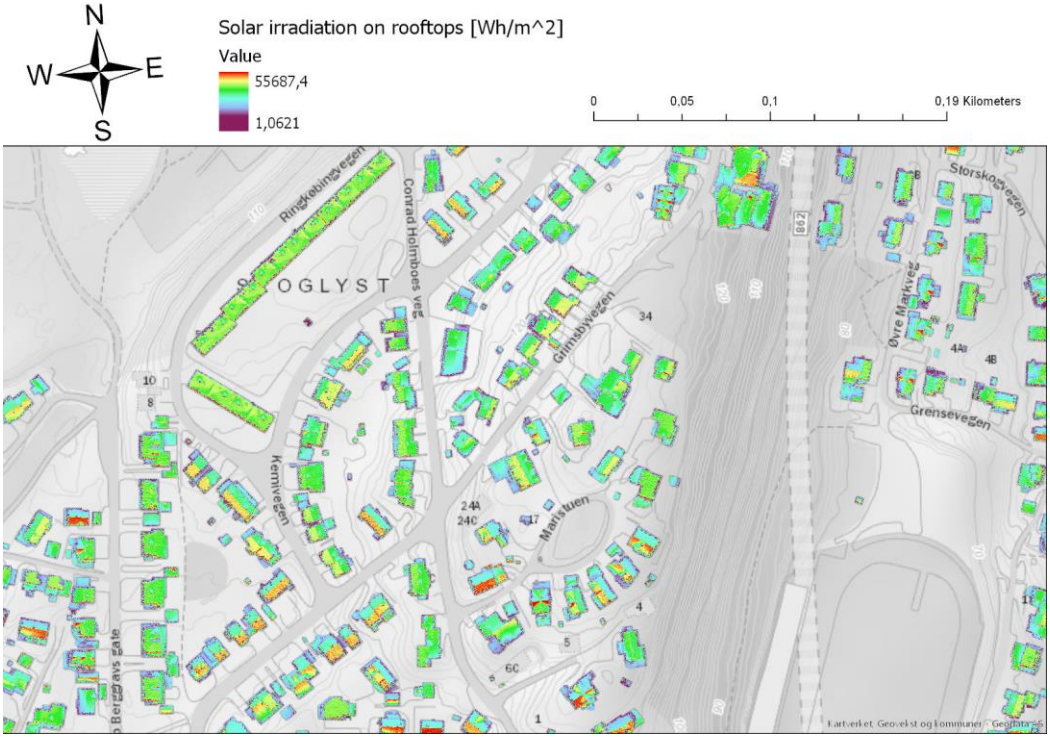

Figure 7-14:High resolution solar map on rooftops in March 2018

Figure 7-15:High resolution solar map on rooftops in April 2018

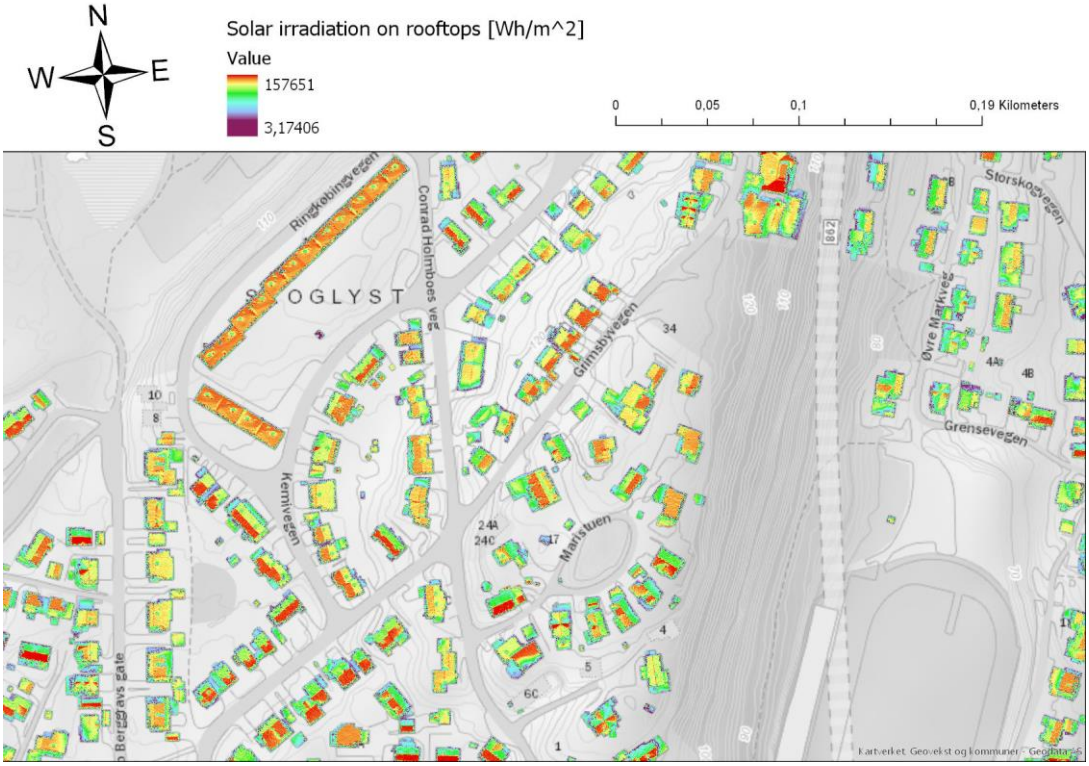

Figure 7-16:High resolution solar map on rooftops in May 2018

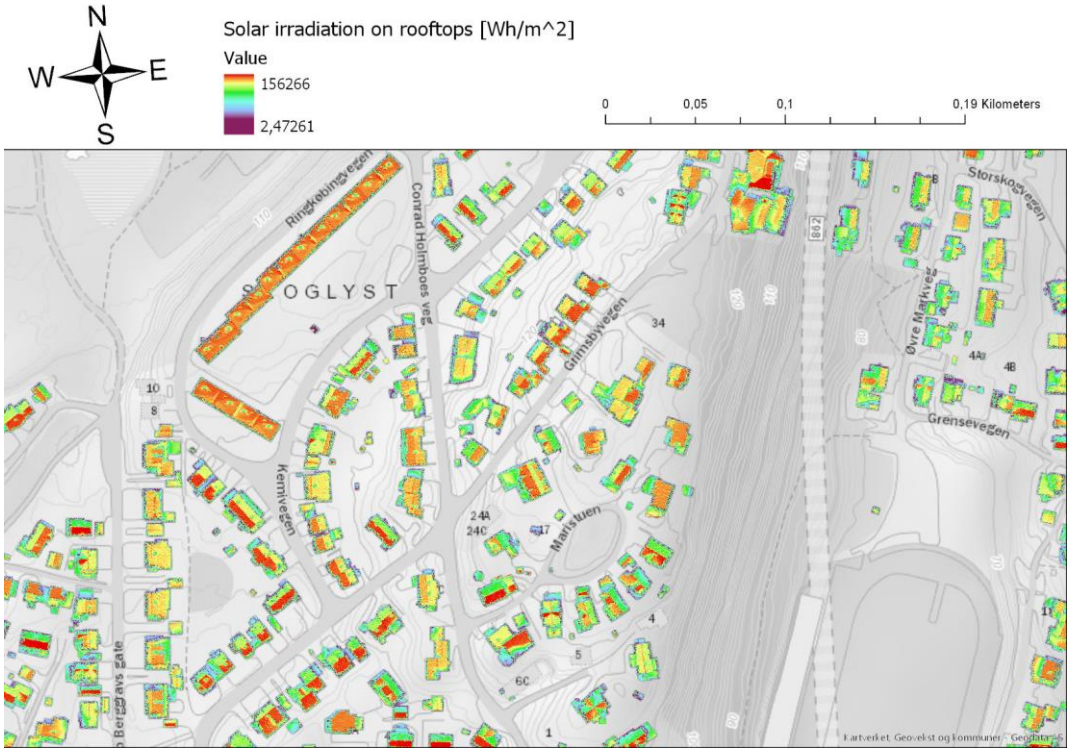

Figure 7-17:High resolution solar map on rooftops in June 2018

Figure 7-18: High resolution solar map on rooftops in July 2018

Figure 7-19: High resolution solar map on rooftops in August 2018

Figure 7-20: High resolution solar map on rooftops in September 2018

Figure 7-21: High resolution solar map on rooftops in October 2018

Figure 7-22: High resolution solar map on rooftops in November 2018

8 Bibliography

8.1

Alternative Energy Tutorials, 2019. *Photovoltaic Solar Cells.* [Online]
Available at: http://www.alternative-energy-tutorials.com/solar-power/photovoltaics.html
[Accessed 12 02 2019].

Anderaa Data Instruments AS, 2013. *Solar Radiation Sensor 2270.* [Online]
Available at: https://www.aanderaa.com/media/pdfs/Solar-Radiation-Sensor-2770.pdf
[Accessed 26 09 2018].

Andrews, J. & Jelley, N., 2013. Principles, Technologies, and impacts. In: *energy science.* Oxford: Oxford University Press, pp. 180-224.

Bellona, 2016. *Bedre klima og smartere økonomi. Landstrøm i norske havner- en mulighetsstudie.* [Online]
Available at: https://network.bellona.org/content/uploads/sites/2/2016/08/Bedre-klima-og-smartere-okonomi-landstrøm-i-norske-havner-en-mulighetsstudie-av-Bellona-SiemensNelfo-og-Efo_-FINAL.pdf
[Accessed 24 04 2019].

Bellona, 2019. *Fakta om landstrøm.* [Online]
Available at: https://bellona.no/assets/sites/2/2015/06/fil_Fakta_om_landstrom-prosjektet1.pdf
[Accessed 20 04 2019].

Berke, J., 2018. *One simple chart shows why an energy revolution is coming — and who is likely to come out on top.* [Online]
Available at: https://www.businessinsider.com/solar-power-cost-decrease-2018-5?r=US&IR=T&IR=T
[Accessed 12 02 209].

Bloch, H., 2002. *Arealstatistikk fra GAB og FKB Bygg.* [Online]
Available at: https://www.ssb.no/a/publikasjoner/pdf/notat_200272/notat_200272.pdf
[Accessed 25 03 2019].

Bowden, S. & Honsberg, C., 2019. *Semiconductur Structure.* [Online]
Available at: https://pveducation.org/pvcdrom/semiconductor-structure
[Accessed 12 02 2018].

Duffie, J. A. & Beckman, W. A., 2013. In: *Solar Engineering of Thermal Processes Fourth Edition.* Honboken, New Jersey: Wiley, pp. 44-53.

Duffie, J. A. & Beckman, W. A., 2013. In: *Solar Engineering of Thermal Processes Fourth Edition.* Honboken, New Jersey: Wiley, p. 48.

Energy Facts Norway, 2019. *Energy Use by sector.* [Online]
Available at: https://energifaktanorge.no/en/norsk-energibruk/energibruken-i-ulike-sektorer/
[Accessed 07 06 2019].

Energysage, 2019. *How has solar panel cost and efficiency changed over time?.* [Online]
Available at: https://news.energysage.com/solar-panel-efficiency-cost-over-time/
[Accessed 30 05 2018].

Enova, 2019. *Hva gjør ENnova.* [Online]
Available at: https://www.enova.no/om-enova/
[Accessed 05 06 2019].

ESA, 2002. *Expert's RoundTable: ASAR Interferometry promises Hyper- Accurate Measurements from orbit.* [Online]
Available at:
http://www.esa.int/Our_Activities/Observing_the_Earth/Expert_s_Roundtable_ASAR_interferometry_promises_hyper-accurate_measurements_from_orbit
[Accessed 21 02 2019].

Esri, 2016. *Cell size of raster data.* [Online]
Available at: http://desktop.arcgis.com/en/arcmap/10.3/manage-data/raster-and-images/cell-size-of-raster-data.htm
[Accessed 23 02 2019].

Esri, 2016. *What is LiDAR data?.* [Online]
Available at: http://desktop.arcgis.com/en/arcmap/10.3/manage-data/las-dataset/what-is-lidar-

data-.htm
[Accessed 22 02 2019].

Esri, 2019. *About ArcGIS.* [Online]
Available at: https://www.esri.com/en-us/arcgis/about-arcgis/overview
[Accessed 18 03 2019].

Esri, 2019. *About ArcGIS Pro.* [Online]
Available at: https://pro.arcgis.com/en/pro-app/get-started/overview-of-arcgis-pro.htm
[Accessed 18 03 2019].

Esri, 2019. *Area Solar Radiation.* [Online]
Available at: http://desktop.arcgis.com/en/arcmap/10.3/tools/spatial-analyst-toolbox/area-solar-radiation.htm
[Accessed 29 05 2019].

Esri, 2019. *What is the ArcGIS Spatial Analyst extension?.* [Online]
Available at: https://pro.arcgis.com/en/pro-app/help/analysis/spatial-analyst/basics/what-is-the-spatial-analyst-extension.htm
[Accessed 30 03 2019].

Falklev, E. H., 2017. Mapping of Solar Energy Potential on Tromsøya Using Solar Analyst in ArcGIS. *Munin- Open research archive*, 1 December, pp. 1-69.

Fjordkraft, 2019. *Strømforbruk.* [Online]
Available at: https://www.fjordkraft.no/privat/stromforbruk/
[Accessed 27 05 2019].

ftexploring, 2011. *Direct, Diffuse and Reflected Radiation.* [Online]
Available at: http://www.ftexploring.com/solar-energy/direct-and-diffuse-radiation.htm
[Accessed 13 09 2018].

Garner, R., 2008. *Solar Irradiance.* [Online]
Available at: https://www.nasa.gov/mission_pages/sdo/science/solar-irradiance.html
[Accessed 17 09 2018].

Geodata, 2019. *3D Clip&Ship.* [Online]
Available at: https://www.geodata.no/webinarer/3d-clip-ship
[Accessed 21 03 2019].

GISgeography, 2018. *How Universal Transverse Mercator (UTM) Works.* [Online]
Available at: https://gisgeography.com/utm-universal-transverse-mercator-projection/
[Accessed 21 02 2019].

GISgeography, 2018. *Passive vs Active Sensors in Remote Sensing.* [Online]
Available at: https://gisgeography.com/passive-active-sensors-remote-sensing/
[Accessed 20 02 2019].

GISgeography, 2018. *Vector vs Raster: What's the Difference Between GIS Spatial Data Types?.* [Online]
Available at: https://gisgeography.com/spatial-data-types-vector-raster/
[Accessed 21 02 2019].

Good, C., Shepero, M., Munkhammar, J. & Boström, T., 2018. Scenario- based modelling of the potential for solar energy charging of electric vehicles in two scandinavian cities. *Energy*, 19 November, pp. 110-125.

Hinckley, A., 2017. *Pyranometers: What you need to know.* [Online]
Available at: https://www.campbellsci.com/blog/pyranometers-need-to-know
[Accessed 22 10 2018].

Honsberg, C. & Bowden, J., 2019. *Introduction.* [Online]
Available at: https://pveducation.org/pvcdrom/introduction/introduction
[Accessed 12 02 2019].

Honsberg, C. & Bowden, S., 2018. *Atmospheric effects.* [Online]
Available at: https://pveducation.org/pvcdrom/properties-of-sunlight/atmospheric-effects
[Accessed 12 12 2018].

Honsberg, C. & Bowden, S., 2018. *Atmospheric Effects.* [Online]
Available at: https://pveducation.org/pvcdrom/properties-of-sunlight/atmospheric-effects
[Accessed 11 02 2019].

Honsberg, C. & Bowden, S., 2018. *Energy of Photons.* [Online]
Available at: https://pveducation.org/pvcdrom/properties-of-sunlight/energy-of-photon
[Accessed 26 09 2018].

Honsberg, C. & Bowden, S., 2018. *Properties of Light.* [Online]
Available at: https://pveducation.org/pvcdrom/properties-of-sunlight/properties-of-light
[Accessed 26 09 2018].

Honsberg, C. & Bowden, S., 2018. *Solar Energy.* [Online]
Available at: https://pveducation.org/pvcdrom/introduction/solar-energy
[Accessed 26 09 2018].

Honsberg, C. & Bowden, S., 2019. *Air Mass.* [Online]
Available at: https://pveducation.org/pvcdrom/properties-of-sunlight/air-mass
[Accessed 11 02 2019].

Honsberg, C. & Bowden, S., 2019. *Effect of temperature.* [Online]
Available at: https://pveducation.org/pvcdrom/solar-cell-operation/effect-of-temperature
[Accessed 12 02 2019].

Honsberg, C. & Bowden, S., 2019. *Fill Factor.* [Online]
Available at: https://pveducation.org/pvcdrom/solar-cell-operation/fill-factor
[Accessed 25 02 2019].

IEA Photovoltaic Power System Programme, 2019. *Photovoltaic power systems in the built environment.* [Online]
Available at: http://www.iea-pvps.org/?id=53
[Accessed 24 03 2019].

Ingenieurbüro Mencke & Tegtmeyer GmbH , 2019. *Silicon Irradiance Sensor.* [Online]
Available at: https://www.imt-solar.com/products/solar-irradiance-sensor/si-sensor/
[Accessed 24 02 2019].

ISO, n.d. *ISO 9000 family- Quality management.* [Online]
Available at: https://www.iso.org/iso-9001-quality-management.html
[Accessed 27 09 2008].

Kartverket, 2019. *Høydedata og terrengmodeller fra Kartverket.* [Online]
Available at: https://www.kartverket.no/data/Hoydedata-og-terrengmodeller/
[Accessed 18 03 2019].

Kipp & Zonen, 2000. *CM11 pyranometer, Instruction Manual.* [Online]
Available at:
file:///C:/Users/Odin%20F.%20Eikeland/AppData/Local/Packages/Microsoft.MicrosoftEdge_8wekyb3d8bbwe/TempState/Downloads/KippZonen_Manual_Pyranometer_Albedometer_CM11_CM14%20(3).pdf
[Accessed 27 09 2018].

Kipp & Zonen, 2018. *Calibration Standards.* [Online]
Available at: http://www.kippzonen.com/ProductGroup/112/Calibration-Standards
[Accessed 27 09 2018].

Kipp and Zonen B.V, 2015. *The working principle of a thermopile pyranometer.* [Online]
Available at: http://www.kippzonen.com/News/572/The-Working-Principle-of-a-Thermopile-Pyranometer#.W5pip_ZuLg9
[Accessed 14 09 2018].

Lingfors, D., 2017. Uppsala Universitetet. In: *Solar Variability Assessment in the Built Environment- Model Development and Application to Grid Integration.* Acta Universitatis Uppsala: Uppsala Universitetet, pp. 49-72.

LOS, 2019. *Historiske Strømpriser.* [Online]
Available at: https://www.los.no/kundeservice/strompris/historiske-strompriser/
[Accessed 16 05 2019].

Luthander, R., Widen, J. & Nilsson Danial, P. J., 2015. Photovoltaic self-consumption in buildings: A review. *Science Direct*, 15 March, pp. 80-94.

Marchant, E. F., 2018. *IPCC: Renewables to Supply 70%-85% of Electricity by 2050 to Avoid Worst Impacts of Climate Change.* [Online]
Available at: https://www.greentechmedia.com/articles/read/ipcc-renewables-85-electricity-

worst-impacts-climate-change#gs.g16dqv
[Accessed 01 06 2019].

Meteonorm, 2019. *Meteonorm.* [Online]
Available at: https://meteonorm.com/
[Accessed 19 05 2019].

Milliano, S. d., 2016. [Online]
Available at: https://www.gim-international.com/content/article/satellite-radar-interferometry
[Accessed 21 02 2019].

Multiconsult, 2018. *Solkraft løfter Norge inn i framtiden.* [Online]
Available at: https://www.multiconsult.no/solkraft-lofter-norge-inn-i-framtiden/
[Accessed 30 05 2019].

NIBIO, 2018. *NIBIO, LandbruksMeterologisk Tjeneste.* [Online]
Available at: http://lmt.bioforsk.no/
[Accessed 26 09 2018].

Opdal, O. A. & Steen, E. H., 2012. Landstrøm i Norge. *En studie av mulighetene for landstrøm i Norge. Case: Hurtigruten*, 1 Mars, pp. 1-40.

Oslo Kommune, 2019. *Oslo Solkart.* [Online]
Available at: https://www.oslo.kommune.no/politikk-og-administrasjon/miljo-og-klima/solkart-for-oslo/
[Accessed 24 03 2019].

PVsyst, 2019. *General description of the PVsyst Software.* [Online]
Available at: https://www.pvsyst.com/
[Accessed 19 05 2019].

Realfsen, E., 2007. *Strømforbruket måned for måned.* [Online]
Available at: https://www.dinside.no/okonomi/stromforbruket-maned-for-maned/62097345
[Accessed 27 05 2019].

Reotemp, 2011. *What is a thermocouple.* [Online]
Available at: https://www.thermocoupleinfo.com/
[Accessed 14 09 2018].

Seale, E., 2016. *Solar Cells.* [Online]
Available at:
http://solarbotics.net/starting/200202_solar_cells/200202_solar_cell_physics.html
[Accessed 12 02 2019].

Sikveland, T., 2019. *Port of Kristiansand.* [Online]
Available at: https://www.portofkristiansand.no/
[Accessed 04 06 2019].

Singh, S., 2016. *Confused Between DEM, DTM and DSM.* [Online]
Available at: http://www.gisresources.com/confused-dem-dtm-dsm/
[Accessed 21 02 2019].

Solar Business Hub, 2019. *Totall installed solar PV capacity exceed 500 GW globally in 2018, IEA PVPS report finds.* [Online]
Available at: https://solarbusinesshub.com/2019/04/21/total-installed-solar-pv-capacity-exceeded-500-gw-globally-in-2018-iea-pvps-report-finds/
[Accessed 30 05 2019].

SSB, 2019. *Bygningsmassen.* [Online]
Available at: https://www.ssb.no/bygningsmasse
[Accessed 25 03 2019].

SSB, 2019. *Tettsteders befolkning og areal.* [Online]
Available at: https://www.ssb.no/befolkning/statistikker/beftett/aar
[Accessed 10 06 2019].

Sustinable Enterprises Media, Inc, 2019. *Global Solar PV Market To See 25% Growth, Reach 129 Gigawatts Of New Capacity In 2019.* [Online]
Available at: https://cleantechnica.com/2019/04/09/global-solar-pv-market-to-see-25-growth-

reach-129-gigawatts-of-new-capacity-in-2019/
[Accessed 30 05 2019].

Tarikhi, P., 2019. *InSAR DEM; why it is better.* [Online]
Available at: https://parviztarikhi.wordpress.com/features-2/dems-from-insar/insar-dem-why-it-is-better/
[Accessed 07 06 2019].

The University of Southampton, 2018. *Data sources for elevation.* [Online]
Available at: http://generic.wordpress.soton.ac.uk/gem/unit-3/3-2-data-sources-for-elevation/
[Accessed 22 02 2019].

Troms Kraft, 2019. *Prisinformasjon.* [Online]
Available at: http://www.tromskraftnett.no/privat/nett/prisinformasjon
[Accessed 10 06 2019].

Tromsø havn, 2019. *Om Tromsø Havn.* [Online]
Available at: https://www.tromso.havn.no/om-oss/
[Accessed 20 04 2019].

UiT, 2019. *ARC- Arctic Centre for Sustainable Energy.* [Online]
Available at: https://en.uit.no/forskning/forskningsgrupper/gruppe?p_document_id=453700
[Accessed 30 05 2019].

yr, 2019. *Klimastatistikk for Tromsø målestasjon.* [Online]
Available at:
https://www.yr.no/sted/Norge/Troms/Tromsø/Tromsø_(Vervarslinga)_målestasjon/klima.html
[Accessed 05 09 2019].